Oncology and Translational Medicine

Volume 8 • Number 6 • December 2022

Oncology and Translational Medicine Volume 8 • Number 6 • December 2022 pp 267-317

邮发代号：38-121
ISSN 2095-9621

GENERAL INFORMATION
≫otm.tjh.com.cn

ISSN 2095-9621
CN 42-1865/R

Oncology and Translational Medicine

肿瘤学与转化医学（英文）

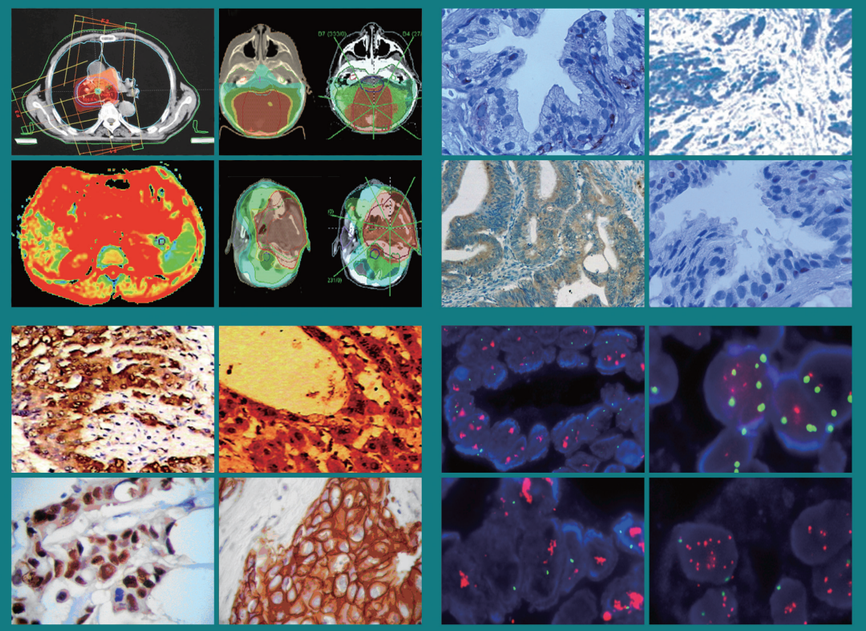

Volume 8
Number 6
December 2022

Oncology and Translational Medicine

Oncology and Translational Medicine
December 2022 Volume 8 Number 6

Contents

Oncology and Translational Medicine

Volume 8 • Number 6 • December 2022

Aims & Scope

Oncology and Translational Medicine is an international professional academic periodical. The Journal is designed to report progress in research and the latest findings in domestic and international oncology and translational medicine, to facilitate international academic exchanges, and to promote research in oncology and translational medicine as well as levels of service in clinical practice. The entire journal is published in English for a domestic and international readership.

Copyright

Supervised by

Ministry of Education of the People's Republic of China.

Administered by

Tongji Medical College, Huazhong University of Science and Technology.

Submission information

Manuscripts should be submitted to:
http://otm.tjh.com.cn
dmedizin@sina.com

Subscription information

ISSN edition: 2095-9621
CN: 42-1865/R

■ Subscription rates
Subscription may begin at any time. Remittances made by check, draft or express money order should be made payable to this journal. The price for 2022 is as follows: US $ 30 per issue; RMB ￥28.00 per issue.

Database

Oncology and Translational Medicine is abstracted and indexed in EMBASE, Index Copernicus, Chinese Science and Technology Paper Citation Database (CSTPCD), Chinese Core Journals Database, Chinese Journal Full-text Database (CJFD), Wanfang Data; Weipu Data; Chinese Academic Journal Comprehensive Evaluation Database.

Business correspondence

All matters relating to orders, subscriptions, back issues, offprints, advertisement booking and general enquiries should be addressed to the editorial office.

Mailing address
Editorial office of
Oncology and Translational Medicine
Tongji Hospital
Tongji Medical College
Huazhong University of Science and Technology
Jie Fang Da Dao 1095
430030 Wuhan, China
Tel.: +86-27-69378388
Email: dmedizin@sina.com

Printer
Changjiang Spatial Information Technology Engineering Co., Ltd. (Wuhan) Hangce Information Cartorgraphy Printing Filial, Wuhan, China
Printed in People's Republic of China

Editors-in-Chief

Managing director

Executive editors

Oncology and Translational Medicine
DOI 10.1007/s10330-022-0598-8
December 2022, Vol. 8, No. 6, P267–P275

ORIGINAL ARTICLE

Hypoxia-inducible factor-2α and its missense mutations: potential role in HCC diagnosis, progression, and prognosis and underlying mechanism

Jun Li[1], Yibo Yan[2], Ganxin Wang[3, 4] (✉), Zaozao Huang[5] (✉)

[1] Emergency Department, Liyuan Hospital, Tongji Medical College, Huazhong University of Science and Technology, Wuhan 430077, China
[2] Division of Cardiology, Liyuan Hospital, Tongji Medical College, Huazhong University of Science and Technology, Wuhan 430077, China
[3] Division of Oncology, Liyuan Hospital, Tongji Medical College, Huazhong University of Science and Technology, Wuhan 430077, China
[4] Cancer Center, Union Hospital, Tongji Medical College, Huazhong University of Science and Technology, Wuhan 430022, China
[5] Yangchunhu Community Hospital, Liyuan Hospital, Tongji Medical College, Huazhong University of Science and Technology, Wuhan 430077, China

Abstract

Objective This study aims to gain further the potential mechanisms of HIF-2α in tumor progression and tumorigenesis.

Methods Mined The Cancer Genome Atlas (TCGA) dataset. In total, 421 participants were enrolled in the TCGAHepatocellular Carcinoma (HCC) study, comprising 371 patients with cancer and 50 healthy controls. From the 371 tumor samples, three samples containing the missense mutation of the HIF-2α gene were compared with 368 wild-type samples to identify differentially expressed genes (DEGs).

Results After filtering, univariate Cox regression and multivariate Cox regression analyses showed that the differentially expressed genes (DEGs) progestagen-associated endometrial protein (PAEP) PNLIPRP2, MIR147B, and pregnancy zone protein (PZP) were significantly correlated with the survival times of patients with HCC. Gene Ontology (GO) and Kyoto Encyclopedia of Genes and Genomes (KEGG) analyses were performed using the Database for Annotation, Visualization, and Integrated Discovery (DAVID) v6.8 database to detect the functional annotation of these four DEGs as well as hub genes obtained from protein-protein interaction (PPI) network analysis using the STRING v10 database. Our analysis focused on the PAEP and PZP genes, whose protein expressions were downregulated in samples with HIF-2α missense mutation. The hub genes of PAEP and PZP were identified using PPI network analysis. Subsequent Kyoto Encyclopedia of Genes and Genomes (KEGG) pathway analysis revealed that PAEP and its hub genes were highly enriched in the TGF-β pathway, which is consistent with the analysis of PZP.

Conclusion Our study proved that the missense mutation of HIF-2α induces the upregulation of PAEP, which is positively related to the poor prognosis of patients with HCC, as it may upregulate the TGF-β pathway. In contrast, PZP downregulation showed the opposite phenomenon, as it may downregulate the TGF-β pathway.

Received: 17 September 2022
Revised: 9 November 2022
Accepted: 1 December 2022

Key words: HIF-2α; TGF-β pathway; ECM; PZP; PAEP; Hypoxia

✉ Correspondence to: Ganxin Wang. Email: Medicine_wgx@163.com
Zaozao Huang. Email: huangzaozao1986@163.com

Hepatocellular carcinoma (HCC) is the fifth most common malignancy in the world. With nearly 500,000 people dying from liver cancer each year, HCC is the third leading cause of cancer-related death [1]. This disease is frequently diagnosed at an advanced stage, when medical and surgical treatments are no longer available. HIF-2α was initially identified as the endothelial PAS domain protein (EPAS1), an endothelium-specific HIF-1α isoform. Thus, HIF-2α was considered to have a more specialized function than HIF-1α, and it also interacts with HIF-1α to execute various biological processes. HIF-2α has been shown to regulate enzymes in the glycolytic pathway in the absence of HIF-1α [2]. HIF-1α and HIF-2α also have common target genes, such as vascular endothelial growth factor A and glucose transporter 1, but the transcriptional activities of HIF-1α and HIF-2α differ in gene regulation [3]. Increased expression of HIF-2α has been observed in lung, breast, colorectal, and gastric cancers and has been associated with poor prognosis in many cases, except for liver cancer and acute myeloid leukemia [4]. Because of the observed opposing HIF-2α expression patterns and their correlation with HCC, special attention has been focused on the relationship between HIF-2α expression and HCC [5]. It has been found that the expression of HIF-2α can be lower or higher in HCC tissues, and HIF-2α expression is associated with a better or worse prognosis for HCC. It has been reported that there were HIF-2α mutations in patients with gangliocytic paraganglioma (GP). The mutated HIF-2α protein attenuated binding to the von Hippel–Lindau (VHL) protein, enhancing HIF-2α stabilization and activation, which consequently upregulate the HIF-2α downstream genes, contributing to the pathogenesis of cancer [6].

Methods

Gene expression and clinical data in The Cancer Genome Atlas database

Tissues from patients with HCC and adjacent normal tissues were obtained from RNA-seq gene expression version 2 (RNASeqV2) level 3 data (Illumina HiSeq platform) in The Cancer Genome Atlas (TCGA) database. All alteration data for missense mutations used in this study were obtained from the cBioPortal for Cancer Genomics (www.cBioPortal.org). Similar expression patterns of target genes were downloaded from the Gene Expression Profiling Interactive Analysis (GEPIA) database.

Functional annotation and protein-protein interaction network analysis

The online database STRING 10.5 (https://string-db.org/) was used to analyze protein interactions. Protein-protein interaction (PPI) network analysis was performed to identify the hub genes, pregnancy zone protein (PZP) and progestagen-associated endometrial protein (PAEP), which were enriched in the targeting pathway. Functional annotation of PAEP, PZP, and their hub genes was performed using the web tool of the updated version of the Database for Annotation, Visualization, and Integrated Discovery (DAVID) version v6.8.

Identification of NRF2-binding sites by in silico analysis

To identify the HIF-2α binding sites within the promoter regions of the putatively HIF-2α regulated genes, we used the transcription factor-binding site finding tool LASAGNA-Search 2.0, with cutoff values of $P \leq 0.01$. The search was limited to the 0–5 kb upstream promoter region relative to the transcription start site.

Gene set enrichment analysis

To further understand the association between the expression level of HIF-2α and biological processes, we performed gene set enrichment analysis (GSEA v2.2; http://www.broad.mit.edu/gsea/). All patients with HCC in the TCGA cohort were divided into two groups based on the median expression value of HIF-2α, and the respective HIF-2α expression level was used as the phenotype label. The thresholds for significance were determined by permutation analysis (1,000 permutations), and the false discovery rate (FDR) was calculated. A gene set was considered to be significantly enriched when the FDR score was < 0.25.

Results

Expression and biological functions of HIF-2α

Initially, HIF-2α was identified as the endothelial PAS domain protein, an endothelium-specific HIF-1α isoform. Therefore, it was considered to have a more specialized function than HIF-1α [2]. However, HIF-2α is also expressed in many other tissues, including the brain, heart, lung, kidney, liver, pancreas, and intestine, suggesting that it also has a widespread role in the response to hypoxia [7].

Recent data show that both HIF-1α and HIF-2α participate in hypoxia-dependent gene regulation through complex and sometimes antagonistic interactions in some cell types, such as kidney cancer cells [3]. HIF-1α preferentially induces the expression of genes encoding glycolytic enzymes, such as phosphofructokinase [8, 9] and lactate dehydrogenase A [10, 11]. In contrast, HIF-2α induces the expression of genes involved in tumor invasion, including matrix metalloproteinases (MMPs) 2 and 13 and the stem cell factor OCT–3/4 [12]. However, HIF-2α has also been shown to regulate enzymes in the glycolytic pathway in the absence of HIF-1α, and HIF-1α

is capable of activating some MMPs, suggesting that HIF-1α and HIF-2α play redundant roles. HIF-1α and HIF-2α also have common target genes, such as the vascular endothelial growth factor A (VEGFA) [3, 13, 14] and glucose transporter 1 [15], but the transcriptional activities of HIF-1α and HIF-2α are different in the regulation of these genes [12].

HIF-2α plays a vital role in embryonic development and is essential for catecholamine homeostasis [16] as well as neural [17] and hematopoietic development [18]. Knockout of HIF-2α in embryos causes developmental defects in several organs, including the retina, heart, lungs, liver, bone marrow, and muscle [19]. Recently, Lin et al. demonstrated that HIF-2α, but not HIF-1α, plays an important role in the embryonic development of hepatic outgrowth in zebrafish by directly controlling the expression of the leg1 gene [20].

The correlation between HIF-2α and cancer

Increased HIF-2α expression has been observed in lung cancer [21–24], breast cancer [25, 26], colorectal cancer [5], gastric cancer [27–29], pancreatic cancer [30, 31], liver cancer [32–35], prostate cancer [36], ovarian cancer [37], head and neck cancer [38, 39], ccRCC cancer [40], oral squamous cell carcinoma [41], and acute myeloid leukemia (AML) [4] and has been associated with different prognoses (Table 1). Special attention has been focused on the relationship between HIF-2α expression and HCC; opposite HIF-2α expression patterns and correlations have been observed in HCC [32–34]. It has been found that the expression of HIF-2α is lower or higher in HCC tissues and is associated with a better or worse prognosis in HCC [32–34].

A direct comparison of the functions of HIF-1α and HIF-2α in a KRAS-driven mouse model of lung tumorigenesis showed that HIF-1α deletion had a surprisingly little effect on tumor burden and progression, whereas the loss of HIF-2α increased tumor growth and progression [42]. The latter effect is correlated with HIF-2α driven expression of Scgb3a1, which encodes the putative tumor suppressor secret globin 3A1 [43]. Surprisingly, overexpression of a stabilized HIF-2α protein in the KRAS lung tumor mouse model also promotes tumor angiogenesis and invasion by increasing the expression of VEGFA and SNAIL [44].

The complex role of HIF-2α is also reflected at the cellular level. It has been reported that HIF-2α inhibits the growth of glioblastoma, SW480 colon cancer, liver cancer, and non-small cell lung cancer (NSCLC) cells but enhances the proliferation of other types of cancer cells, including gastric cancer, breast cancer, and Renalcellcarcinoma (RCC) cells [28, 45, 46]. Taken together, these findings prove that HIFs have dual and even opposite effects on tumor growth, which warrants careful consideration when using HIF inhibitors as cancer therapeutic agents.

The expression of HIF-2α is correlated with different cancer prognoses

To identify the relationship between the expression level of HIF-2α and various types of cancer, we mined data from TCGA. TCGA analysis revealed that the HIF-2α expression level in normal tissue was higher than that in tumor tissue in breast invasive carcinoma, prostate adenocarcinoma, ovarian serous cystadenocarcinoma, AML, lung adenocarcinoma, and lung squamous cell HCC (LUSC). We then determined whether HIF-2α expression level correlated with overall survival (OS) in cancer (Fig. 1a). We analyzed the data downloaded from TCGA using the R package version 3.4.3. The Kaplan-Meier curve revealed that patients with lower HIF-2α expression levels exhibited longer OS in HCC, which was consistent with the results for kidney renal clear cell HCC (KIRC) (Fig. 1b).

Identification of the expression of the different genes associated with HIF-2α in HCC

Our investigation revealed missense mutations in patients with HCC. To elucidate the mechanism of HIF-2α in HCC, we divided the 377 patients into two groups, which comprised three missense mutation samples or 368 wild-type samples, using the online analysis tool cBioPortal (www.cBioPortal.org) (Fig. 1c). Using the R-package "edgeR" for the identification of differentially expressed genes (DEGs) with RNA-seq expression profiles, we found 68 genes that were all downregulated (Fig. 1d). After filtering with $|\log FC| > 2$ and $P < 0.05$, we identified 40 DEGs between missense mutation and wild-type samples (Fig. 3). We also identified the DGEs between the 50 normal and 370 tumor tissues with the R-package "edgeR," the result of which revealed that there were 5,887 DEGs between the two groups. Using the Venny 2.1 tool, we obtained 19 overlapping downregulated genes by integrating the two datasets (Fig. 1e).

A risk score of four genes as an indicator for patients with HCC

Univariate Cox regression analyses were used to filter the identified 19 DEGs and selected genes with values of $P < 0.05$. The genes PAEP, PNLIPRP2 (pancreatic lipase-related protein 2), MIR147B (microRNA 147b), and PZP were significantly correlated with the survival time of patients with HCC. These four genes were selected for multivariate Cox regression analyses, which revealed that PAEP, PNLIPRP2, and MIR147B were highly expressed in the high-score group, and PZP was highly expressed in the low-score group (Fig. 2a). The coefficients of the four-gene signature are displayed in Table 2. Patients with high scores had significantly worse survival times than

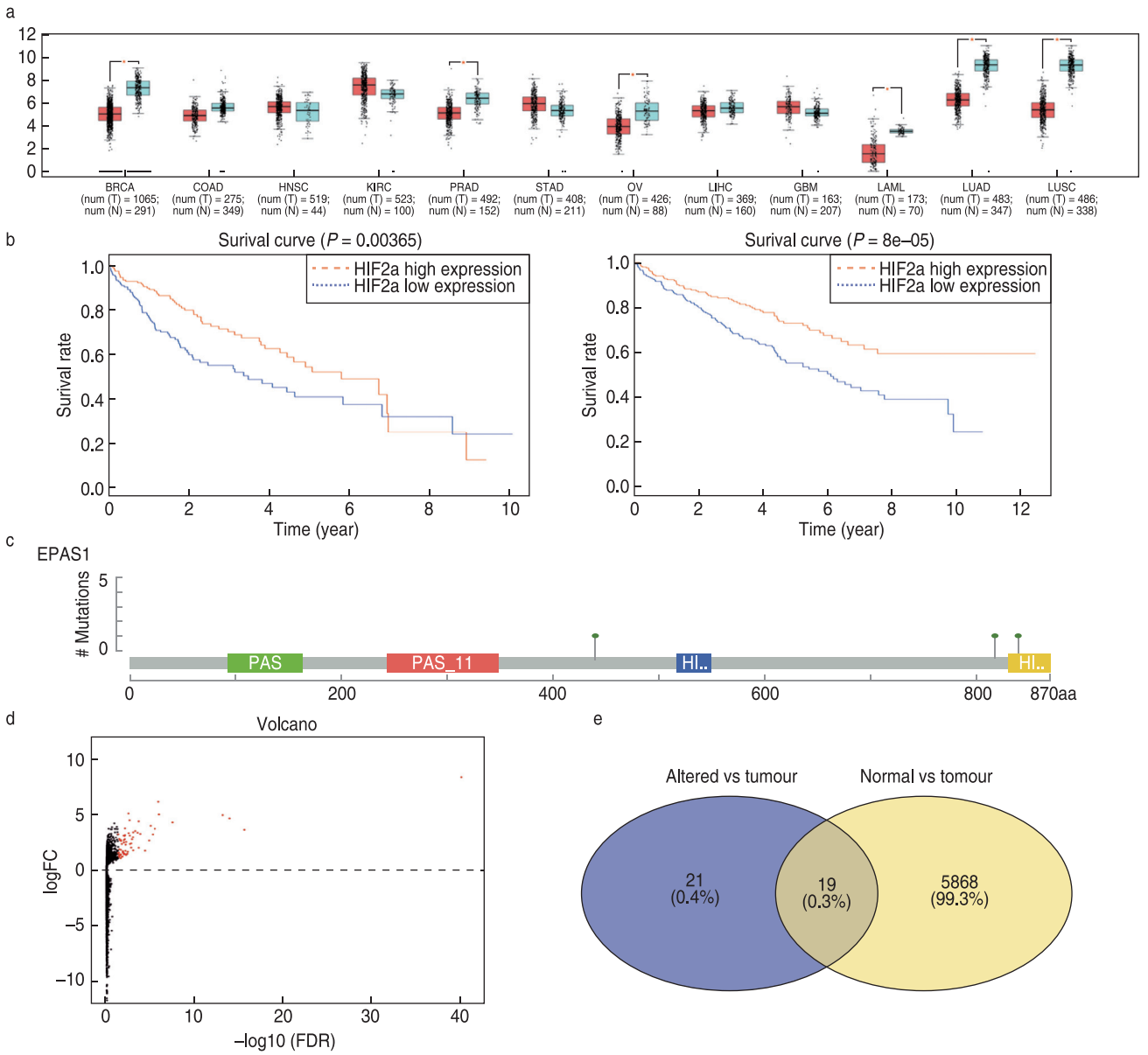

Fig. 1 The expression of HIF-2α correlated with different cancer prognosis and identification of the expression of the different genes associated with HIF-2α in HCC. (a) The gene expression of HIF-2α in normal tissue (green) compared with the tumor tissue (red); (b) KM overall survival curve in HCC and KIRC were according to the median value of the expression of HIF-2α; (c) cBioprotal-predicted mutation maps (lollipop plots) showing the mutation position of HIF-2α; (d) The upregulated genes in the missense mutation group exhibited in the volcano plot; (e) Nineteen overlapping upregulated genes were obtained by integrating the two datasets by utilizing the Venny 2.1 tool

those with low scores (Fig. 2b). Furthermore, these four genes exhibited superior capacity in predicting the 5-year survival rate, with an AUC value of 0.677 (Fig. 2c). Taken together, the score model of these four genes might serve as a significant predictive factor for prognosis in patients with HCC.

HIF-2α regulates the expression of putative oncogenes PAEP and PZP at the transcriptional level

To verify whether the transcription factor HIF-2α affects the gene expression of the four DEGs, we used LASAGNA-Search 2.0. The results revealed that HIF-2α

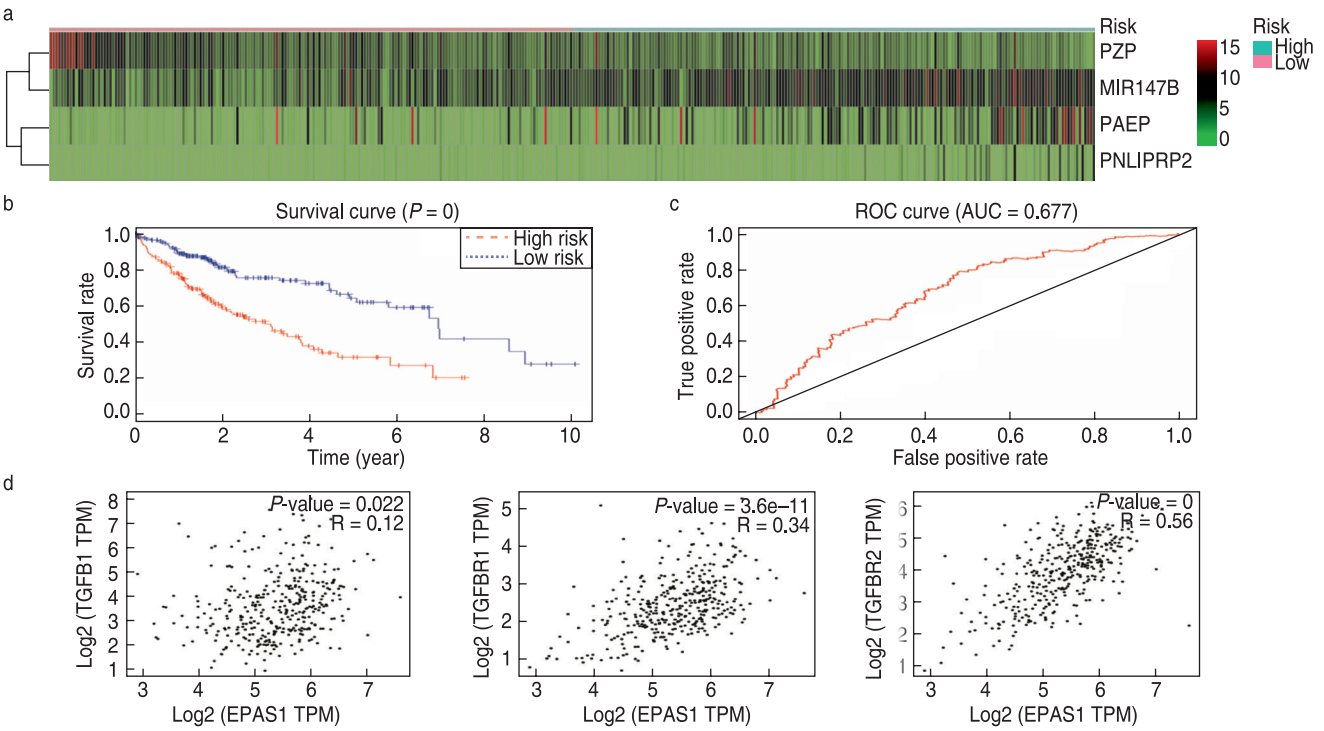

Fig. 2 Risk score of four genes as indicator in patients with HCC and GSEA plot showing that HIF-2α expression positively correlated with the TGF-β pathway and ECM Receptor Interaction in HCC. (a) Heat map showing the differential expression and risk of the four genes in HCC; (b) Kaplan-Meier survival curve: overall survival in patients with hepatocellular carcinoma according to the risk score; (c) The area under the curve was 0.677, demonstrating that the four-gene signature had high sensitivity and specificity for the classification of HCC patients from normal; (d) Expression levels of TF HIF-2α were positively correlated with the levels of TGFB1, TGFBR1, and TGFBR2 in TCGA dataset

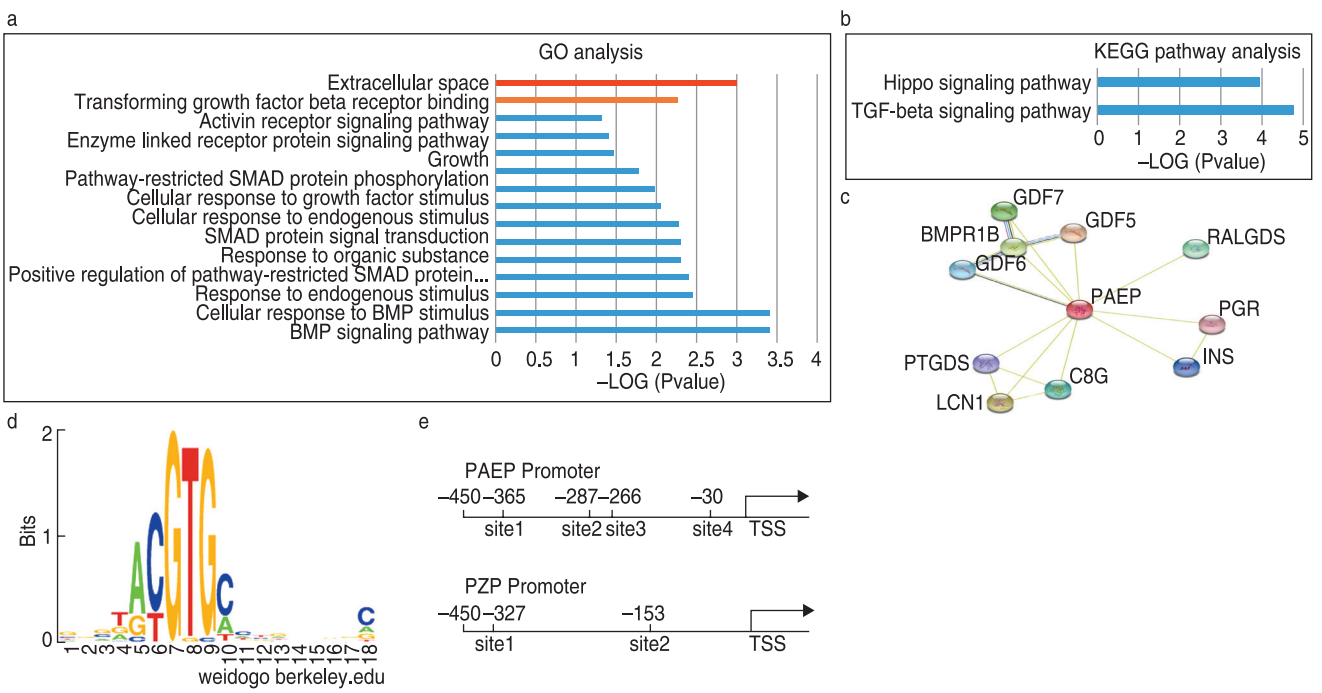

Fig. 3 HIF-2α binds to the ARE sequences of two putative genes identified in the four-gene signature and the KEGG, GO pathway prediction analysis, and PPI analysis of PAEP. (a–c). KEGG and GO pathway prediction analysis of PAEP, along with 10 hub genes. (d–e) Positions of in silico predicted HIF-2α binding sites (AREs) in the promoter regions of human PAEP and PZP

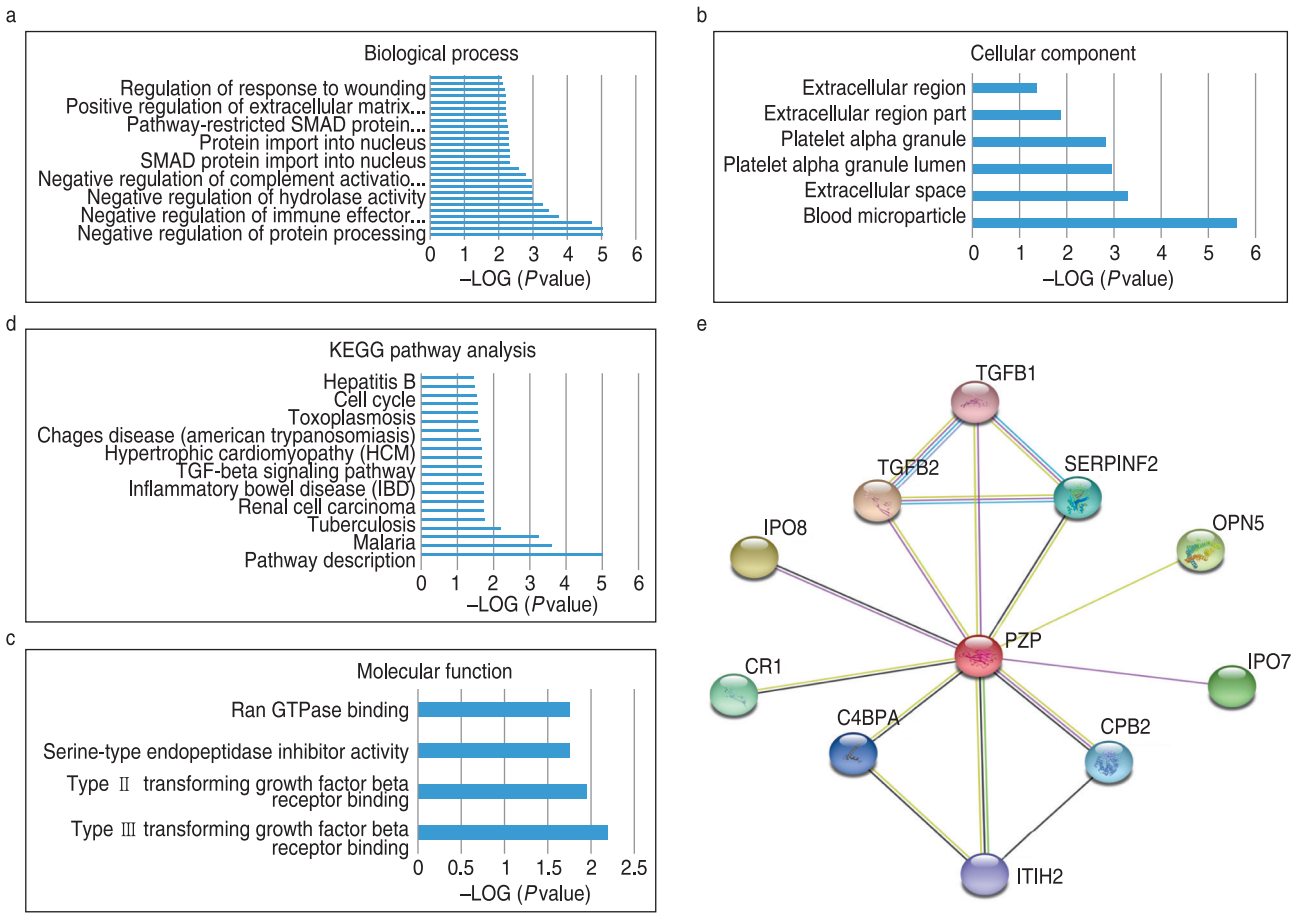

Fig. 4 KEGG, GO pathway prediction analysis, and PPI analysis of PZP. (a–c) GO Biological process, cellular component, and molecular function of PZP, along with its hub genes; (d) KEGG analysis for PZP and its hub genes; (e) Protein-protein interaction analysis for PZP and its hub genes

directly binds to the promoter regions of PAEP and PZP (Fig. 4d-e), which implies that HIF-2α affects the expression of PAEP and PZP by regulating their transcriptional levels. We then analyzed the functional annotation of PZP and the 10 hub genes from KEGG, GO pathway prediction analysis, and PPI analysis. The latter revealed that 10 hub genes were correlated with PZP (Fig. 3e). These genes are associated with 28 significant biological processes: negative regulation of cellular protein metabolic process, negative regulation of proteolysis, negative regulation of immune effector process, negative regulation of immune response, regulation of extracellular matrix organization, negative regulation of hydrolase activity, regulation of immunoglobulin-mediated immune response, negative regulation of macrophage cytokine production, negative regulation of complement activation, classical pathway, negative regulation of plasminogen activation, negative regulation of endopeptidase activity, SMAD protein import into the nucleus, negative regulation of fibrinolysis, platelet degranulation, protein import into the nucleus, protein targeting the nucleus, negative regulation of response to stimulus, pathway-restricted SMAD protein phosphorylation, regulation of catalytic activity, and regulation of response to stress (Fig. 3a). The TGF-β and Hippo signaling pathways were significantly enriched ($P < 0.05$) in the KEGG pathway analysis (Fig. 3d). By analyzing the PAEP using the same method, we found that PAEP, along with the 10 hub genes, highly enriched 13 significant biological processes: BMP signaling pathway, cellular response to BMP stimulus, response to endogenous stimulus, positive regulation of pathway-restricted SMAD protein phosphorylation, and response to organic substances (Fig. 4b–c), the TGF-β and Hippo signaling pathways were significantly enriched ($P < 0.01$) in the KEGG pathway analysis (Fig. 4a).

Discussion

At the transcriptional level, HIF-2α is a transcription factor that regulates the expression of other proteins. HIF-2α also interacts with proteins to execute different functions, which affects the progress and prognosis of various types of cancer. We have summarized that there are conflicting results in HCC xenograft tumor models.

He et al. found that downregulation of HIF-2α inhibits the growth of HCC tumors [47], and Sun et al. discovered that HIF-2α suppression does not affect HCC tumor growth, whereas HIF-2α overexpression reduces tumor growth [33]. GSEA revealed that HIF-2α was positively correlated with the TGF-β signaling pathway and ECM receptor interaction in patients with HCC. To further verify the mechanism of HIF-2α in HCC, we used the TCGA dataset to determine differences in the expression of DEGs between a missense mutation group and the corresponding wild-type group using cBioPortal (www.cBioPortal.org). We identified 19 overlapping upregulated genes by integrating the two datasets. Univariate and multivariate Cox regression analyses indicated that PAEP, PNLIPRP2, MIR147B, and PZP could predict the 5-year survival rate in patients with HCC. We used GEPIA to identify 100 genes with expression patterns similar to those of the four DEGs. After performing GO and KEGG pathway analyses with DAVID and STRING, we focused on biological processes, molecular functions, cellular components, and the pathways of PAEP and PZP in normal and tumor cells.

PAEP is a conflicting gene that affects the progression of various types of cancer. Overexpression of PAEP stimulates cell migration in human endometrial adenocarcinomas, and vascular endothelial growth factor mediates PAEP to facilitate neovascularization by increasing the migration and tube formation of human umbilical vein endothelial cells during embryogenesis and tumor development [48]. However, the overexpression of PAEP is correlated with differentiated epithelia and induces cell differentiation, which reduces the malignancy of cancer cells. Patients with high PAEP expression have worse survival times, which indicates that PAEP acts as a tumor gene in HCC. GO and KEGG pathway analyses, as well as PPI network analysis, revealed that PAEP interacts with 10 hub genes to increase the malignant characteristics of HCC cells and mediates the poor prognosis of patients with HCC by activating the TGF-β pathway. Taken together, the missense mutation of HIF2-α upregulated the expression of PAEP, which led to a worse prognosis in HCC.

The encoded protein of PZP is highly expressed in the late-pregnancy serum. It has been reported that the expression of PZP increases in the serum of individuals who later develop Alzheimer's disease (AD) [49]. In our study, we confirmed that the expression of PZP increased in HIF-2α missense-mutated samples compared with wild-type samples. Univariate Cox regression analyses revealed that PZP functions as a protective factor in HCC. Taken together, the missense mutation of HIF-2α upregulated PZP expression, which led to a better prognosis in HCC.

Taken together, we hypothesized that the missense mutation HIF-2α enhances the stabilization and activation of HIF-2α, which consequently upregulates the HIF-2α downstream genes PAEP and PZP, contributing to the conflicting roles of HIF-2α in HCC. HIF-2α is an endothelium-specific HIF-1α isoform with conflicting roles in various types of cancer. The mechanism of HIF-2α in tumor pathogenesis has not yet been elucidated, and further insight into the role of HIF-2α in cancer is required.

Acknowledgments

Not applicable.

Funding

This research did not receive any specific grants from funding agencies in the public, commercial, or not-for-profit sectors.

Conflicts of interest

The authors declared that they have no conflicts of interest.

Author contributions

Not applicable.

Data availability statement

All data generated or analyzed during this study are included in this published article (and its supplementary information files).

Ethical approval

Not applicable.

References

1. von Felden J, Schulze K, Gil-Ibanez I, et al. First- and Second-Line Targeted Systemic Therapy in Hepatocellular Carcinoma-An Update on Patient Selection and Response Evaluation. Diagnostics (Basel). 2016;6(4):44.
2. Tian H, McKnight SL, Russell DW. Endothelial PAS domain protein 1 (EPAS1), a transcription factor selectively expressed in endothelial cells. Genes Dev. 1997;11(1):72-82.
3. Zou JX, Chen K. Roles and molecular mechanisms of hypoxia-inducible factors in renal cell carcinoma. Hereditas (Beijing) (Chinese). 2018;40(5):341-356.
4. Forristal CE, Brown AL, Helwani FM, et al. Hypoxia inducible factor (HIF)-2α accelerates disease progression in mouse models of leukemia and lymphoma but is not a poor prognosis factor in human AML. Leukemia. 2015;29(10):2075-2085.
5. Yang Q, Guo X, Yang L. Metformin Enhances the Effect of Regorafenib and Inhibits Recurrence and Metastasis of Hepatic Carcinoma After Liver Resection via Regulating Expression of Hypoxia Inducible Factors 2α (HIF-2α) and 30 kDa HIV Tat-Interacting Protein (TIP30). Med Sci Monit. 2018;24:2225-2234.
6. Zhuang Z, Yang C, Ryska A, et al. HIF2A gain-of-function mutations detected in duodenal gangliocytic paraganglioma. Endocr Relat Cancer. 2016;23(5):L13-6.

7. Wiesener MS, Maxwell PH. HIF and oxygen sensing; as important to life as the air we breathe? Ann Med. 2003;35(3):183-190.
8. Du D, Liu C, Qin M, et al. Metabolic dysregulation and emerging therapeutical targets for hepatocellular carcinoma. Acta Pharm Sin B. 2022;12(2):558-580.
9. Fuhrmann DC, Brüne B. miR-193a-3p increases glycolysis under hypoxia by facilitating Akt phosphorylation and PFKFB3 activation in human macrophages. Cell Mol Life Sci. 2022;79(2):89.
10. Cheng L, Qin T, Ma J, et al. Hypoxia-inducible Factor-1α Mediates Hyperglycemia-induced Pancreatic Cancer Glycolysis. Anticancer Agents Med Chem. 2019;19(12):1503-1512.
11. Cui XG, Han ZT, He SH, et al. HIF1/2α mediates hypoxia-induced LDHA expression in human pancreatic cancer cells. Oncotarget. 2017;8(15):24840-24852.
12. Keith MP, Pitchford C, Bernstein WB. Treatment of hemophagocytic lymphohistiocytosis with alemtuzumab in systemic lupus erythematosus. J Clin Rheumatol. 2012;18(3):134-137.
13. Feng N, Chen H, Fu S, et al. HIF-1α and HIF-2α induced angiogenesis in gastrointestinal vascular malformation and reversed by thalidomide. Sci Rep. 2016;6:27280.
14. Shui YB, Wang X, Hu JS, et al. Vascular endothelial growth factor expression and signaling in the lens. Invest Ophthalmol Vis Sci. 2003;44(9):3911-3919.
15. Ryan HE, Lo J, Johnson RS. HIF-1 alpha is required for solid tumor formation and embryonic vascularization. EMBO J. 1998;17(11):3005-3015.
16. Nurse CA, Salman S, Scott AL. Hypoxia-regulated catecholamine secretion in chromaffin cells. Cell Tissue Res. 2018;372(2):433-441.
17. Påhlman S, Mohlin S. Hypoxia and hypoxia-inducible factors in neuroblastoma. Cell Tissue Res. 2018;372(2):269-275.
18. Chabi S, Uzan B, Naguibneva I, et al. Hypoxia Regulates Lymphoid Development of Human Hematopoietic Progenitors. Cell Rep. 2019;29(8):2307-2320.e6.
19. Schellinger IN, Cordasic N, Panesar J, et al. Hypoxia inducible factor stabilization improves defective ischemia-induced angiogenesis in a rodent model of chronic kidney disease. Kidney Int. 2017;91(3):616-627.
20. Lin TY, Chou CF, Chung HY, et al. Hypoxia-inducible factor 2 alpha is essential for hepatic outgrowth and functions via the regulation of leg1 transcription in the zebrafish embryo. PLoS One. 2014;9(7):e101980.
21. Wu XH, Qian C, Yuan K. Correlations of hypoxia-inducible factor-1α/hypoxia-inducible factor-2α expression with angiogenesis factors expression and prognosis in non-small cell lung cancer. Chin Med J (Engl). 2011;124(1):11-18.
22. Giatromanolaki A, Koukourakis MI, Sivridis E, et al. Relation of hypoxia inducible factor 1 alpha and 2 alpha in operable non-small cell lung cancer to angiogenic/molecular profile of tumours and survival. Br J Cancer. 2001;85(6):881-890.
23. Gao ZJ, Wang Y, Yuan WD, et al. HIF-2α not HIF-1α overexpression confers poor prognosis in non-small cell lung cancer. Tumour Biol. 2017;39(6):1010428317709637.
24. Luan Y, Gao C, Miao Y, et al. Clinicopathological and prognostic significance of HIF-1α and HIF-2α expression in small cell lung cancer. Pathol Res Pract. 2013;209(3):184-189.
25. Helczynska K, Larsson AM, Holmquist Mengelbier L, et al. Hypoxia-inducible factor-2alpha correlates to distant recurrence and poor outcome in invasive breast cancer. Cancer Res. 2008;68(22):9212-20.
26. Wang W, He YF, Sun QK, et al. Hypoxia-inducible factor 1α in breast cancer prognosis. Clin Chim Acta. 2014;428:32-37.
27. Griffiths EA, Pritchard SA, McGrath SM, et al. Hypoxia-associated markers in gastric carcinogenesis and HIF-2alpha in gastric and gastro-oesophageal cancer prognosis. Br J Cancer. 2008;11;98(5):965-973.
28. Tong WW, Tong GH, Chen XX, et al. HIF2α is associated with poor prognosis and affects the expression levels of survivin and cyclin D1 in gastric carcinoma. Int J Oncol. 2015;46(1):233-242.
29. Li N, Wang HX, Qin C, et al. Relationship between clinicopathological features and HIF-2α in gastric adenocarcinoma. Genet Mol Res. 2015;14(1):1404-1413.
30. Zhang Q, Lou Y, Zhang J, et al. Hypoxia-inducible factor-2α promotes tumor progression and has crosstalk with Wnt/β-catenin signaling in pancreatic cancer. Mol Cancer. 2017;16(1):119.
31. Wang M, Chen MY, Guo XJ, et al. Expression and significance of HIF-1α and HIF-2α in pancreatic cancer. J Huazhong Univ Sci Technolog Med Sci. 2015;35(6):874-879.
32. Bangoura G, Liu ZS, Qian Q, et al. Prognostic significance of HIF-2alpha/EPAS1 expression in hepatocellular carcinoma. World J Gastroenterol. 2007;13(23):3176-3182.
33. Sun HX, Xu Y, Yang XR, et al. Hypoxia inducible factor 2 alpha inhibits hepatocellular carcinoma growth through the transcription factor dimerization partner 3/ E2F transcription factor 1-dependent apoptotic pathway. Hepatology. 2013;57(3):1088-1097.
34. Yang SL, Liu LP, Niu L, et al. Downregulation and pro-apoptotic effect of hypoxia-inducible factor 2 alpha in hepatocellular carcinoma. Oncotarget. 2016;7(23):34571-34581.
35. Jiang L, Liu QL, Liang QL, et al. Association of PHD3 and HIF2α gene expression with clinicopathological characteristics in human hepatocellular carcinoma. Oncol Lett. 2018;15(1):545-551.
36. Nanni S, Benvenuti V, Grasselli A, et al. Endothelial NOS, estrogen receptor beta, and HIFs cooperate in the activation of a prognostic transcriptional pattern in aggressive human prostate cancer. J Clin Invest. 2009;119(5):1093-1108.
37. Osada R, Horiuchi A, Kikuchi N, et al. Expression of hypoxia-inducible factor 1alpha, hypoxia-inducible factor 2alpha, and von Hippel-Lindau protein in epithelial ovarian neoplasms and allelic loss of von Hippel-Lindau gene: nuclear expression of hypoxia-inducible factor 1alpha is an independent prognostic factor in ovarian carcinoma. Hum Pathol. 2007;38(9):1310-1320.
38. Winter SC, Shah KA, Han C, et al. The relation between hypoxia-inducible factor (HIF)-1alpha and HIF-2alpha expression with anemia and outcome in surgically treated head and neck cancer. Cancer. 2006;107(4):757-766.
39. Sivridis E, Giatromanolaki A, Gatter KC, et al; Tumor and Angiogenesis Research Group. Association of hypoxia-inducible factors 1alpha and 2alpha with activated angiogenic pathways and prognosis in patients with endometrial carcinoma. Cancer. 2002;95(5):1055-1063.
40. Kim H, Shim BY, Lee SJ, et al. Loss of Von Hippel-Lindau (VHL) Tumor Suppressor Gene Function: VHL-HIF Pathway and Advances in Treatments for Metastatic Renal Cell Carcinoma (RCC). Int J Mol Sci. 2021;22(18):9795.
41. Lim E, Kuo CC, Tu HF, et al. The prognosis outcome of oral squamous cell carcinoma using HIF-2α. J Chin Med Assoc. 2017;80(10):651-656.
42. Mazumdar J, Hickey MM, Pant DK, et al. HIF-2alpha deletion promotes Kras-driven lung tumor development. Proc Natl Acad Sci U S A. 2010;107(32):14182-14187.
43. Krop I, März A, Carlsson H, et al. A putative role for psoriasin in breast tumor progression. Cancer Res. 2005;65(24):11326-11334.
44. Kim J, Bagchi IC, Bagchi MK. Signaling by hypoxia-inducible factors is critical for ovulation in mice. Endocrinology. 2009;150(7):3392-

3400.
45. Choudhry H, Albukhari A, Morotti M, et al. Tumor hypoxia induces nuclear paraspeckle formation through HIF-2α dependent transcriptional activation of NEAT1 leading to cancer cell survival. Oncogene. 2015;34(34):4482-4490.
46. Ma X, Zhang H, Xue X, et al. Hypoxia-inducible factor 2α (HIF-2α) promotes colon cancer growth by potentiating Yes-associated protein 1 (YAP1) activity. J Biol Chem. 2017;292(41):17046-17056.
47. He C, Sun XP, Qiao H, et al. Downregulating hypoxia-inducible factor-2α improves the efficacy of doxorubicin in the treatment of hepatocellular carcinoma. Cancer Sci. 2012;103(3):528-534.
48. Weber R, Meister M, Muley T, et al. Pathways regulating the expression of the immunomodulatory protein glycodelin in non-small cell lung cancer. Int J Oncol. 2019;54(2):515-526.
49. Lake F. Serum proteome analyzed to reveal increased levels of PZP in Alzheimer's patients. Expert Rev Proteomics. 2011;8(6):686.

DOI 10.1007/s10330-022-0598-8
Cite this article as: Li J, Yan YB, Wang GX, et al. Hypoxia-inducible factor-2α and its missense mutations: potential role in HCC diagnosis, progression, and prognosis and underlying mechanism. Oncol Transl Med. 2022;8(6): 267-275.

Oncology and Translational Medicine
DOI 10.1007/s10330-022-0593-3

December 2022, Vol. 8, No. 6, P276–P284

ORIGINAL ARTICLE

Construction and validation of a prognostic risk model for uterine corpus endometrial carcinoma based on alternative splicing events*

Yi Cheng, Long Li, Chen Gong, Kai Qin (✉)

Department of Oncology, Tongji Hospital, Tongji Medical College, Huazhong University of Science and Technology, Wuhan 430030, China

Abstract

Objective To establish a prognostic risk model for uterine corpus endometrial carcinoma (UCEC) based on alternative splicing (AS) event data from The Cancer Genome Atlas (TCGA) and assess the accuracy of the model.

Methods TCGA and SpliceSeq databases were used to acquire a summary of AS events and clinical data related to UCEC. Bioinformatic analysis was performed to identify differentially expressed AS events in UCEC. Least absolute shrinkage and selection operator (LASSO) regression and multivariate Cox regression analyses were used for constructing a prognostic risk model. Next, using the receiver operating characteristic (ROC) curve, Kaplan-Meier survival analysis, and independent prognostic analysis, we assessed the accuracy of the model. In addition, a splicing network was established based on the association between potential splicing factors and AS events.

Results We downloaded clinical data and AS events of 527 UCEC cases from TCGA and SpliceSeq databases, respectively. We obtained 18,779 survival-associated AS events in UCEC using univariate Cox regression analysis and 487 AS events using LASSO regression analysis. Multivariate Cox regression analysis established a prognostic risk model for UCEC based on the percentage splicing value of 13 AS events. Independent prognostic effect on UCEC risk was then assessed using multivariate and univariate Cox regression analyses ($P < 0.001$). The area under the curve was 0.827. The pathological stage and risk score were independent prognostic factors for UCEC. Herein, we established a regulatory network between alternative endometrial cancer-related splicing events and splicing factors.

Conclusion We constructed a prognostic model of UCEC based on 13 AS events by analyzing datasets from TCGA and SpliceSeq databases with medium accuracy. The pathological stage and risk score were independent prognostic factors in the prognostic risk model.

Received: 7 August 2022
Revised: 21 September 2022
Accepted: 12 October 2022

Key words: TCGA; SpliceSeq; uterine corpus endometrial carcinoma; alternative splicing event; prognostic model

Uterine corpus endometrial carcinoma (UCEC) is a major malignancy affecting the female reproductive system. UCEC is the second most common cancer of the genital system in China [1]. Given the aging population in China, the incidence and mortality of endometrial cancer are gradually increasing. However, the 5-year survival rate of recurrent/metastatic endometrial cancer is currently 10%–20% [2]. The Cancer Genome Atlas research project (TCGA) aims to classify endometrial cancer into four subtypes by applying high-throughput genome analysis technology and comprehensive analysis: polymerase epsilon (POLE) ultramutated, microsatellite unstable, copy number low/microsatellite stable, and copy number high/'serous-like' [3]. The World Health Organization classification of female genital tumors in 2020 refers to the ProMisE molecular classification. The main obstacle to the application of this method is the need for diverse high-tech cooperation, which is difficult to implement

✉ Correspondence to: Kai Qin. Email: qinkaitj@126.com
* Supported by a grant from the Natural Science Foundation of Hubei Province (No. 2020CFB592).

and popularize in clinical settings [4]. Therefore, there is an urgent need to identify novel biomarkers to predict the prognosis of endometrial cancer and guide precise treatment.

Alternative splicing (AS) refers to the organization of exons from original gene transcripts (pre-mRNAs) in different ways to generate structurally and functionally distinct mRNA and protein variants. The concept of AS was first derived from the "split gene" discovered by Philip Sharp and Richard Roberts in 1977 [5]. AS and its regulation are crucial for exploring cancer. Simultaneously, the regulation of AS constitutes a hallmark of cancer [6]. More than 8,000 tumor samples from 32 different types of cancers analyzed by Kahles et al. revealed that there exist thousands of AS variants when compared with non-malignant tissues [7]. These splicing variants may provide cancer-specific markers and new antigens, which are potentially critical for cancer treatment. With the development of genome sequencing, growing evidence suggests that AS events are crucial for the prognosis of multiple malignancies [8]. Herein, we constructed a prognostic risk model of endometrial cancer by integrating the AS data in the TCGA SpliceSeq database and clinical data from the TCGA database and verified its efficacy.

Materials and methods

Data collection of alternative splicing events and data processing

We downloaded the transcript profiles (https://portal.gdc.cancer.gov/) from the TCGA data portal of the UCEC cohort on August 22, 2021. In addition, we collected AS event data from TCGA SpliceSeq (https://bioinformatics.mdanderson.org/TCGASpliceSeq/). The percentage splicing (PSI) value, typically used to quantify AS events, was calculated for each AS event. AS events included 35 non-tumor samples and 527 UCEC samples, and mRNA sequencing profiles included 23 non-tumor samples and 552 UCEC samples. Additionally, we downloaded the complete clinical data of 548 UCEC samples (including sex, age, survival status, and overall survival time), as shown in Table 1.

Table 1 Clinical characteristics of uterine corpus endometrial carcinoma

Clinical characteristics	Patients	
	n	%
Age (years)		
≤ 60	181	33
> 60	364	66.4
Unknow	3	0.6
Grade		
G1	99	18.1
G2	122	22.3
G3	316	57.7
High grade	11	1.9
Survival status		
Alive	467	85.2
Dead	81	14.8
Survival time (months)		
< 90	42	7.7
≥ 90	505	92.1
Unknown	1	0.2

Screening for prognostic AS events of UCEC

There are seven types of AS events: mutually exclusive exons (MEs), alternate donor sites (ADs), retained introns (RIs), alternate acceptor sites (AAs), alternate promoters (APs), alternate terminators (ATs), and exon skipping (ES). In total, 28,281 AS events in patients with endometrial cancer are shown in the UpSet plots. The most frequent types of AS events were AT, ES, AT& ES, AP, and ES & AP events (Fig. 1a). The PSI values of AS events in patients with endometrial cancer were supplemented by the Knn function in the R language impute package, subsequently combined with the survival time and survival status of patients. Univariate Cox regression analysis was used to screen for prognostic AS events in endometrial cancer. The screening threshold was set to $P < 0.05$, and the prognostic AS events are shown in UpSet (Fig. 1b), Volcano (Fig. 2a), and Bubble (Fig. 2b–2h).

Establishment of the prognostic model related to AS events of UCEC

Least absolute shrinkage and selection operator (LASSO) regression analysis was used to screen survival-associated AS events of endometrial cancer to construct a prognostic model that prevents overfitting of the model and improves accuracy. Next, the risk score of each UCEC was calculated and divided into high- or low-risk groups based on the median risk score. Subsequently, the screened AS events were analyzed using multivariate Cox regression analysis to construct a prognostic risk model for UCEC. The formula was as follows: Risk score = $\beta_{gene1} \times expr_{gene1} + \beta_{gene2} \times Expr_{gene2} + \cdots + \beta_{genen} \times Expr_{genen}$. A $P < 0.05$ was considered statistically significant, and the PSI value of AS was indicated by $Expr_{genen}$.

Evaluation of prognostic models

To assess the predictive ability of this prognostic model, receiver operating characteristic (ROC) curves and Kaplan–Meier curve survival analysis were performed. In addition, heatmaps, risk scores, and scatter plots of survival-associated AS events were plotted according to the ranking of risk scores. The clinical characteristics of UCEC were analyzed using univariate and multivariate Cox regression analyses ($P < 0.05$).

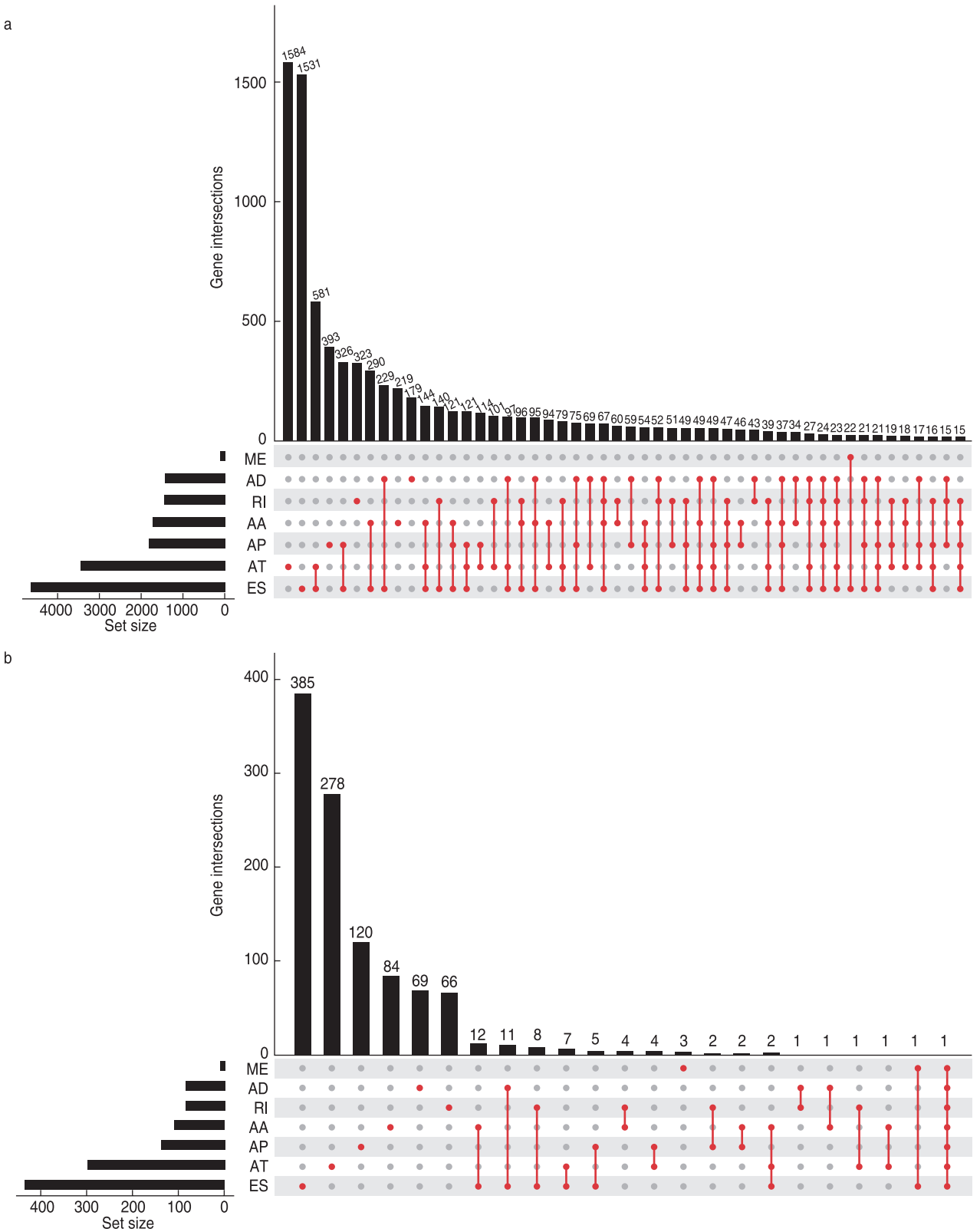

Fig. 1 The UpSet plot shows the distribution of seven types of prognostic AS events in uterine corpus endometrial carcinoma. (a) The distributions of seven different types of AS-related genes in uterine corpus endometrial carcinoma; (b) Distribution of seven AS events that significantly correlate with overall survival. AS, alternative splicing; ME, mutually exclusive exons; AD, alternate donor site; RI, retained intron; AA, alternate acceptor; AP, alternate promoter; AT, alternate terminator; ES, exon skipping

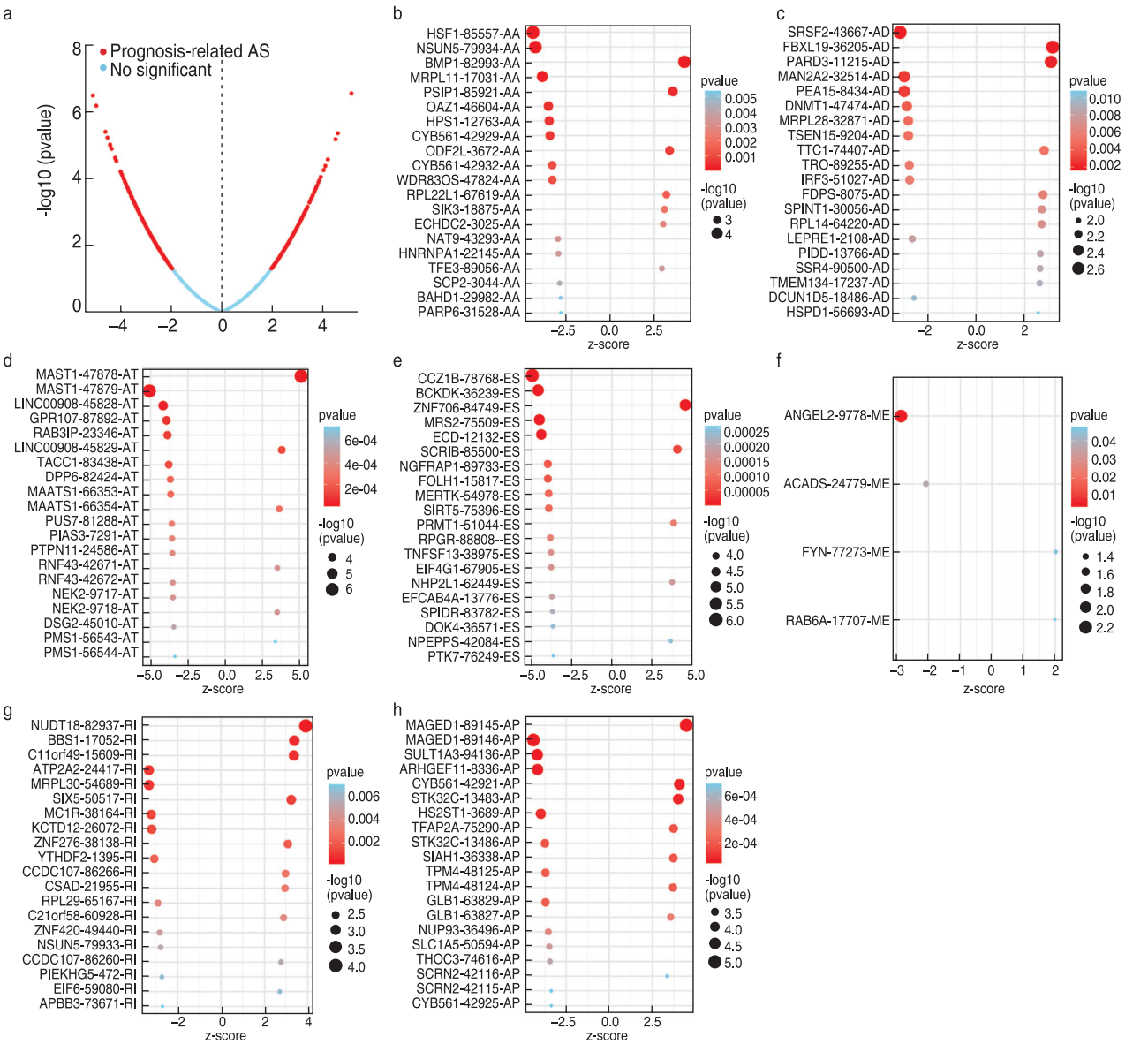

Fig. 2 Prognostic AS events in uterine corpus endometrial carcinoma. (a) Volcano plots of prognostic AS events; (b–h) Forest plots: hazard ratios of the top 20 overall survival-associated AA, AD, AT, ES, ME, RI and AP events. *P* values are indicated by the color scale on the right side. AA, alternate acceptor; AD, alternate donor site; AP, alternate promoter; AS, alternative splicing; AT, alternate terminator; ES, exon skipping; ME, mutually exclusive exons; RI, retained intron

Construction of splicing regulatory network

To better explore the biological processes and pathways of AS-related genes, Cytoscape (version 3.7.2) was used to construct and visualize the regulatory network between survival-related AS events and splicing factors (SFs).

Statistical analysis

Statistical analyses were performed using R version 4.1.1 (R packages: UpSetR, BiocManager, Survival, ggplot, ggplot2, glmnet, Survminer, Survival ROC, estimate, Vioplot, pheatmap, and forestplot). For all analyses, a two-tailed $P < 0.05$ was deemed statistically significant.

Results

Overview of prognostic AS events in UCEC

A total of 2630 prognostic AS events of endometrial cancer were screened using univariate Cox regression analysis ($P < 0.05$), among which ES, AT, AP, AA, and AD events exhibited a higher frequency (Fig. 1b). In addition, prognostic AS events are shown in volcano plots, with the red dots representing prognostic AS (Fig. 2a). Seven types of AS events were most prominently displayed in the forest plots (Fig. 2b–2h). These are indicated by the gene-AS number-AS event type. The size of dots indicates –

log10 (*P* value) using univariate Cox regression analysis, and the color of dots indicates the *P* value (Fig. 1d).

Establishment of a prognostic prediction model for UCEC

On reducing the number of AS events to 18, as indicated by the LASSO regression analysis, the lambda error value of the prognostic model had the minimum error and highest accuracy (Fig. 3a). The coefficients of each PSI value were calculated using the LASSO regression analysis (Table 2).

Evaluation of the prognostic model of UCEC

The overall survival time of the low-risk group was remarkably longer than that of the high-risk group, as determined using the Kaplan–Meier curve analysis (P = 2.148E-11, Fig. 3d). The area under the ROC curve for this score was 0.827 (Fig. 3c). The heatmap, risk score, and scatter plots of prognostic AS events in UCEC indicated that the higher the risk score, the shorter the survival time and greater the number of deaths (Fig. 4a–4c). According to the results of the heatmap, the frequency of 13 AS events, including MAST1|47879|AT, increased the risk score, indicating that all 13 AS events were high-risk AS events (Fig. 4a). Univariate and multivariate Cox regression analyses revealed that the risk score of the prognostic model could be used as a prognostic biomarker (P < 0.001) (Table 3). Tumor grade could be employed as an independent prognostic factor (Table 3).

Network analysis of prognostic AS and SFs

To elucidate the potential mechanism of AS regulation, we constructed a correlation network between the expression level of SFs and the PSI value of prognostic AS events. Two high-risk AS events (red ellipse), four low-risk AS events (green ellipse), and six SFs were identified (purple triangle) (Fig. 5). In our regulatory network, the first four most important nodes were termed central SFs or AS events, including two downregulated AS events (HNRNPA1-22149-ES and TIMM13-46608-AD). Therefore, these key AS factors are involved in the dysregulation of AS in endometrial cancer and further

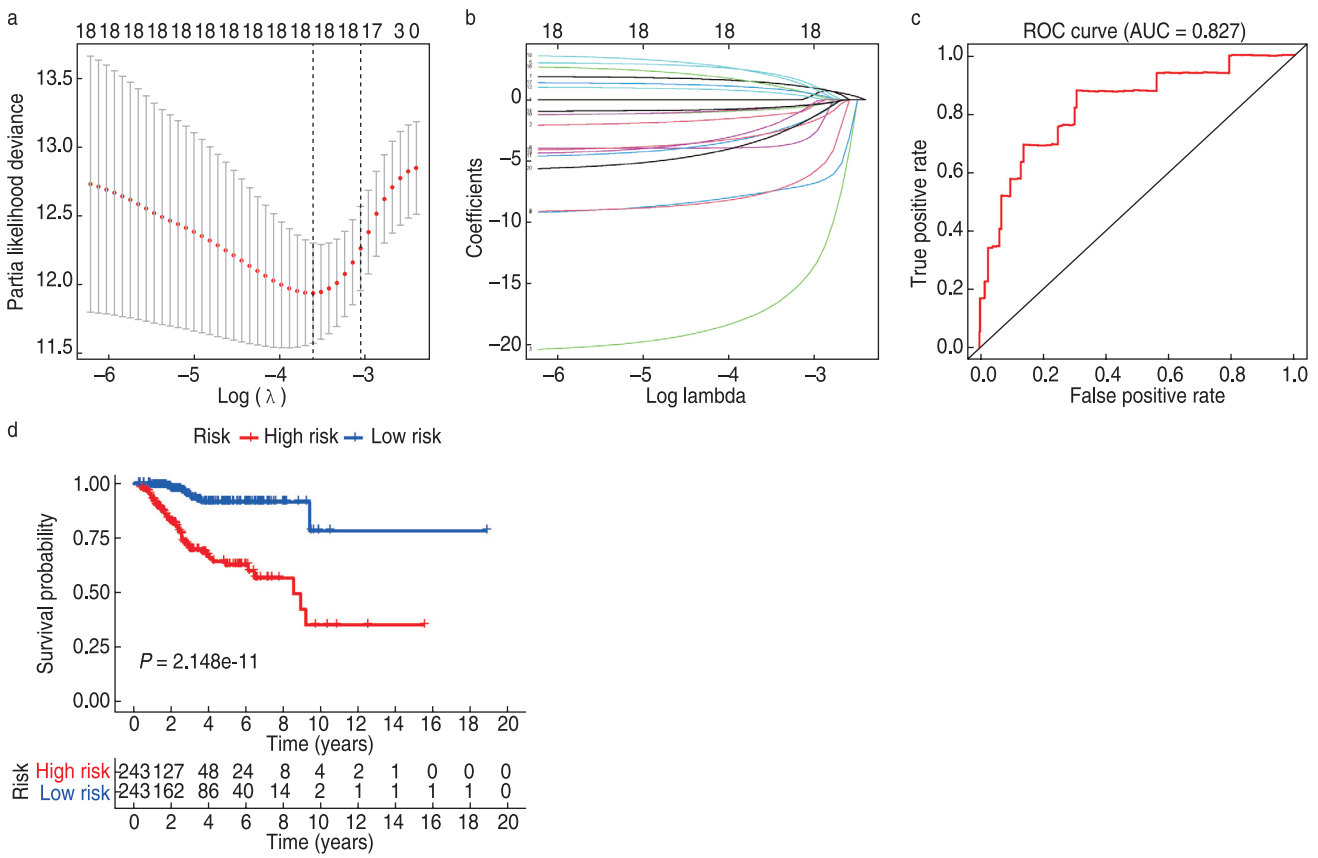

Fig. 3 Confirmation of 13 survival-associated AS event-based prognostic signatures. (a) LASSO coefficient profiles of all AS events; (b) Ten-time cross-validation for tuning parameter selection in the LASSO regression; (c) ROC analysis of risk scores for overall survival prediction. The AUC was calculated for ROC curves, and sensitivity and specificity were calculated to assess score performance; (d) Kaplan–Meier curve of the risk score model based on the characteristic 13 AS events. AS, alternative splicing; AUC, area under the curve; ROC, receiver operating characteristic

Table 2 Survival-associated AS events in uterine corpus endometrial carcinoma identified by multivariate Cox regression analysis

Survival-associated AS events	Coef	HR (95%CI)	*P* value
MAST1|47879|AT	−1.875	0.0153 (0.051–0.464)	0.001
CCZ1B|78768|ES	−21.536	4.43E-10 (2.06E-16–0.001)	0.004
ZNF706|84749|ES	3.660	38.869 (1.155–1307.78)	0.041
MAGED1|89145|AP	2.138	8.483 (0.527–136.567)	0.132
ECD|12132|ES	−15.883	1.27E-07 (1.02E-12–0.016)	0.008
NSUN5|79934|AA	−5.959	0.003 (0.000–0.061)	< 0.001
SULT1A3|94136|AP	−1.460	0.232 (0.050–1.078)	0.062
ARHGEF11|8336|AP	−4.486	0.011 (0.001–0.150)	0.001
CYB561|42921|AP	3.073	21.616 (3.505–133.292)	0.001
SCRIB|85500|ES	1.521	4.579 (0.770–27.235)	0.094
STK32C|13483|AP	4.028	56.151 (6.000–525.480)	< 0.001
NGFRAP1|89733|ES	−7.963	0.0003 (2.31E-07–0.525)	0.033
FOLH1|15817|ES	−5.876	0.003 (0.000–0.037)	8.05E-06

AS, alternative splicing; HR, hazard ratio; coef, coefficient

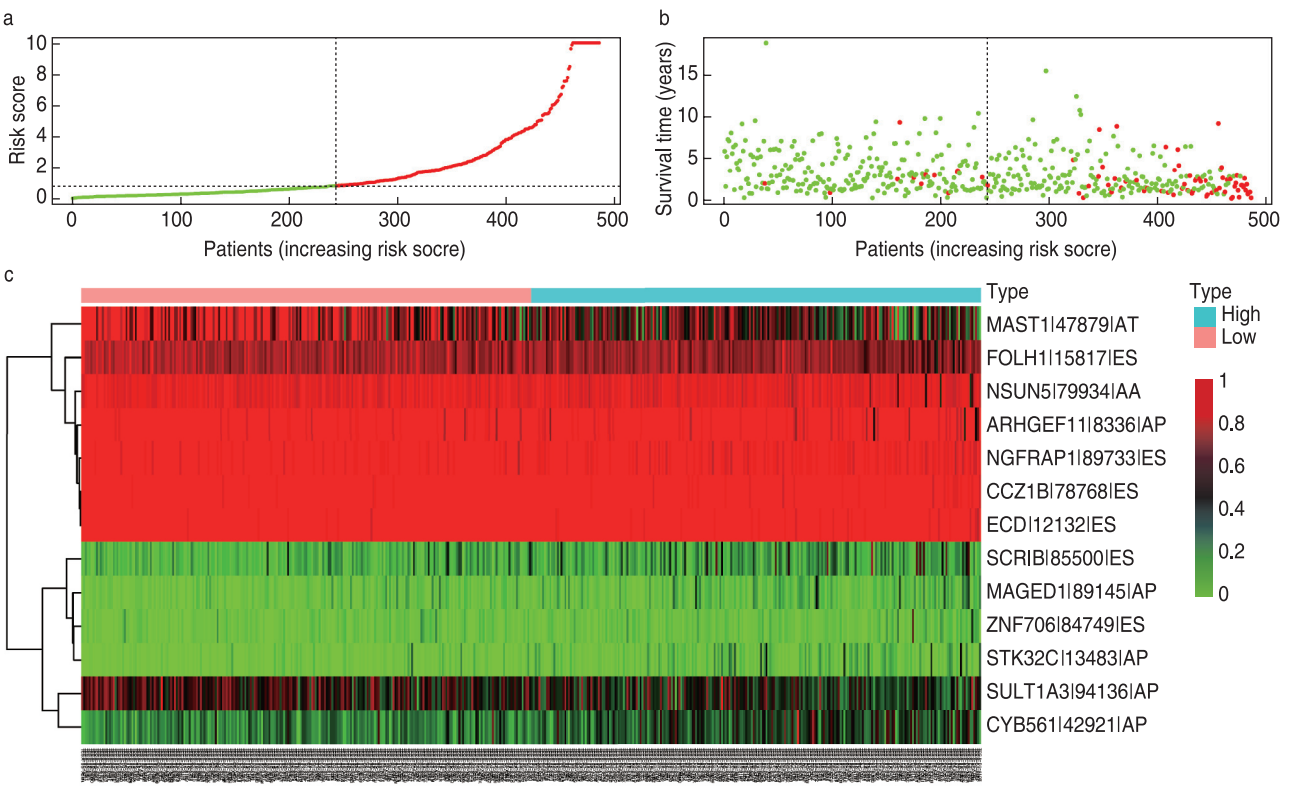

Fig. 4 a–c: Risk score, scatter plots, and heatmap of prognostic AS events in uterine corpus endometrial carcinoma. AS, alternative splicing

mediate cancer occurrence and development.

Discussion

As one of the most common malignant reproductive tumors in females, UCEC has a high incidence worldwide, and the prognosis of patients with advanced disease remains poor [1, 2]. Given the complex molecular mechanisms, such as genomic complexity and epigenetic diversity, endometrial cancer is highly heterogeneous from clinical and molecular perspectives. Moreover, it can be challenging to implement and popularize the prognostic risk model of endometrial cancer predicted by ProMisE and TCGA, owing to technical reasons [3, 4, 9]. Therefore, there is an urgent need to develop a powerful tool for predicting the prognosis of endometrial

Table 3 Univariate and multivariate Cox regression analyses of clinical characteristics in uterine corpus endometrial carcinoma

Clinical characteristic	Univariate Cox regression		Multivariate Cox regression	
	HR (95%CI)	*P* value	HR (95%CI)	*P* value
Age	1.032 (1.008–1.056)	0.008	1.011 (0.987–1.036)	0.364
Grade	2.501 (1.602–3.904)	5.50E-05	2.557 (1.584–4.128)	< 0.001
Risk score	1.070 (1.057–1.083)	1.56E-27	1.071 (1.056–1.086)	3.35E-22

CI, confidence interval; HR, hazard ratio

carcinoma and providing new insights for individualized treatment strategies.

A growing body of research has provided strong evidence indicating the role of AS (post-transcriptional modification process) in the physiological and pathological processes of malignant tumors [8]. Abnormal AS events play an important role in the occurrence and development of endometrial carcinoma [10, 11].

To identify prognostic AS events of UCEC, we obtained 527 AS events of endometrial cancers from TCGA SpliceSeq and clinical data from TCGA database. LASSO Cox regression and univariate/multivariate Cox regression were used for constructing a prognostic risk model based on the 13 AS events. The 13 AS events were MAST1|47879|AT, CCZ1B|78768|ES, ZNF706|84749|ES, MAGED1|89145|AP, ECD|12132|ES, NSUN5|79934|AA and SULT1A3|944. AP, SCRIB|85500|ES, STK32C|13483|AP, NGFRAP1|89733|ES, and FOLH1|15817|ES. Folic acid hydrolase-1 (FOLH1) is a type II transmembrane protein expressed in the lumen of the new vascular system in solid tumors. FOLH1 is widely expressed in the neovascularization of primary and metastatic Merkel cell carcinoma, and the monoclonal antibody J591 can be used for brachytherapy based on the FOLH1 monoclonal antibody in Merkel cell carcinoma [12]. The neurotransmitter N-acetylaspartyl glutamate (NAAG) is a selective endogenous agonist of the metabotropic glutamate receptor 3. Increasing NAAG levels may improve cognition. Glutamate carboxypeptidase II (GCP II) is encoded by the folate hydrolase 1 (*FOLH1*) gene, which regulates synaptic NAAG levels. Increasing the level of NAAG by inhibiting FOLH1/GCPII could improve cognition [13]. In the present study, we found that low expression of FOLH1 was related to poor prognosis in endometrial carcinoma. The B-module protein is a conserved regulator of cell polarity. Originally identified as a tumor suppressor in *Drosophila melanogaster*, the destruction of the Scrib protein can lead to tumorigenesis in mammals and is associated with human cancers (ovarian cancer, gastric cancer, and colorectal cancer) [14–17]. Scrib plays a key role in the establishment of cell polarity during migration [18]. STK32C, a member of the AGC superfamily serine/threonine protein kinase, was found to be highly

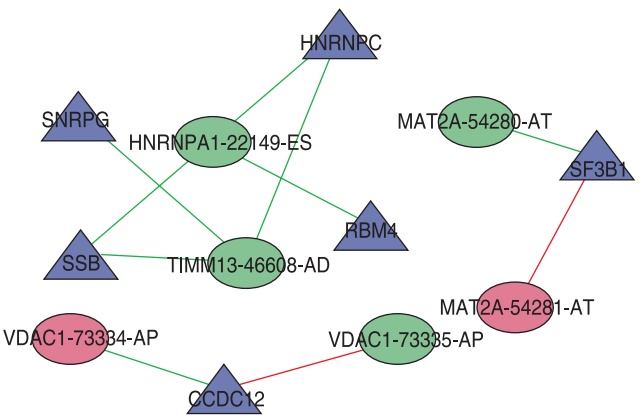

Fig. 5 Gene interaction networks between alternative splicing (AS) factors and prognostic AS events. Purple triangle: spliced factors, green ellipse: low-risk AS events, red ellipse: high-risk AS events, green line: a negative correlation, red line: a positive correlation

expressed in brain tissue. Erlsun et al. have shown that high STK32C protein expression in tumor tissues was significantly related to poor clinicopathological features and short-term recurrence-free survival rate in patients with bladder cancer [19]. STK32C inhibits tumor cell migration, proliferation, and invasion *in vitro* Cytochrome B561 (CYB561) is a conserved transmembrane transport protein with chelating reductase activity that specifically acts on secretory vesicles of neuroendocrine substances (catecholamine and neuropeptide). It is widely expressed in human tissues and promotes the growth and metastasis of castrated neuroendocrine prostate cancer cells. The low expression level of CYB561 mRNA in ovarian cancer has been associated with poor prognosis and may serve as a prognostic biomarker. Zhou *et al.* have reported that CYB561 can be used as a prognostic biomarker for breast cancer [20]. Rho guanine nucleotide exchange factor 11 (ARHGEF11) has been shown to promote tumor metastasis in glioblastoma and ovarian cancer. Du et al. have found that ARHGEF11 can promote the proliferation and metastasis of liver cancer by activating the β-catenin pathway and that ARHGEF11 may be a potential prognostic biomarker of liver cancer [21]. NSUN5 encodes cytosine-5 RNA methyltransferase. Jiang et al. have determined that NSUN5 is a promoter of colorectal

development mediated via cell cycle regulation [22]. Melanoma antigen D1 (MAGED1) is a member of the type II melanoma antibody (MAGE) family. Downregulation of MAGED1 expression has been documented in glioma stem cells and breast cancer cell lines and may play a critical role in cancer and apoptosis. Zeng et al. have reported a correlation between the expression of melanoma antigen D1 in colorectal cancer and prognosis [23]. Microtubule-related serine/threonine kinase 1 (MAST1) is the main driver of cisplatin resistance in human cancer. Mechanistically, cisplatin inhibits the mitogen-activated protein kinase (MAPK) pathway by separating cRaf from MEK1, whereas MAST1 replaces cRaf to reactivate the MAPK pathway in a cRaf-independent manner [24].

According to the prognostic risk model constructed based on AS events of these 13 genes, the AUC of the ROC curve was 0.827, indicating that the model presented medium accuracy. However, this study has some limitations: (1) Data were from a single database, the sample size was relatively small, and a single ethnicity was evaluated. In the future, this needs to be verified in a larger sample population, using multicenter and multi-region populations. (2) The clinical information from the TCGA database is incomplete, and some information, such as tumor stage, was lacking. (3) Currently, few studies are available on the parental genes of AS, and their function in endometrial cancer remains unclear. Additional basic research is needed to further explore the mechanisms underlying these AS events.

In conclusion, we identified 13 AS events based on data from TCGA and TCGA SpliceSeq databases and established a prognostic risk model with moderate predictive accuracy. Furthermore, we identified risk score and tumor grade as independent prognostic factors for UCEC.

Acknowledgments
Not applicable.

Funding
Supported by a grant from the Natural Science Foundation of Hubei Province (No. 2020CFB592).

Conflicts of interest
The authors indicated no potential conflicts of interest.

Author contributions
Kai Qin conceived and designed the experiments and revised the manuscript; Yi Cheng, Long Li and Chen Gong analyzed the data; Yi Cheng drafted the manuscript. All authors have read and approved the final manuscript.

Data availability statement
Not applicable.

Ethical approval
Not applicable.

References

1. Xia C, Dong X, Li H, et al. Cancer statistics in China and United States, 2022: profiles, trends, and determinants. Chin Med J (Engl). 2022;135(5):584-590.
2. Morice P, Leary A, Creutzberg C, et al. Endometrial cancer. Lancet. 2016;387(10023):1094-1108.
3. Cancer Genome Atlas Research Network, Kandoth C, Schultz N, et al. Integrated genomic characterization of endometrial carcinoma. Nature. 2013;497(7447):67-73.
4. Kommoss S, McConechy MK, Kommoss F, et al. Final validation of the ProMisE molecular classifier for endometrial carcinoma in a large population-based case series. Ann Oncol. 2018;29(5):1180-1188.
5. Chow LT, Gelinas RE, Broker TR, et al. An amazing sequence arrangement at the 5' ends of adenovirus 2 messenger RNA. Cell. 1977;12(1):1-8.
6. Ladomery M. Aberrant alternative splicing is another hallmark of cancer. Int J Cell Biol. 2013;2013:463786.
7. Jin H, Wang C, Jin G, et al. Regulator of calcineurin 1 gene isoform 4, down-regulated in hepatocellular carcinoma, prevents proliferation, migration, and invasive activity of cancer cells and metastasis of orthotopic tumors by inhibiting nuclear translocation of NFAT1. Gastroenterology. 2017;153(3):799-811.e33.
8. Bessa C, Matos P, Jordan P, et al. Alternative splicing: expanding the landscape of cancer biomarkers and therapeutics. Int J Mol Sci. 2020;21(23):9032.
9. Marín-Jiménez JA, García-Mulero S, Matías-Guiu X, et al. Facts and hopes in immunotherapy of endometrial cancer. Clin Cancer Res. 2022:clincanres.1564.2022.
10. Konno R, Takano T, Sato S, et al. Serum soluble fas level as a prognostic factor in patients with gynecological malignancies. Clin Cancer Res. 2000;6(9):3576-3580.
11. Sun D, Zhang A, Gao B, et al. Identification of alternative splicing-related genes CYB561 and FOLH1 in the tumor-immune microenvironment for endometrial cancer based on TCGA data analysis. Front Genet. 2022;13:770569.
12. Ramirez-Fort MK, Meier-Schiesser B, Lachance K, et al. Folate hydrolase-1 (FOLH1) is a novel target for antibody-based brachytherapy in Merkel cell carcinoma. Skin Health Dis. 2021;1(1):e9.
13. Zink CF, Barker PB, Sawa A, et a. Association of missense mutation in FOLH1 with decreased NAAG levels and impaired working memory circuitry and cognition. Am J Psychiatry. 2020;177(12):1129-1139.
14. Nakajima YI. Scrib module proteins: Control of epithelial architecture and planar spindle orientation. Int J Biochem Cell Biol, 2021. 136: 106001.
15. Shen H, Huang C, Wu J, et al. SCRIB promotes proliferation and metastasis by targeting Hippo/YAP signalling in colorectal cancer. Front Cell Dev Biol. 2021;9:656359.
16. Hussein UK, Ha SH, Ahmed AG, et al. FAM83H and SCRIB stabilize β-catenin and stimulate progression of gastric carcinoma. Aging (Albany NY). 2020;12(12):11812-11834.
17. Hussein UK, Ahmed AG, Choi WK, et al. SCRIB is involved in the progression of ovarian carcinomas in association with the factors linked to epithelial-to-mesenchymal transition and predicts shorter survival of diagnosed patients. Biomolecules. 2021;11(3):405.
18. Osmani N, Vitale N, Borg JP, et al. Scrib controls Cdc42 localization

and activity to promote cell polarization during astrocyte migration. Curr Biol. 2006;16(24):2395-2405.
19. Sun E, Liu K, Zhao K, et al. Serine/threonine kinase 32C is overexpressed in bladder cancer and contributes to tumor progression. Cancer Biol Ther. 2019;20(3):307-320.
20. Zhou X, Shen G, Ren D, et al. Expression and clinical prognostic value of CYB561 in breast cancer. J Cancer Res Clin Oncol. 2022;148(8):1879-1892.
21. Du JP, Zhu ZX, et al. ARHGEF11 promotes proliferation and epithelial-mesenchymal transition of hepatocellular carcinoma through activation of beta-catenin pathway. Aging (Albany NY), 2020. 12(20): 20235-20253.
22. Jiang Z, Li S, Han MJ, et al. High expression of NSUN5 promotes cell proliferation via cell cycle regulation in colorectal cancer. Am J Transl Res. 2020 Jul 15;12(7):3858-3870. Erratum in: Am J Transl Res. 2020 Oct 15;12(10):6976.
23. Zeng ZL, Wu WJ, Yang J, et al. Prognostic relevance of melanoma antigen D1 expression in colorectal carcinoma. J Transl Med. 2012 10:181.
24. Jin L, Chun J, Pan C, et al. MAST1 drives cisplatin resistance in human cancers by rewiring cRaf-Independent MEK activation. Cancer Cell. 2018;34(2):315-330.e7.

DOI 10.1007/s10330-022-0593-3
Cite this article as: Cheng Y, Li L, Gong C, et al. Construction and validation of a prognostic risk model for uterine corpus endometrial carcinoma based on alternative splicing events. Oncol Transl Med. 2022;8(6):276-284.

Oncology and Translational Medicine
DOI 10.1007/s10330-022-0596-6
December 2022, Vol. 8, No. 6, P285–P292

ORIGINAL ARTICLE

A novel derivative of Genistein inhibits proliferation of ovarian cancer HO-8910 cells by regulating reactive oxygen species*

Yanping Gao[1], Zhiyong Dong[2], Jun Bai[1, 3] (✉)

[1] Department of Gynecology, The First People's Hospital of Datong (Women and Children's Hospital of Shanxi Datong University), Datong 037000, China
[2] Department of Gynecology, The First Affiliated Hospital of Jinan University, Guangzhou 510630, China
[3] Institute of Oncology, Shanxi Datong University, Datong 037000, China

Abstract

Objective To investigate the anticancer effect of a novel derivative of genistein (5-hydroxy-4'-nitro-7-propionyloxy-genistein, HNPG) on human ovarian cancer HO-8910 cells and its possible molecular mechanism.

Methods HO-8910 cells were cultured *in vitro,* and the inhibitory effect of HNPG on proliferation was determined using MTT [3-(4,5-dimethylthiazol-2-yl)-2,5-diphenyltetrazolium bromide] assay. The effect of HNPG on inducing apoptosis was examined using FCM with Annexin V-FITC and propidium iodide staining. The effect of HNPG on regulating reactive oxygen species (ROS) was measured using FCM with 2',7'-di chlorodihydro-fluorescein diacetate staining. The effect of HNPG on modulating mitochondrial membrane potential (MMP) was determined using FCM with lipophilic cationic dye 2 (6 Amino 3 imino 3H xanthen 9 yl) benzoic acid methyl ester (Rh123) staining. The bioactivity of superoxide dismutase (SOD) and catalase (CAT) and the content of glutathione (GSH) and malondialdehyde (MDA) were detected using enzyme-linked immunosorbent assay. The related apoptotic proteins, including bcl-2, bax, cyt-c, and cleaved-caspase-3, were assessed using western blotting.

Results HNPG exhibited dramatic antitumor activity against HO-8910 cells *in vitro*, inhibited proliferation, and induced apoptosis in a time- and dose-dependent manner. These effects were accompanied by reduced bioactivity of SOD and CAT, reduced GSH content, and enhanced MDA content. Simultaneously, the amount of ROS was increased and the level of MMP was reduced, along with upregulation of mitochondrial apoptosis pathway-related proteins, bax, cyt-c, and cleaved-caspase-3; bcl-2 protein was downregulated.

Conclusion HNPG inhibited proliferation of human ovarian cancer HO-8910 cells *in vitro*, which might be related to decreased bioactivity of SOD and CAT. HNPG also reduced GSH content, which resulted in ROS accumulation in cells, damaged the integrity of mitochondrial membrane, and induced cell apoptosis.

Received: 10 September 2022
Revised: 30 November 2022
Accepted: 15 December 2022

Key words: ovarian cancer; 5-hydroxy-4'-nitro-7-propionyloxy-genistein; reactive oxygen species; proliferation; apoptosis

Chemotherapy plays an extremely important role in the treatment of ovarian cancer; postoperative chemotherapy and preoperative neoadjuvant chemotherapy have greatly improved patient prognosis in recent years [1]. Not only can chemotherapy kill residual cancer foci, control recurrence, alleviate symptoms, prolong survival time, and reduce cancer volume to create satisfactEory conditions for surgeons, it also serves as the main treatment for patients who cannot tolerate surgery [2]. Therefore, the development of new anticancer drugs with more anticancer effects and fewer side-effects has become one of the hot spots in clinical research [1, 2].

It was reported that Genstein (GEN) caused extensive pharmacological effects and could inhibit proliferation and induce apoptosis of cancer cells, but its clinical application was limited due to its poor solubility and low bioavailability [3]. However, the solubility and bioavailability of GEN could be improved, and

✉ Correspondence to: Jun Bai. Email: baijunjinanu@163.com
* Supported by a grant from the Scientific Research Project of Shanxi Provincial Health Commission (No. 2021166).

the antitumor activity increased through chemical modification of its structure [4]. 5-hydroxy-4'-nitro-7-pro-pionyloxy-genistein (HNPG) is a novel derivative of GEN, which includes nitro-4' and propionyloxy-7 in the parent nucleus of GEN [5]. HNPG reportedly possesses more anticancer activity than GEN, though its effect against ovarian cancer and its molecular mechanism have not yet been reported [6].

This study examined the inhibitory effect of HNPG on the proliferation of ovarian cancer HO-8910 cells, further investigated its possible molecular biological mechanism, and provided an experimental basis for the clinical treatment of ovarian cancer with HNPG.

Materials and methods

Cells and reagents

Human ovarian cancer HO-8910 cells were purchased from the China Center for Type Culture Collection and cultured in Dulbecco's modified Eagle medium (DMEM) medium containing 10% fetal bovine serum at 37 °C with 5% CO_2 and saturated humidity. HNPG (molecular formula $C_{18}H_{13}O_7N$, molecular weight 355, faint yellow powder, 98% purity) was synthesized by Professor Jin Yongsheng (Biochemical Laboratory of Naval Military Medical University of China). Primary antibodies of bcl-2 (A00040-1), bax (A00183), cyt-c (BA0774), cleaved caspase-3 (BM3937), and glyceraldehyde-3-phosphate dehydrogenase (GAPDH) (A00227-1) were purchased from Boster Biotechnology Co., LTD. The determination kits of reactive oxygen species (ROS) (E004-1-1), superoxide dismutase (SOD) (A001-3), catalase (CAT) (A007-1-1), glutathione (GSH) (A006-1), and malondialdehyde (MDA) (A003-4) were bought from Nanjing Jiancheng Institute of Biology. Annexin V-FITC apoptosis detection kit (C0162) and mitochondrial membrane potential detection kit (C2006) were obtained from Shanghai Beyond Biological Company. MTT (C0009), penicillin-streptomycin solution (C0022), pancreatic protein digestive enzyme (C0205), and bicinchoninic acid (BCA) protein concentration determination kit (P0012S) were purchased from Beyotime Biotechnology Institute. Cell lysate (ARAR0107) and standard fetal bovine serum (PYG0001) were purchased from Boster Biotechnology LTD.

MTT analysis

HO-8910 cells in logarithmic growth phase were plated on a 96-well culture plate at a density of 5,000/well for 24 h. After the cells completely adhered to the culture plate, different concentrations of HNPG (0.625, 1.25, 2.5, 5, 10, 20, 40 μmol/L) were added to each well for 48 h. The inhibitory effect on proliferation of HO-8910 cells was detected, and the optimal concentration and action time associated with optimal bioactivity were selected and administrated for subsequent experiments. The cells were incubated using DMEM medium containing cisplatin 5 μmol/L, GEN 160 μmol/L, or HNPG (5, 10, or 20 μmol/L) for 48 h. The culture medium was then removed, and 5 mg/L MTT was added to each well for further incubation for 4 h. Next, the MTT suspension was removed, and 100 μL Dimethyl sulfoxide (DMSO) was added. The wavelength of 570 nm was selected to detect the optical density (model: ELX-800 Type). Cell proliferation inhibition rate (IR) was calculated as follows: IR = (1 − mean of experimental group A/mean of blank control group A) × 100%. IC50 was obtained using the improved Koch method. The experiment was repeated three times, and the mean values were used for statistical analysis.

FCM of annexin V-FITC (AV) and propidium iodide (PI) staining

HO-8910 cells in logarithmic phase were cultured for 24 h to ensure that the cells completely adhered to the bottle bottom. The culture medium was renewed with EMEM medium containing DDP (5 μmol/L), GEN (160 μmol/L), or HNPG (2.5, 5, or 10 μmol/L). After 48 h, the treatment media were discarded and the cells were cleaned twice with PBS. The cells were digested with 0.25% trypsin and beaten into single cell suspension. The suspended cells were centrifuged at 2,000 rpm for 5 min, and the supernatant was discarded. The cellular precipitate was resuspended in 1 mL 50 mmol AV and 50 mmol PI solution, incubated at 37 °C for 30 min in a dark room, then washed with serum-free DMEM solution three times. The apoptotic cells were measured using FCM with an excitation wavelength of 488 nm and an emission wavelength of 530 nm. The experiment was conducted three times, and the average values were taken for statistical analysis.

FCM of DCFH-DA staining

HO-8910 cells in logarithmic phase were incubated and completely adhered to the bottle bottom for 24 h. The culture medium was changed to fresh DMEM medium containing DDP (5 μmol/L), GEN (160 μmol/L), or HNPG (2.5, 5, 10 μmol/L), and the cells continued to incubate for 48 h. The treatment media were discarded and the bottle bottom was cleaned twice with PBS. The cells were digested with 0.25% trypsin and resuspended in culture medium. The cellular suspension was centrifuged at 2,000 rpm for 5 min, and the supernatant was discarded. The cellular precipitate was suspended in 1 mL 50 mmol 2',7'-dichlorodihydrofluorescein diacetate (DCFH-DA) solution, and incubated at 37 °C for 30 min in a dark room, then washed three times with serum-free DMEM solution to remove DCFH-DA that did not enter

the cells. The cells were passed through a 40 μm filter. The fluorescence intensity of DCFH-DA was measured using FCM with an excitation wavelength of 488 nm and emission wavelength of 530 nm. The experiment was performed three times, and the average values were adopted for statistical analysis.

FCM of Rhodamine 123 staining

HO-8910 cells in logarithmic phase were cultured and completely adhered to the bottle bottom for 24 h. The culture medium was replaced with new DMEM medium containing DDP (5 μmol/L), GEN (160 μmol/L), or HNPG (2.5, 5, or 10 μmol/L). The cells continued to incubate for 48 h; then the culture medium was discarded, and the bottle bottom was cleaned twice with PBS. The cells were digested with 0.25% trypsin and resuspended. The cell suspension was centrifuged at 2,000 rpm for 5 min, and the supernatant was discarded. The cell precipitate was suspended in 500 μL Rh123 solution (final concentration 5 μg/mL), and incubated at 37 °C for 30 min in a dark room. The cells were washed three times with serum-free DMEM solution and two times with PBS, then passed through a 40 μm filter. The fluorescence intensity of Rh123 was measured uisng FCM with an excitation wavelength of 475 nm and emission wavelength of 525 nm. The experiment was repeated three times, and the average values were calculated for statistical analysis.

Enzyme-linked immunosorbent assay (ELISA) method

HO-8910 cells in logarithmic phase were incubated for 24 h until they completely adhered to the bottle bottom. The culture medium was changed with new DMEM medium containing DDP (5 μmol/L), GEN (160 μmol/L), or HNPG (2.5, 5, or 10 μmol/L), and the cells continued to incubate for 48 h. The cells were digested with 0.25% trypsin and resuspended. The cellular suspension was centrifuged at 800 rpm for 5 min, the supernatants were discarded, and the cell precipitates were suspended twice with ice PBS. As a final step, the cellular precipitate was lysed using cell lysis solution for 30 min, and the supernatant was centrifuged at 1,2000 rpm at 4 °C for 10 min. Protein density in the supernatant was determined with a BCA protein quantitation kit. In accordance with the appropriate kit instructions, SOD activity, CAT activity, GSH contents, and MDA contents were measured at 550 nm, 405 nm, 420 nm, and 532 nm, respectively. The calculation formulas of enzyme activity/content were as follows: Total SOD activity (U/mg) = $([OD_{control\ group} - OD_{experimental\ group}] / OD_{control\ group}) / 50\% \times (V_{total\ reaction\ liquid}/V_{sample}) / C_{protein}$; CAT activity (U/mgprot) = $(OD_{control\ group} - OD_{experimental\ group}) \times 271 \times 1/(60 \times V_{sample}) / C_{protein}$ (gprot/mL); GSH content (mgGSH/gprot) = $([OD_{Determinationvalue} - OD_{blankvalue}] / [OD_{standard\ value} - OD_{blank\ value}]) \times C_{standard\ concentration}$ (20×10^{-3} mmol/ L) $\times W_{molecular\ weight\ (307)} \times R_{dilution\ ratio\ of\ sample\ before\ test} / C_{homogenate\ protein(gprot/l)}$; MDA content (nmol/mgprot) = $([OD_{experimental\ group} - OD_{control\ group}]/[OD_{standard\ value} - OD_{standard\ value}]) \times C_{standard\ product} / C_{protein\ content}$. The experiment was performed three times, and the average values were taken for statistical analysis.

Western blotting assay

HO-8910 cells in logarithmic phase were cultured for 24 h until they completely adhered to the bottle bottom. The culture medium was discarded and new DMEM media with different concentrations of HNPG (2.5, 5, or 10 μmol/L) were added for a 48 h incubation. The cells on the bottle bottom were washed three times with ice-cold PBS, and the cell lysis solution was added to extract proteins. A 30 μg sample was separated uisng sodium dodecyl sulfate-polyacrylamide gel electrophoresis (SDS-PAGE), and the protein was transferred to polyvinylidene fluoride (PVDF) membrane. The protein was blocked with 5% nonfat milk in Tris-buffered saline with Tween-20 (TBST) in a room temperature shaker for 2 h. The primary antibody was incubated at 37 °C for 3 h, and the secondary antibody was incubated at 37 °C for 1 h. The fluorescence of antigen-antibody reactions was stimulated using enhanced chemiluminescent agents, and the film was exposed to the reacting fluorescence. The resulting film image was processed and analyzed using a grayscale scanner. The experiment was repeated three times, and the average values were used for statistical analysis.

Statistical analyses

The data were analyzed using statistical product and service solutions 21.0 software. All experimental data were expressed as mean ± standard deviation ($\bar{\chi} \pm s$). Comparisons between the two groups were analyzed using student's *t* test, and multiple groups were analyzed using one-way analysis of variance. $P < 0.05$ indicated statistical differences.

Results

Effect of HNPG on proliferation of HO-8910 cells

The different concentrations of HNPG (0.625, 1.25, 2.5, 5, 10, 20, and 40 μmol/L) were administrated to HO-8910 cells for 48 h, and it was found that the cellular proliferation was inhibited in a concentration-dependent manner. The most significant inhibition by HNPG occurred at a concentration between 1.25 and 20 μmol/L. Compared with the normal saline (NS) group, the inhibition rates of different concentrations of HNPG were statistically significant ($P < 0.05$), as shown in Fig. 1a. HNPG was found to inhibit the proliferation of HO-

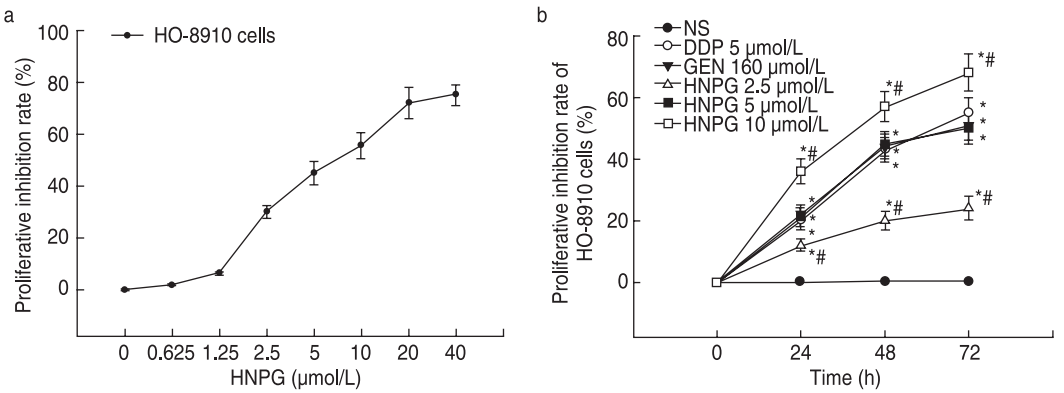

Fig. 1 The inhibitory effect of HNPG on proliferation of HO-8910 cells. (a) The inhibition rate of HO-8910 cells treated with different concentrations of HNPG for 48 h; (b) The inhibition rate of HO-8910 cells treated with different concentrations of HNPG at different times. **P* < 0.05 *vs.* the NS group; #*P* < 0.05 *vs.* the 5 μmol/L DDP group, or 160 μmol/L GEN group

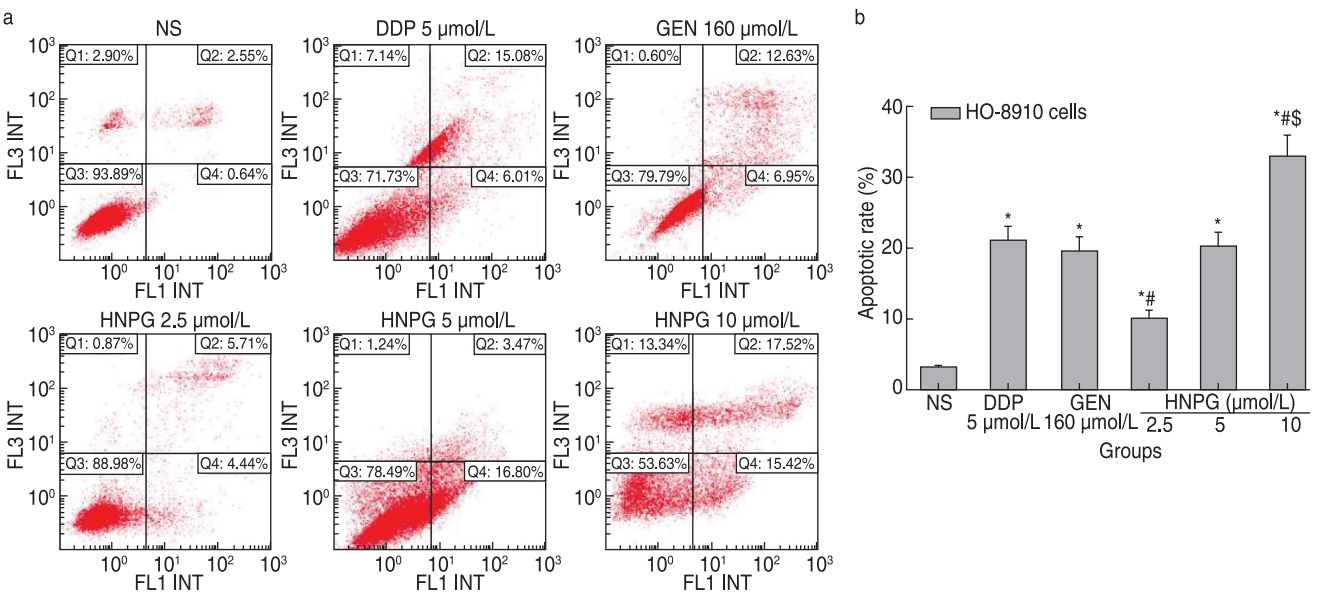

Fig. 2 The effect of HNPG on apoptosis of HO-8910 cells. **P* < 0.05 *vs.* the NS group; #*P* < 0.05 *vs.* 5 μmol/L DDP group, 5 μmol/L HNPG group, or 160 μmol/L GEN group; $*P* < 0.05 *vs.* 5 μmol/L DDP group, 5 μmol/L HNPG group, or 160 μmol/L GEN group

8910 cells in a time-dependent manner. The different groups of HNPG (2.5, 5, and 10 μmol/L) at different time-points (24, 48, and 72 h) showed statistical differences in the inhibition rate of HO-8910 cells ($P < 0.05$), and the IC50 of HO-8910 cells treated with HNPG for 48 h was 4.8 ± 0.6 μmol/L. The inhibitory effect of 5 μmol/L HNPG on the proliferation of HO-8910 cells was similar to 5 μmol/L DDP or 160 μmol/L GEN, and there was no significant difference between the latter two groups ($P < 0.05$) (Fig. 1b).

Effect of HNPG on induced apoptosis of HO-8910 cells

HO-8910 cells in logarithmic phase were cultured with NS, DDP (5 μmol/L), GEN (160 μmol/L), or HNPG (2.5, 5, and 10 μmol/L) for 48 h. FCM showed that HO-8910 cells underwent apoptosis to varying degrees. The apoptotic rates of NS, DDP (5 μmol/L), GEN (160 μmol/L), and HNPG (2.5, 5, and 10 μmol/L) groups were 3.19 ± 0.42%, 21.06 ± 1.47%, 19.65 ± 1.69%, 10.24 ± 1.13%, 20.25 ± 2.04%, and 32.83 ± 3.12%, respectively, and the apoptotic rates of each research group were higher than that of the NS group ($P < 0.05$). There were statistical differences between each concentration of HNPG (2.5, 5, and 10 μmol/L) groups ($P < 0.05$). The apoptotic rate of the 5 μmol/L HNPG group was close to that of the 160 μmol/L GEN or 5 μmol/L DDP groups, and there was no significant difference between the latter two groups ($P > 0.05$), as shown in Fig. 2.

Effect of HNPG on ROS regulation in HO-8910 cells

HO-8910 cells in logarithmic phase were incubated with NS, DDP (5 μmol/L), GEN (160 μmol/L), or HNPG (2.5, 5, and 10 μmol/L) for 48 h. FCM indicated that the fluorescence intensity of DCFH-DA in HO-8910 cells was increased to varying degrees. The fluorescence intensity of the DDP (5 μmol/L), GEN (160 μmol/L), and HNPG (2.5, 5, 10 μmol/L) groups were 0.78 ± 0.08, 4.45 ± 0.47, 4.29 ± 0.49, 2.24 ± 0.13, 4.38 ± 0.44, and 6.26 ± 0.52, respectively, and there were statistical differences between each research group and the NS group (P < 0.05). There were also statistically significant differences between the HNPG (2.5, 5, and 10 μmol/L) groups (P < 0.05). The fluorescence intensity of the 5 μmol/L HNPG group was close to the 160 μmol/L GEN or 5 μmol/L DDP group, and there was no statistical difference between the latter two groups (P > 0.05), as shown in Fig. 3.

Effect of HNPG on mitochondrial membrane potential (MMP) adjustment in HO-8910 cells

HO-8910 cells in logarithmic phase were cultured in medium containing NS, DDP (5 μmol/L), GEN (160 μmol/L), or HNPG (2.5, 5, and 10 μmol/L) for 48 h. FCM demonstrated that Rh 123 fluorescence intensity of HO-8910 cells decreased to varying degrees. The fluorescence intensity of the NS, DDP (5 μmol/L), GEN (160 μmol/L), and HNPG (2.5, 5, 10 μmol/L) groups were 10.02±0.86, 5.5 ± 0.42, 5.66 ± 0.48, 8.38 ± 0.63, 6.16 ± 0.54, and 2.28 ± 0.12, respectively, and there were statistical differences compared with the NS group (P < 0.05). There were statistically significant differences between each pair of HNPG concentrations (P < 0.05). The fluorescence intensity of the 5 μmol/L HNPG group was analogous to the 160 μmol/L GEN and 5 μmol/L DDP groups, and there was no significant difference between the latter two groups (P > 0.05), as shown in Fig. 4.

Effect of HNPG on SOD, CAT, GSH, and MDA modulation in HO-8910 cells

HO-8910 cells in logarithmic phase were incubated with DMEM medium, including DDP (5 μmol/L), GEN (160 μmol/L), or HNPG (2.5, 5, and 10 μmol/L) for 48 h. ELISA assays indicated that SOD and CAT activity were reduced, GSH content was reduced, and MDA content was increased. There was statistical significance compared with the NS group (P < 0.05). There were statistical differences in SOD activity, CAT activity, GSH content, and MDA content between any two HNPG groups (P < 0.05). SOD/CAT activity in the 5 μmol/L HNPG group was similar to the 160 μmol/L GEN or 5 μmol/L DDP group, and GSH/MDA content in 5 μmol/L HNPG groups were similar to the 5 μmol/L GEN or 5 μmol/L DDP groups, while there was no statistical significance between the latter two groups (P > 0.05), as shown in Table 1.

Effect of HNPG on mitochondrial apoptosis pathway-related proteins regulated in HO-8910 cells

Logarithmic proliferating HO-8910 cells were cultured with DMEM medium containing different concentrations of HNPG (2.5, 5, and 10 μmol/L) for 48 h, the cellular proteins were extracted, and the average relative gray values of western blots were detected. The expression of bcl-2 protein was downregulated in a concentration-dependent manner, and there was a statistical difference

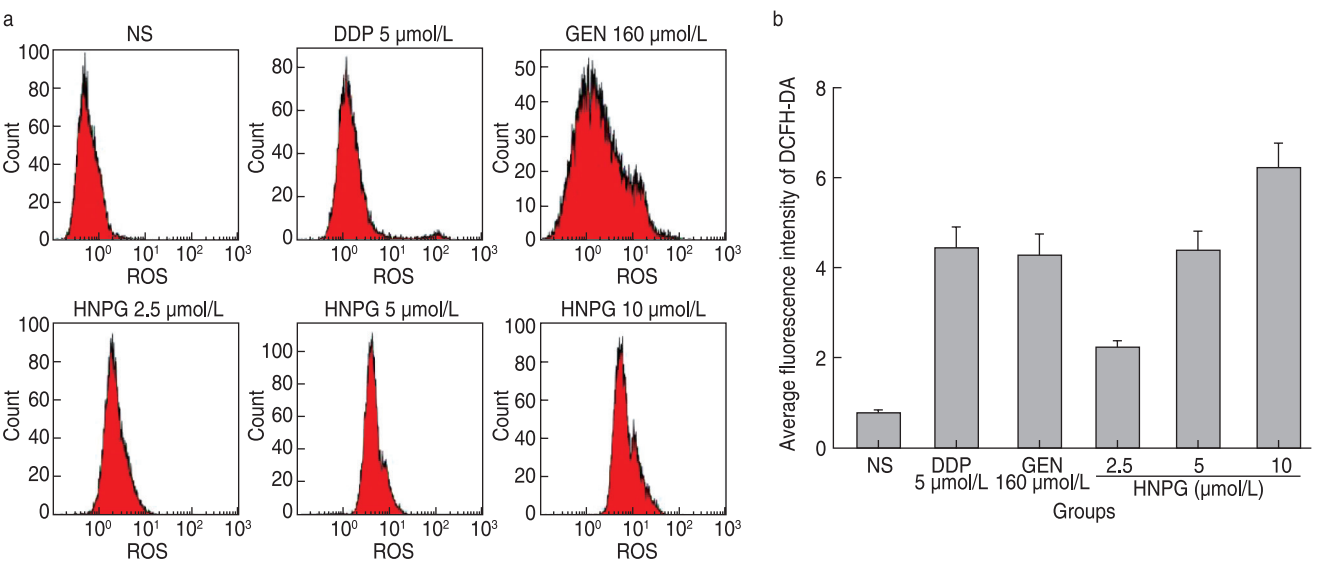

Fig. 3 The effect of HNPG on ROS regulation in HO-8910 cells. *P < 0.05 *vs.* the NS group; #P < 0.05 *vs.* 5 μmol/L DDP group, 5 μmol/L HNPG group, or 160 μmol/L GEN group; $$P$ < 0.05 *vs.* 5 μmol/L DDP group, 5 μmol/L HNPG group, or 160 μmol/L GEN group

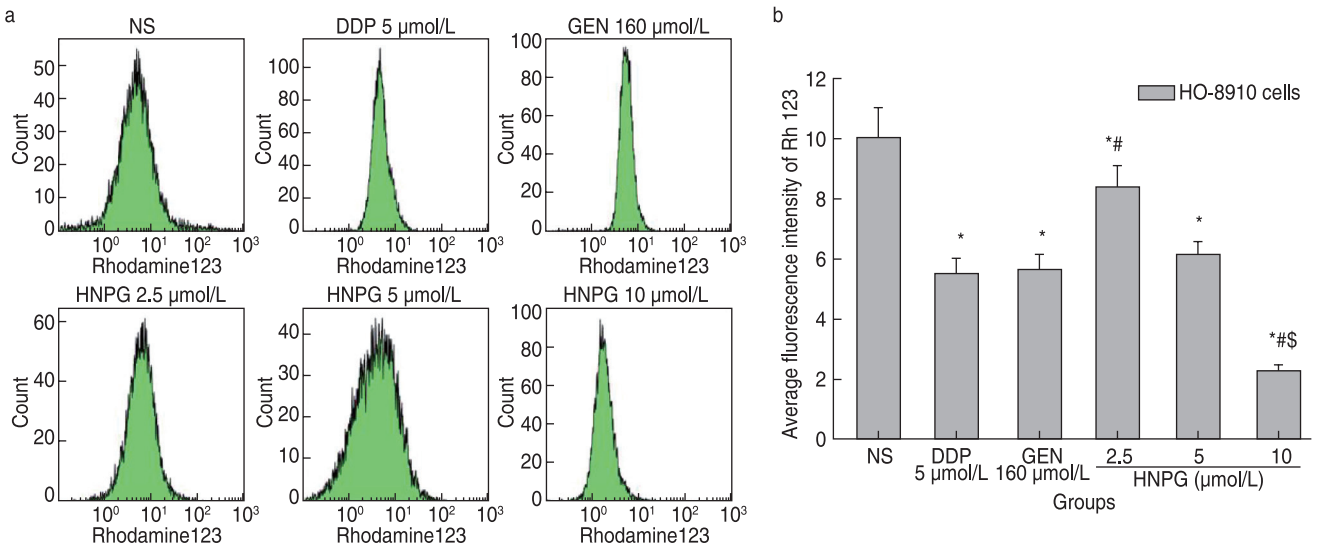

Fig. 4 The effect of HNPG on MMP adjustment in HO-8910 cells. * $P < 0.05$ *vs.* the NS group; # $P < 0.05$ *vs.* 5 μmol/L DDP group, 5 μmol/L HNPG group, or 160 μmol/L GEN group; $ $P < 0.05$ *vs.* 5 μmol/L DDP group, 5 μmol/L HNPG group, or 160 μmol/L GEN group

Table 1 Effect of HNPG on SOD, CAT, GSH and MDA modulation in HO-8910 cells

Groups	SOD (U/mgprot)	CAT (U/mgprot)	GSH (mg/gprot)	MDA (nmol/mgprot)
NS	46.59 ± 2.21	10.89 ± 1.12	12.47 ± 1.07	4.43 ± 0.27
DDP 5 μmol/L	31.08 ± 1.84*	5.98 ± 0.12*	6.28 ± 0.37*	8.54 ± 0.47*
GEN 160 μmol/L	32.90 ± 3.31*#	6.52 ± 0.09*#	6.45 ± 0.11*#	8.76 ± 0.27*#
HNPG 2.5 μmol/L	43.85 ± 2.04*#	8.65 ± 0.52*#	9.52 ± 0.48*#	5.04 ± 0.41*#
HNPG 5 μmol/L	32.70 ± 3.06*	6.70 ± 0.43*	6.97 ± 0.44*	8.49 ± 0.31*
HNPG 10 μmol/L	25.72 ± 3.08*#$	4.18 ± 0.47*#$	4.46 ± 0.63*#$	10.62 ± 0.22*#$

*$P < 0.05$ *vs* the NS group; #$P < 0.05$ *vs* 5 μmol/L DDP group, or 5 μmol/L HNPG group, or 160 μmol/L GEN group; $$P < 0.05$ *vs.* 5 μmol/L DDP group, or 5 μmol/L HNPG group, or 160 μmol/L GEN group

compared with the NS group ($P < 0.05$). However, bax, cyt-c, and cleaved caspase-3 proteins were upregulated in a concentration-dependent manner, and there were statistical differences compared with the NS group ($P < 0.05$; Fig. 5).

Discussion

Atypical proliferation is one of the malignant manifestations of cancer; the rapidly and abnormally proliferating cancer cells not only compress, infiltrate, and damage the surrounding tissue, but also cause metastasis. Simultaneously, the cancer cells release harmful substances into the blood, lymph, and tissue fluid, which threaten the regulatory function of the immune system and affect the balance and stability of the internal environment. Therefore, inhibiting proliferation of cancer cells has become one of the key steps in cancer treatment [7]. Apoptosis is a kind of programmed cell death in which signal transduction pathways are initiated by factors originating internally and externally to the body. Death signals are received by apoptosis-related genes, and various enzymes implementing apoptosis, such as endogenous nuclease and caspase, are synthesized [8]. Apoptosis plays an important role in modern oncology chemotherapy; many chemical medicines exert their antitumor role via induction of tumor cell apoptosis [8]. Chemotherapy remains the most important method to treat ovarian cancer aside from surgery. Chemical medicines, which have entered organisms can kill malignant cells, inhibit cancer cell proliferation, and induce tumor cell apoptosis, thereby playing a crucial role in reducing various damages caused by cancer proliferation and invasion [9, 10]. In this study, we found that HNPG could inhibit proliferation and induce apoptosis of ovarian cancer HO-8910 cells, with an effect similar to DDP or GEN, suggesting that HNPG has potential as a chemical substance to treat ovarian cancer. These findings indicate that the possible molecular biological mechanism is worth investigating.

A balanced oxidation-antioxidant enzyme system exists in organisms, which plays an important role in

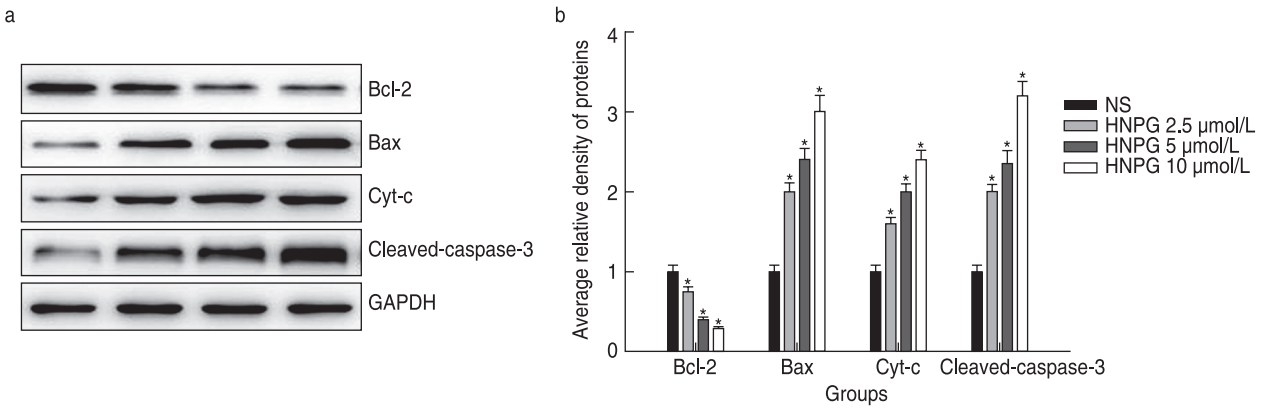

Fig. 5 Effect of HNPG on apoptosis-related protein regulation in HO-8910 cells. * $P < 0.05$ *vs.* the NS group

maintaining the balance and stability of the internal environment [11]. The antioxidant system includes SOD, CAT, GSH, and other enzymes [11]. SOD is one of most important antioxidant enzymes and can directly withstand oxygen free radicals and ROS in the body; this enzyme can take superoxide anion free radicals as the substrate to catalyze its disproportionation reaction to generate nontoxic oxygen or hydrogen peroxide [12]. CAT is another key enzyme in the defense system, which can effectively catalyze hydrogen peroxide into nontoxic oxygen [13]. GSH can also effectively catalyze hydrogen peroxide into nontoxic oxygen and water [14]. SOD, CAT, and GSH play significant roles in the antioxidant enzyme system. The determination of SOD activity, CAT activity, and GSH content can indirectly reflect the antioxidant capacity of organisms, including oxygen free radicals and purged ROS [15]. Organisms can produce oxygen free radicals or ROS via enzyme systems themselves, which can attack polyunsaturated fatty acids in biofilms, induce lipid peroxidation, and form lipid peroxides, such as MDA; therefore, the amount of MDA can reflect the degree of lipid peroxidation in body, which indirectly indicates the degree of cell damage [16]. In this study, it was found that the content of ROS in HO-8910 cells was improved by HNPG, accompanied by decreased SOD and CAT bioactivity, reduced GSH content, and enhanced MDA content. This suggested that the effect of HNPG on inhibiting proliferation and inducing apoptosis of HO-8910 cells was closely related to the function of the oxidant-antioxidant enzyme system brought down, which led to ROS accumulation in HO-8910 cells and damaged the mitochondrial phospholipid membrane.

Mitochondria are vital organelles for cellular oxidative phosphorylation, and transformation holes jointly assembled by bcl-2 and bax proteins in the phospholipid bilayer of mitochondria maintain the normal communication between the intra and extra-mitochondrial environments [17, 18]. When the mitochondrial membrane is damaged, the substances in the mitochondrion spill out, which not only directly reduces MMP, but also initiates a cellular apoptotic reaction [19]. When MMP is downregulated and mitochondrial substances leak, a vicious cycle develops that promotes the initiation of cellular apoptosis. Simultaneously, bcl-2 and/or bax proteins are abnormally regulated and their ratio unbalanced, which will also lead to downregulation of MMP and cause mitochondrial substances to spill over, including cyt-c, apoptosis inductive factor, or apoptosis protease-activating factor. Once the mitochondrial substances are released into the cytoplasm, the caspase family cascade reaction is activated [20, 21]. Finally, the apoptotic effector protein-cleaved caspase-3 is activated and cellular apoptosis is induced [22]. In this study, it was found that MMP decreased when HO-8910 cells were treated with HNPG. This was accompanied by reduced expression of bcl-2 protein, increased expression of bax and cleaved caspase-3, and a downregulated ratio of bcl-2/bax, which together suggest that the proliferation inhibition and induced apoptosis might be related to the mitochondrial apoptosis pathway, in which mitochondrial contents are released into the cytoplasm and the caspase family cascade reactions are activated for mitochondrial injury.

In summary, HNPG significantly inhibited proliferation and induced apoptosis of HO-8910 *in vitro*, and the molecular biological mechanism might be closely related to the downregulation of the cellular antioxidant enzyme system. In turn, this downregulation reduced the capacity of scavenging ROS, contributed to ROS accumulation in cells, damaged mitochondrial lipid membrane, reduced cellular MMP, caused mitochondrial dysfunction, released cyt-c and other apoptosis-inducing substances into the cytoplasm, activated the caspase enzyme chain reaction, and resulted in cell apoptosis. However, to determine whether HNPG inhibits the growth and proliferation of ovarian cancer cells *in vivo* and whether HNPG possesses synergistic effects with other traditional anticancer drugs, further study is needed.

Acknowledgments

The authors would like to thank the researchers who worked on Genistein in anti-tumor cells. The authors would also like to thank Professor Wanyu Xie (The First Affiliated Hospital of University of South China, Hengyang, Hunan, China) for her technical assistance.

Funding

Supported by a grant from the Scientific Research Project of Shanxi Provincial Health Commission (No. 2021166).

Conflicts of interest

The authors indicated no potential conflicts of interest.

Author contributions

Yanping Gao and Zhiyong Dong contributed to data acquisition. Jun Bai contributed to data acquisition, data interpretation, and reviewed and approved the final version of this manuscript.

Data availability statement

The data that support the findings of this study are available from the corresponding author upon reasonable request.

Ethical approval

Not applicable.

References

1. Okusaka T, Furuse J. Recent advances in chemotherapy for pancreatic cancer: evidence from Japan and recommendations in guidelines. J Gastroenterol. 2020;55(4):369-382.
2. Feldmann G. Medikamentöse Therapie des Pankreaskarzinoms : Immer noch eine Domäne der Chemotherapie? [Medicinal treatment of pancreatic cancer: Still a domain of chemotherapy?]. Internist (Berl). 2020;61(2):226-232. German.
3. Jaiswal N, Akhtar J, Singh SP; Badruddeen, Ahsan F. An overview on genistein and its various formulations. Drug Res (Stuttg). 2019;69(6):305-313.
4. Ardito F, Di Gioia G, Pellegrino MR, et al. Genistein as a potential anticancer agent against head and neck squamous cell carcinoma. Curr Top Med Chem. 2018;18(3):174-181.
5. Bai J, Luo X. 5-Hydroxy-4'-Nitro-7-Propionyloxy-Genistein Inhibited Invasion and Metastasis via Inactivating Wnt/b-Catenin Signal Pathway in Human Endometrial Carcinoma Ji Endometrial Cells. Med Sci Monit. 2018;24:3230-3243.
6. Bai J, Yang BJ, Luo X. Effects of 5-hydroxy-4'-nitro-7-propionyloxy-genistein on inhibiting proliferation and invasion via activating reactive oxygen species in human ovarian cancer A2780/DDP cells. Oncol Lett. 2018;15(4):5227-5235.
7. Brioude F, Toutain A, Giabicani E, et al. Overgrowth syndromes - clinical and molecular aspects and tumour risk. Nat Rev Endocrinol. 2019;15(5):299-311.
8. D'Arcy MS. Cell death: a review of the major forms of apoptosis, necrosis and autophagy. Cell Biol Int. 2019;43(6):582-592.
9. Spencer SH, Menard SM, Labedz MZ, et al. Enteral tube administration of oral chemotherapy drugs. J Oncol Pharm Pract. 2020;26(3):703-717.
10. Foster CH, Dave P, Sherman JH. Chemotherapy for the management of cerebral metastases. Neurosurg Clin N Am. 2020;31(4):603-611.
11. Nada HA, El-Shabrawy MM, Ibrahim SH, et al. Measurement of serum glutathione peroxidase, catalase and superoxide dismutase concentration in patients with external anogenital warts before and after treatment with intralesional tuberculin purified protein derivative. Andrologia. 2020;52(9):e13661.
12. Pudlarz AM, Czechowska E, S Karbownik M, et al. The effect of immobilized antioxidant enzymes on the oxidative stress in UV-irradiated rat skin. Nanomedicine (Lond). 2020; 15(1):23-39.
13. Chen R, Zhu Q, Fang Z, et al. Aluminum induces oxidative damage in Saccharomyces cerevisiae. Can J Microbiol. 2020;66(12):713-722.
14. Tatar Ş, Türkmenoğlu Y. Investigation of antioxidant responses in Gammarus pulex exposed to Bisphenol A. Environ Sci Pollut Res Int. 2020;27(11):12237-12241.
15. Cui N, Pozzobon V, Guerin C, et al. Effect of increasing oxygen partial pressure on Saccharomyces cerevisiae growth and antioxidant and enzyme productions. Appl Microbiol Biotechnol. 2020;104(18):7815-7826.
16. Habashy WS, Milfort MC, Rekaya R, et al. Cellular antioxidant enzyme activity and biomarkers for oxidative stress are affected by heat stress. Int J Biometeorol. 2019;63(12):1569-1584.
17. Edlich F. BCL-2 proteins and apoptosis: Recent insights and unknowns. Biochem Biophys Res Commun. 2018;500(1):26-34.
18. Cui L, Bu W, Song J, et al. Apoptosis induction by alantolactone in breast cancer MDA-MB-231 cells through reactive oxygen species-mediated mitochondrion-dependent pathway. Arch Pharm Res. 2018;41(3):299-313.
19. Senichkin VV, Pervushin NV, Zuev AP, et al. Targeting Bcl-2 family proteins: What, Where, When? Biochemistry (Mosc). 2020;85(10):1210-1226.
20. Chea EE, Deredge DJ, Jones LM. Insights on the conformational ensemble of Cyt C reveal a compact state during peroxidase activity. Biophys J. 2020;118(1):128-137.
21. Barayeu U, Lange M, Méndez L, et al. Cytochrome c autocatalyzed carbonylation in the presence of hydrogen peroxide and cardiolipins. J Biol Chem. 2019;294(6):1816-1830.
22. Hentzen NB, Mogaki R, Otake S, et al. Intracellular photoactivation of caspase-3 by molecular glues for spatiotemporal apoptosis induction. J Am Chem Soc. 2020;142(18):8080-8084.

DOI 10.1007/s10330-022-0596-6
Cite this article as: Gao YP, Dong ZY, Bai J. A novel derivative of Genistein inhibits proliferation of ovarian cancer HO-8910 cells by regulating reactive oxygen species. Oncol Transl Med. 2022;8(6): 285–292.

Oncology and Translational Medicine
DOI 10.1007/s10330-022-0584-4
December 2022, Vol. 8, No. 6, P293–P300

ORIGINAL ARTICLE

Downregulated lncRNA *DRAIC* enhances the radiotherapy sensitivity of human HCC cell line *HepG2* by targeting *miR-223-3p*

Shuyan Li, Jian Zhang, Zhengming Wang, Wenjun Li (✉)

Department of Radiotherapy, PLA Rocket Force Characteristic Medical Center, Beijing 100088, China

Abstract

Objective This study aims to investigate the effects of the long noncoding RNA (lncRNA) *DRAIC* on the proliferation, apoptosis, and radiosensitivity of hepatocellular carcinoma (HCC) cells and the molecular mechanisms involved.

Methods Cancer tissues and their corresponding adjacent tissues from 30 patients with HCC were collected, and the expression levels of *DRAIC* and *miR-223-3p* were detected via RT-qPCR. *DRAIC* interference and *miR-223-3p* overexpression vectors were transfected into *HepG2* cells. In addition, *DRAIC* and *miR-223-3p* interference vectors were co-transfected into *HepG2* cells. The constructed cells were irradiated at 4 Gy. Cell colony formation assay, MTT assay, and flow cytometry were performed to detect the radiosensitivity, proliferation inhibition rate, and apoptosis rate of *HepG2* cells, respectively. Dual luciferase reporter gene assay was performed to detect the targeted regulation of *DRAIC* on *miR-223-3p* expression.

Results The expression level of *DRAIC* in HCC tissues was higher than that in paracancer tissues, whereas the expression level of *miR-223-3p* was lower in HCC tissues than that in paracancer tissues ($P < 0.05$). Inhibition of *DRAIC* expression or overexpression of *miR-223-3p* increased the proliferation inhibition and apoptosis rates of *HepG2* cells ($P < 0.05$). After irradiation, cell survival fraction decreased and cell proliferation inhibition and apoptosis rates increased ($P < 0.05$). *DRAIC* targeted the regulation of *miR-223-3p* expression, and interference of *miR-223-3p* expression reversed the effects of inhibiting *DRAIC* expression on the proliferation, apoptosis, and radiosensitivity of *HepG2* cells.

Conclusion Inhibition of *DRAIC* expression can inhibit the proliferation of *HepG2* cells, promote cell apoptosis, and enhance the radiosensitivity of cells via upregulation of *miR-223-3p*.

Received: 22 June 2022
Revised: 29 August 2022
Accepted: 11 October 2022

Key words: the long noncoding RNA (lncRNA) *DRAIC*; *miR-223-3p*; hepatocellular carcinoma (HCC); radiosensitivity medium classification

Hepatocellular carcinoma (HCC) is a common malignant tumor in China, and is often treated with surgery and chemotherapy [1]. With the popularization and development of precision radiotherapy in recent years, radiotherapy has become an effective means to treat liver cancer [2]. However, the resistance of HCC cells to radiotherapy reduces the sensitivity and limits the wide application of radiotherapy. Finding biomarkers that are predictive of neoadjuvant therapy and have a prognostic effect on the overall survival is a research hotspot in the field of neoadjuvant therapy. Long noncoding RNAs (lncRNAs) are transcripts of more than 200 nucleotides and are closely associated with various diseases, including cancer. LncRNAs are considered potential biomarkers for cancer diagnosis, specifically as tumor promoters or suppressors [3]. Studies have reported that the lncRNA *DRAIC* is upregulated in gastric cancer tissues and cell lines, which can be used as an indicator of poor prognosis in patients with gastric cancer. Inhibition of *DRAIC* can inhibit the proliferation, migration, and invasion of gastric cancer cells [4]. The lncRNA *DRAIC* regulates the DNA damage response of nasopharyngeal carcinoma cells to achieve radiation resistance [5]. However, its role in HCC and whether it affects the radiosensitivity of HCC

✉ Correspondence to: Wenjun Li. Email: queyun175837@163.com

cells remain unclear. *DRAIC* has been reported to have binding sites for *miR-223-3p*. Overexpression of *miR-223-3p* can inhibit the proliferation and migration of HCC cells [6]. Therefore, this experiment was conducted to investigate the effects of the lncRNA *DRAIC* on the proliferation, apoptosis, and radiosensitivity of HCC cells and whether the mechanism was related to *miR-223-3p*.

Materials and methods

Specimens

Thirty patients with HCC with complete clinicopathological data were admitted to our hospital (PLA Rocket Force Characteristic Medical Center, Beijing, China) from June 2015 to June 2020. All patients were checked through pathological examination, and their cancer and paracancer tissues were surgically removed. In addition, all patients signed informed consent forms. This experiment was reviewed and approved by the Ethics Committee of our hospital.

Cells and reagents

Human HCC cell line, *HepG2*, was purchased from Shanghai Cell Bank (Chinese Academy of Sciences, China). The main reagents were as follows: RPMI-1640 complete medium was purchased from Gibco (San Diego, California, USA); Fluorescence quantitative PCR kit (Dingguochangsheng, Beijing, China); methyl thiazolyl tetrazolium (MTT) kit (Tongwei, LTD, Shanghai, China). The apoptosis detection kit (Emijie, Wuhan, China), protein lysate (Yuanye, Shanghai, China), double luciferase reporter gene detection kit (Biyuntian, Shanghai, China). The rabbit polyclonal antibodies cyclin D1 (AB39570), Bcl-2 (AB25644) and rabbit monoclonal antibodies p21 (AB13662), Bax (AB25436), and cleaved caspase-3 (AB66254) were purchased from Abcam (Boston, Massachusetts, USA).

Experimental grouping

HepG2 cells were cultured in RPMI-1640 complete medium. *DRAIC* interference expression vector and a negative control and *miR-223-3p* mimics and a negative control were transfected into *HepG2* cells at the logarithmic growth stage. They were classified as short interfering (si)-*DRAIC*, *si*-NC, *miR-223-3p*, and *miR*-NC groups, respectively. The *DRAIC* interference expression vector was co-transfected with *miR-223-3p* inhibitor or a negative control into *HepG2* cells and was classified as *si-DRAIC* + anti-*miR-223-3p* and *si-DRAIC* + anti-*miR*-NC groups, respectively. Cells in the *si*-NC, *si-DRAIC*, *miR*-NC, *miR-223-3p*, *si-DRAIC* + anti-*miR*-NC, and *si-DRAIC* + anti-*miR-223-3p* groups were irradiated with 4 Gy radiation and were recorded as 4 Gy + *si*-NC, 4 Gy + *si*-DRAIC, 4 Gy + *miR*-NC, 4 Gy + *miR-223-3*, 4 Gy + *si-DRAIC* + anti-*miR*-NC, and 4 Gy + *si-DRAIC* + anti-*miR-223-3p* groups, respectively.

Real-time quantitative PCR (RT-qPCR) detection

RNA was extracted from tissues and cells. Next, RT-qPCR was performed according to the kit instructions, with GAPDH and U6 as internal controls, and the relative expression level was calculated via the $2^{-\Delta\Delta Ct}$ method. The following primers were used: *DRAIC* upstream primer sequence: 5'-CTGCCTCCACCCGTGTACCG-3' and downstream primer sequence: 5'-ATCGGCGTGGGTGTCTCACC-3'; GAPDH upstream primer sequence: 5'-TGGTCr-CCCAAGCGTCGATag-3' and downstream primer sequence: 5'-AGCTTGGACGAGATCGGGGAA-3'; *miR-223-3p* upstream primer sequence: 5'-AcACTT-ATCGGTAGTGTGGTC-3' and downstream primer sequence: 5'-AGCTCGTCTCTCCCGTCCCT-3'; U6 upstream primer sequence: 5'-CCAACGA-AACCGTCGCATCCAGT-3' and downstream primer sequence: 5'-AgGAAAAGTTCACAatCTCGA-3'.

Cell colony formation assay

Cells of the *si*-NC, *si-DRAIC*, *miR*-NC, *miR-223-3p*, *si-DRAIC* + anti-*miR*-NC, and *si-DRAIC* + anti-*miR-223-3p* groups were inoculated in a 60 mm petri dish and irradiated with 0, 2, 4, 6 and 8 Gy radiation. After irradiation, the cultures were continued for two weeks. The cells were subjected to Giemsa staining, and colonies of more than 50 cells were counted under an optical microscope (BX53, Olympus, Japan). GraphPad Prism 5 (National Institutes of Health) was used to fit the cell survival curve.

MTT assay

The cells were cultured for 48 h, MTT assay was performed according to the manufacturer's instructions, and MTT solution and dimethyl sulfoxide were added. The absorbance (*A*) value at 490 nm was detected using a microplate reader (Multiskan FC, Thermo). The proliferation inhibition rate was calculated using the following formula: [1 – *A* (experimental group)] / *A* (blank group) × 100%.

Flow cytometry

HepG2 cells were digested with 0.25% trypsin and centrifuged. Flow buffer was then added to the cells according to the manufacturer's instructions, and the cells were resuspended (Phosphate buffer). Next, 5 μL annexin V-APC was added and the cells were incubated for 30 min, and then 5 μL PI was added.

Western blot

The cells were collected (1×10^6 cells/mL) and subjected to total protein extraction. The proteins (100 μg) were then denatured, separated via SDS-PAGE, transferred to the PVDF membrane, and then sealed for 1 h. They were incubated with the primary antibody (diluted 1:500) overnight at 4 °C and with the secondary antibody for 1 h. ECL developing solution A and the same volume of liquid B was dropped onto the PVDF membrane, and an image was captured using the AI600 imaging system. The absorbance value was analyzed using Image J software (Ver. 1.48, Bethesda, MD, USA) and was compared with β-actin as the internal control.

Double luciferase reporter gene assay

The wild-type *DRAIC* sequence containing the predicted *miR-223-3p* binding site or mutants at each site was cloned into the PsichecK-2 plasmid and named *DRAIC*-WT or *DRAIC*-MUT reporter gene. The luciferase reporter gene was transfected into *HepG2* cells with *miR-223-3p*, anti-*miR-223-3p*, or the corresponding controls. After 48 h, luciferase activity was measured using the dual luciferase reporter gene assay system (Promega).

Statistical analysis

SPSS 20.0 software was used for statistical analysis. The measurement data consistent with normal distribution were expressed as mean ± standard deviation ($X \pm S$). *T*-test and LSD-*T* test were performed for comparison between two groups, and one-way ANOVA was used for comparison between multiple groups. $P < 0.05$ was considered to indicate a statistically significant difference.

Results

Expression of lncRNA *DRAIC* and *miR-223-3p* in HCC tissues

DRAIC expression level in HCC tissues was higher than that in paracancer tissues, whereas the *miR-223-3p* expression level in HCC tissues was lower than that in paracancer tissues ($P < 0.05$; Fig. 1).

Effect of inhibiting lncRNA *DRAIC* expression on the radiosensitivity of *HepG2* cells

The cell survival fraction of the *si-DRAIC* group decreased after irradiation at different doses ($P < 0.05$), and the radiosensitization ratio was 1.725 (Fig. 2).

Effects of inhibition of lncRNA *DRAIC* expression combined with 4 Gy radiation on the proliferation and apoptosis of *HepG2* cells

The proliferation inhibition and apoptosis rates of *HepG2* cells in the *si-DRAIC* group were higher than those in the *si*-NC group. The expression levels of cyclin D1 and Bcl-2 in the *si-DRAIC* group were lower than those in the *si*-NC group, whereas the expression levels of p21, Bax, and cleaved caspase-3 in the *si-DRAIC* group were higher than those in the *si*-NC group ($P < 0.05$). Furthermore, the proliferation inhibition and apoptosis rates of cells in the 4 Gy + *si-DRAIC* group were higher than those in 4 Gy + *si*-NC group. The expression levels of cyclin D1 and Bcl-2 in the 4 Gy + *si-DRAIC* group were lower than those in 4 Gy + *si*-NC group, whereas the expression levels of p21, Bax, and cleaved caspase-3 in the 4 Gy + *si-DRAIC* group were higher than those in the 4 Gy + *si*-NC group ($P < 0.05$; Fig. 3).

LncRNA *DRAIC* targeted regulation of *miR-223-3p* expression

starBase prediction showed that the lncRNA *DRAIC* contained binding sites for *miR-223-3p* (Fig. 4a). The luciferase activity of *HepG2* cells co-transfected with WT-*DRAIC* and *miR-223-3p* was lower than that of cells co-transfected with WT-*DRAIC* and *miR*-NC ($P < 0.05$; Fig. 4b). Overexpression of *DRAIC* decreased *miR-223-3p* expression levels, inhibited *DRAIC* expression, and increased *miR-223-3p* expression levels ($P < 0.05$; Fig. 4c). The *DRAIC* expression level was negatively correlated with *miR-223-3p* expression level in tumor and fat cancer tissues ($r = -0.528$, $P < 0.001$; Fig. 4d).

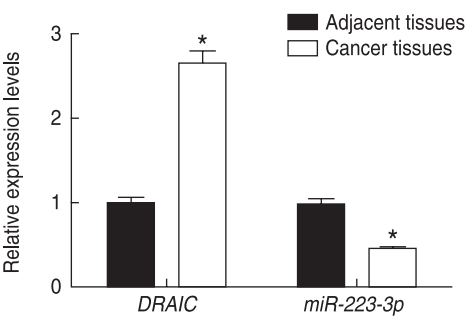

Fig. 1 Expression of lncRNA *DRAIC* and *miR-223-3p* in HCC tissues. * $P < 0.05$ compared with adjacent tissues

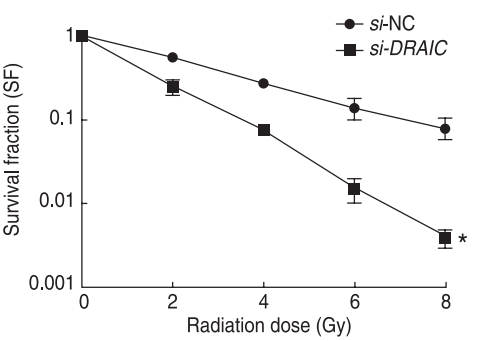

Fig. 2 Effect of inhibition of lncRNA *DRAIC* expression on *HepG2* cell survival score. * $P < 0.05$ compared with *si*-NC group

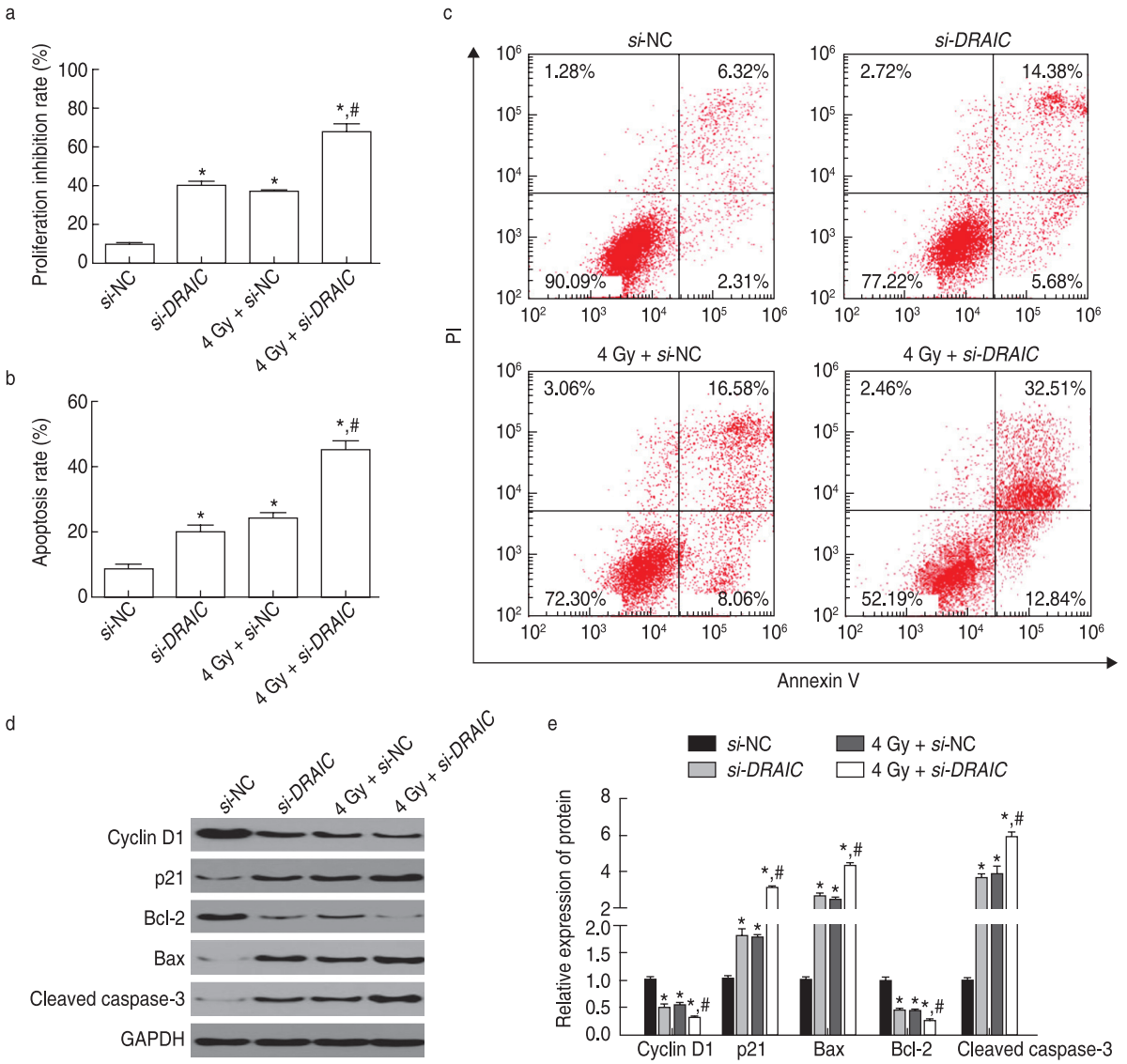

Fig. 3 Effects of inhibition of lncRNA *DRAIC* expression combined with 4 Gy radiation on the proliferation and apoptosis of *HepG2* cells. (a) Proliferation inhibition rate; (b) Apoptosis rate; (c) Apoptosis was detected via flow cytometry; (d) Western blotting was performed to detect protein expression; (e) Relative expression of proteins. * $P < 0.05$ compared with *si*-NC group; # $P < 0.05$ compared with 4 Gy + *si*-NC group

Effect of *miR-223-3p* overexpression on the radiosensitivity of *HepG2* cells

The cell survival score of the *miR-223-3p* group decreased after irradiation at different doses ($P < 0.05$). The radiosensitization ratio of cells was 1.701 (Fig. 5).

Effects of *miR-223-3p* overexpression combined with 4 Gy irradiation on the proliferation and apoptosis of *HepG2* cells

The proliferation inhibition and apoptosis rates of *miR-223-3p* group cells were higher than those of *miR*-NC group cells. The expression levels of cyclin D1 and Bcl-2 in the *miR-223-3p* group were lower than those in the *miR*-NC group, whereas the expression levels of p21, Bax, and cleaved caspase-3 in the *miR-223-3p* group were higher than those in the *miR*-NC group ($P < 0.05$). Furthermore, the proliferation inhibition and apoptosis rates of cells in the 4 Gy + *miR-223-3p* group were higher than those in 4 Gy + *miR*-NC *group*. The expression levels of cyclin D1 and Bcl-2 in the 4 Gy + *miR-223-3p* group were lower than those in 4 Gy + *miR*-NC group, whereas the expression levels of p21, Bax, and cleaved caspase-3 in the 4 Gy + *miR-223-3p* group were higher than those in the 4 Gy + *miR*-NC group ($P < 0.05$; Fig. 6).

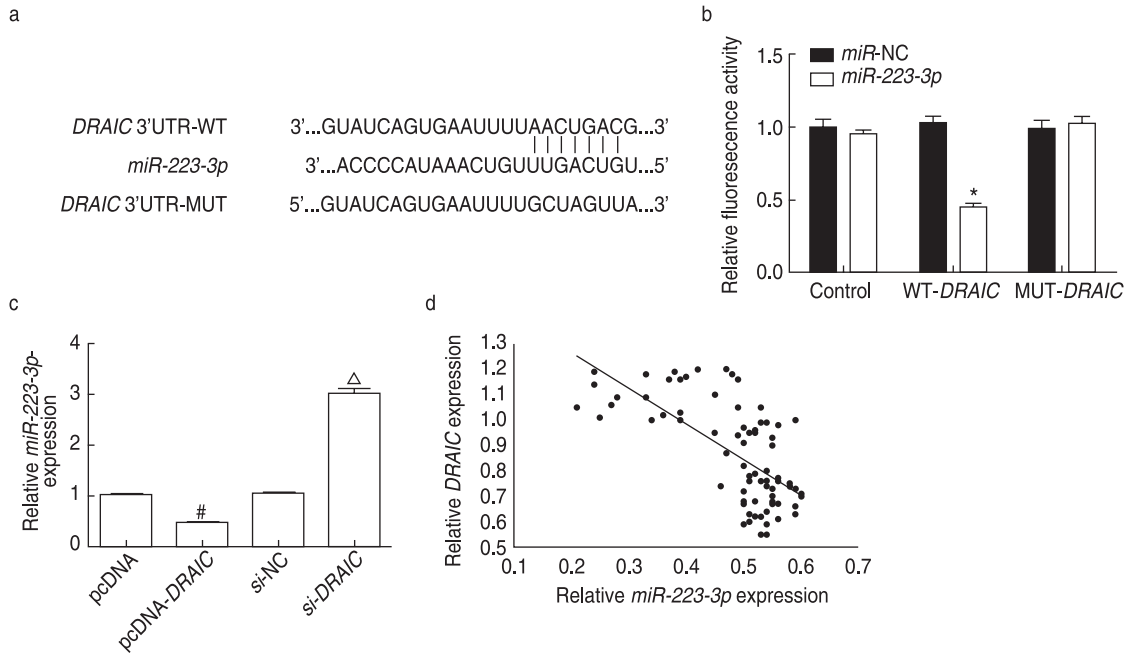

Fig. 4 LncRNA *DRAIC* targeting regulated the expression of *miR-223-3p*. (a) Schematic of lncRNA *DRAIC* and *miR-223-3p* binding; (b) luciferase reporter gene assay verified that *miR-223-3p* was the target of the lncRNA *DRAIC*; (c) lncRNA *DRAIC* was detected to affect endogenous *miR-223-3p* levels via RT-qPCR; (d) Pearson linear analysis of the correlation between lncRNA *DRAIC* and *miR-223-3p* in lung cancer tissues. * $P < 0.05$ compared with *miR*-NC group; # $P < 0.05$ compared with pcDNA group; △ $P < 0.05$ compared with *si*-NC group

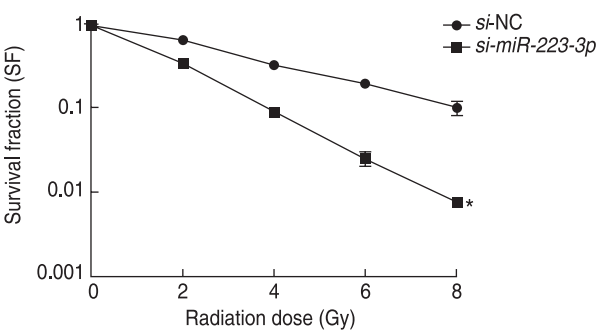

Fig. 5 Effect of *miR-223-3p* overexpression on the survival score of *HepG2* cells. * $P < 0.05$ compared with *miR*-NC

Interference with *miR-223-3p* expression reversed the effect of inhibiting *DRAIC* expression on the radiosensitivity of HCC *HepG2* cells

After irradiation at different doses, the cell survival score of the *si-DRAIC* + anti-*miR*-NC group was lower than that of the *si*-NC group, and the radiosensitization ratio was 1.745. In contrast, the cell survival score of the *si-DRAIC* + anti-*miR-223-3p* group was higher than that of the *si-DRAIC* + anti-*miR*-NC group, and the radiosensitization ratio was 1.140. Furthermore, the proliferation inhibition and apoptosis rates of cells in the 4 Gy + *si-DRAIC* + anti-*miR-223-3p* group were lower than those in the 4 Gy + *si-DRAIC* + anti-*miR*-NC group. The expression levels of cyclin D1, Bcl-2, and caspase-3 in the 4 Gy + *si-DRAIC* + anti-*miR-223-3p* group were higher than those in the 4 Gy + *si-DRAIC* + anti-*miR*-NC group, whereas the expression levels of p21, Bax, and cleaved caspase-3 in the 4 Gy + *si-DRAIC* + anti-*miR-223-3p* group were lower than those in the 4 Gy + *si-DRAIC* + anti-*miR*-NC group ($P < 0.05$; Fig. 7 and 8).

Discussion

HCC is a common malignant tumor in China, with a high degree of malignancy, recurrence, and mortality. The treatment methods mainly include surgery, chemotherapy, and radiotherapy. However, the resistance of HCC cells to radiotherapy limits its efficacy; thus, improving the radiotherapy sensitivity of HCC cells has important clinical significance for the treatment of HCC. LncRNAs usually regulate gene expression, including the transcriptional or post-transcriptional regulation of oncogenes and tumor suppressor genes. The lncRNA *DRAIC* is a novel lncRNA located at the 15Q23 position of the human chromosome, which has been recently reported to play an important role in the regulation of cancer occurrence and development. Saha *et al* [4] found that the lncRNA *DRAIC* inhibits the activation of the NF-κB pathway through interacting with the inhibitors

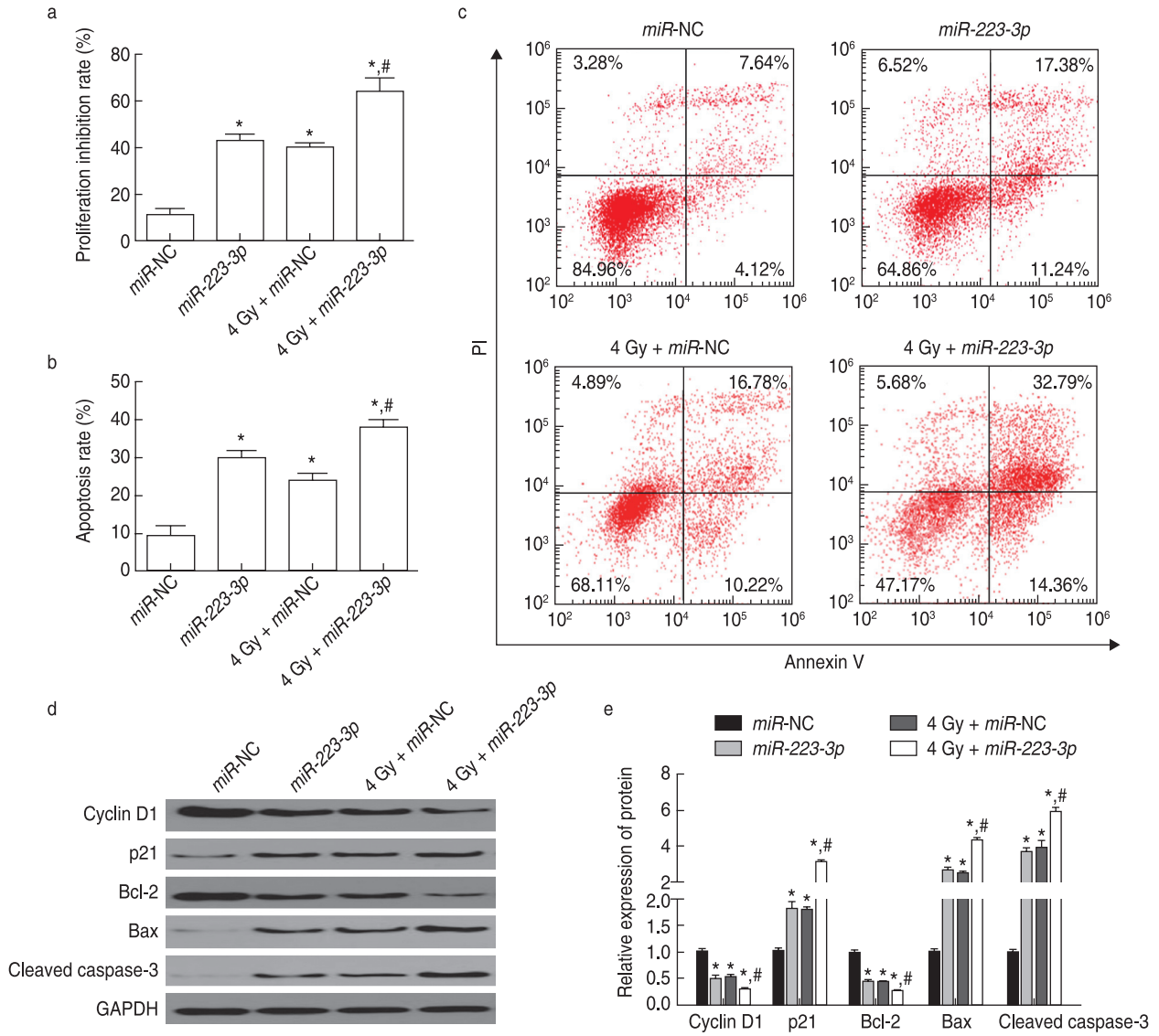

Fig. 6 Effects of inhibition of *miR-223-3p* expression combined with 4 Gy radiation on the proliferation and apoptosis of *HepG2* cells. (a) Proliferation inhibition rate; (b) apoptosis rate; (c) apoptosis was detected via flow cytometry; (d) Western blotting was performed to detect protein expression; (e) relative expression of proteins. * $P < 0.05$ compared with *miR*-NC group; # $P < 0.05$ compared with 4 Gy + *miR*-NC group

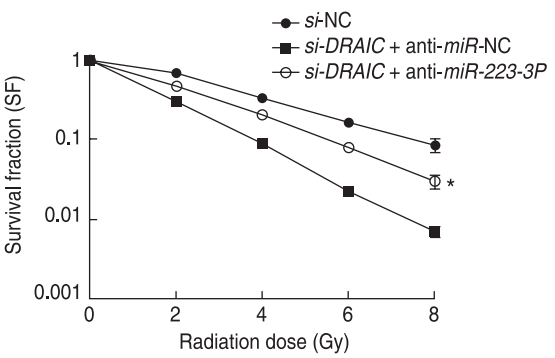

Fig. 7 Interference with *miR-223-3p* expression reversed the effect of inhibition of *DRAIC* expression on the survival scores of *HepG2* cells. * $P < 0.05$ compared with *si-DRAIC* + anti-*miR*-NC group

of IκB kinase β, thereby inhibiting the proliferation and invasion of prostate cancer cells, growth of xenograft tumors, and progression of prostate cancer.

Deng *et al* [7] found that the lncRNA *DRAIC* regulates the expression of *miR-223-3p*, and the inhibited expression can inhibit the migration and invasion of gastric cancer cells and promote their apoptosis. Li *et al* [8] found that *DRAIC* is highly expressed in esophageal cancer tissues and cells, and interference with *DRAIC* expression can inhibit the proliferation and autophagy of liver cancer cells. Although TCGA and RNA sequencing data have indicated that the lncRNA *DRAIC* is upregulated in HCC cells, its mechanism in HCC development has not been clarified. In this study, the expression of *DRAIC*

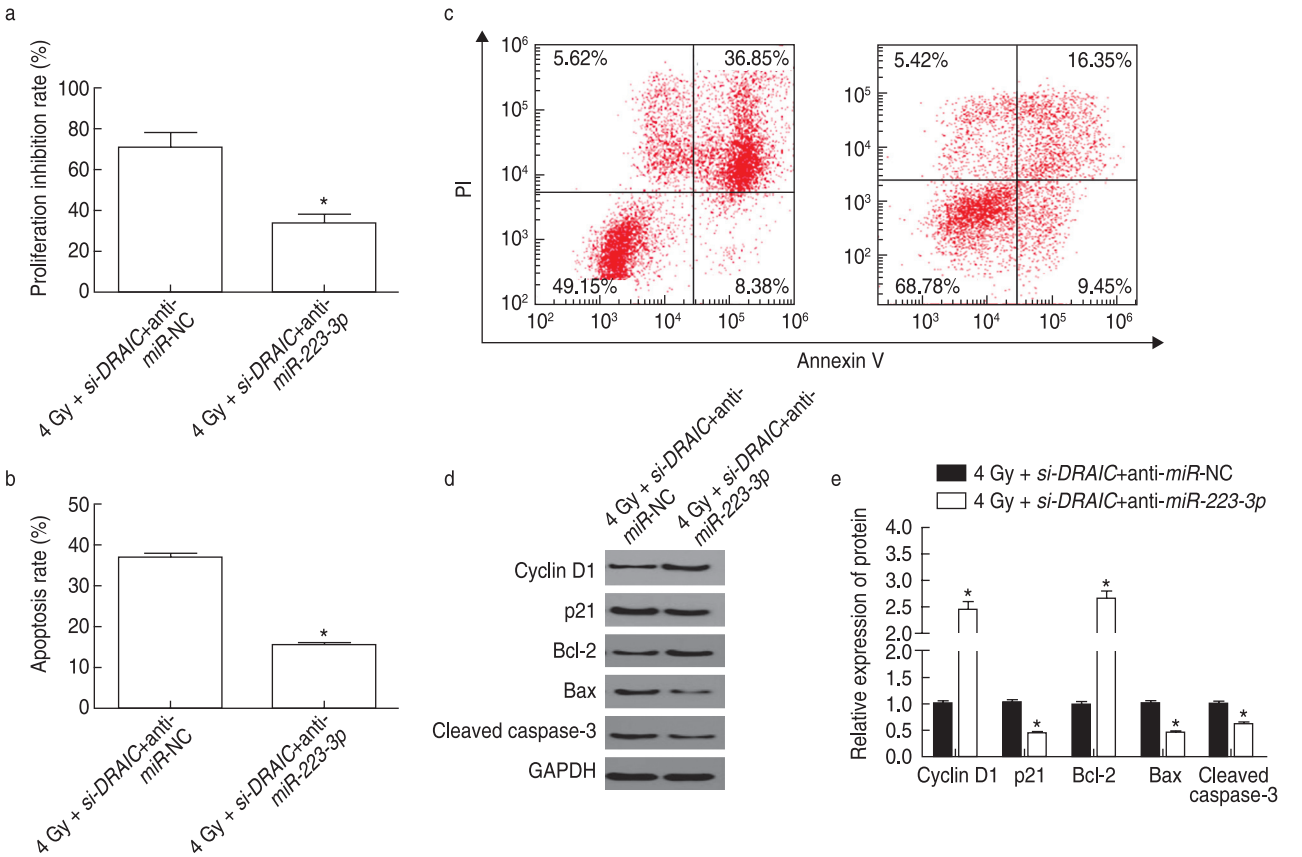

Fig. 8 Interference with *miR-223-3p* expression reversed the effects of inhibition of *DRAIC* expression combined with 4 Gy irradiation on the proliferation and apoptosis of *HepG2* cells. (a) Proliferation inhibition rate; (b) apoptosis rate; (c) apoptosis was detected via flow cytometry; (d) Western blotting was performed to detect protein expression; (e) relative expression of proteins. * $P < 0.05$ compared with 4 Gy + *si-DRAIC* + anti-*miR*-NC group

in HCC tissues was significantly higher than that in the adjacent tissues ($P < 0.05$). After transfection with *DRAIC* interference expression vector, the cell proliferation inhibition and apoptosis rates increased. These results indicated that inhibition of *DRAIC* could inhibit the proliferation and apoptosis of *HepG2* cells. The cells transfected with *DRAIC* interference expression vector were irradiated at different doses. The results showed that the survival fraction of cells decreased, indicating that inhibition of *DRAIC* expression increased the sensitivity of cancer cells to radiation. In addition, the proliferation inhibition and apoptosis rates of *HepG2* cells were significantly increased after transfection with *DRAIC* interference expression vector combined with 4 Gy radiation, indicating that the combination of inhibition of *DRAIC* expression and irradiation had a stronger tumor inhibition effect on *HepG2* cells than interference alone.

Bioinformatic analysis of the lncRNA *DRAIC* was performed to identify and verify *miR-223-3p* as a binding target. The *miR-223-3p* presents low expression in a variety of cancers, and its overexpression can inhibit the proliferation and migration of a variety of cancer cells [9–10]. Xu *et al* [11] found that the expression of *miR-223-3p* was reduced in HCC cells, and *miR-223-3p* can inhibit the proliferation, migration, invasion, and other malignant phenotypes of HCC cells through targeting the adipocyte atypical cadherin 1. Wang *et al* [12] showed that *miR-223-3p* is underexpressed in breast cancer tissues and its overexpression can inhibit the expression of an oncogene in epithelial cell transformation sequence 2, thus inhibiting the invasion and migration of breast cancer cells and promoting cell apoptosis. Sun *et al* [13] also found that the expression of *miR-223-3p* was decreased in oral squamous cell carcinoma tissues and cell lines, and its overexpression inhibited the proliferation, migration, and invasion of oral squamous cell carcinoma cells and induced cell apoptosis. The results of this study showed that the expression level of *miR-223-3p* in HCC tissues was decreased, which was consistent with the results of previous studies, suggesting that *miR-223-3p* plays a tumor suppressive role in HCC. Dong *et al* [14] demonstrated that *miR-223-3p* was downregulated in HCC cell lines, and *miR-223-3p* overexpression inhibited cell proliferation and migration and increased cisplatin sensitivity. The results of this study also showed that *miR-223-3p* overexpression alone or combined with irradiation

increased the proliferation inhibition and apoptosis rates of *HepG2* cells, and the cell survival fraction decreased after irradiation at different doses. These results indicated that the overexpression of *miR-223-3p* could inhibit the proliferation of *HepG2* cells, promote apoptosis, and increase the radiosensitivity of cells. This study also found that the lncRNA *DRAIC* regulated and interfered with *miR-223-3p* expression, which reversed the effects of inhibiting *DRAIC* expression on *HepG2* cell proliferation, apoptosis, and radiosensitivity.

In conclusion, inhibition of the lncRNA *DRAIC* expression can inhibit the proliferation of *HepG2* cells, promote apoptosis, and enhance the radiosensitivity of cells, and the mechanism may be related to *miR-223-3p*.

Acknowledgments
Not applicable.

Funding
Not applicable.

Conflicts of interest
The authors indicated no potential conflicts of interest.

Author contributions
All authors contributed to data acquisition, data interpretation, and reviewed and approved the final version of this manuscript.

Data availability statement
Not applicable.

Ethical approval
Not applicable.

References

1. Zhao SN, Chen AX, Cao JY, et al. Neurotrophin 3 hinders the growth and metastasis of hepatocellular carcinoma cells. Oncol Transl Med. 2020;6(4):143-152.
2. Kang J, Huang X, Dong W, et al. Long non-coding RNA LINC00630 facilitates hepatocellular carcinoma progression through recruiting transcription factor E2F1 to up-regulate cyclin-dependent kinase 2 expression. Hum Exp Toxicol. 2021;40(12_suppl):S257-S268.
3. Zhu HX, Lu WJ, Zhu WP, et al. Comprehensive analysis of N6 -methyladenosine-related long non-coding RNAs for prognosis prediction in liver hepatocellular carcinoma. J Clin Lab Anal. 2021;35(12):e24071.
4. Saha S, Kiran M, Kuscu C, et al. Long noncoding RNA DRAIC inhibits prostate cancer progression by interacting with IKK to inhibit NF-κB activation. Cancer Res. 2020;80(5):950-963.
5. Liao B, Wang Z, Zhu Y, et al. Long noncoding RNA DRAIC acts as a microRNA-122 sponge to facilitate nasopharyngeal carcinoma cell proliferation, migration and invasion via regulating SATB1. Artif Cells Nanomed Biotechnol. 2019;47(1):3585-3597.
6. Qi X, Wang HZ, Chen XD, et al. miR-223-3p regulates the proliferation and apoptosis of hepatocellular carcinoma SMMC-7721 cells by targeting RAC1. Chin J Cancer Biother. 2020;27(6):664-670.
7. Deng Q, Zhang TQ, Le WJ, et al. Effects of DRAIC on the migration and invasion of SGC-7901 gastric cancer cell by regulating miR-223. Med J West China (Chinese). 2018;30(12):1753-1757.
8. Li F, Zhou X, Chen M, et al. Regulatory effect of LncRNA DRAIC/miR-149-5p/NFIB molecular network on autophagy of esophageal cancer cells and its biological behavior. Exp Mol Pathol. 2020;116:104491.
9. Zhou K, Wei Y, Li X, et al. MiR-223-3p targets FOXO3a to inhibit radiosensitivity in prostate cancer by activating glycolysis. Life Sci. 2021;282:119798.
10. Ji Q, Xu X, Song Q, et al. miR-223-3p inhibits human osteosarcoma metastasis and progression by directly targeting CDH6. Mol Ther. 2018;26(5):1299-1312.
11. Xu J, Wang B, Liu ZT, et al. miR-223-3p regulating the occurrence and development of liver cancer cells by targeting FAT1 gene. Math Biosci Eng. 2019;17(2):1534-1547.
12. Wang X, Tong Z, Liu H. MiR-223-3p targeting epithelial cell transforming sequence 2 oncogene inhibits the activity, apoptosis, invasion and migration of MDA-MB-468 breast cancer cells. Onco Targets Ther. 2019;12:7675-7684.
13. Sun C, Liu XH, Sun YR. MiR-223-3p inhibits proliferation and metastasis of oral squamous cell carcinoma by targeting SHOX2. Eur Rev Med Pharmacol Sci. 2019;23(16):6927-6934.
14. Dong Z, Qi R, Guo X, et al. MiR-223 modulates hepatocellular carcinoma cell proliferation through promoting apoptosis via the Rab1-mediated mTOR activation. Biochem Biophys Res Commun. 2017;483(1):630-637.

DOI 10.1007/s10330-022-0584-4
Cite this article as: Li SY, Zhang J, Wang ZM, et al. Downregulated lncRNA *DRAIC* enhances the radiotherapy sensitivity of human HCC cell line *HepG2* by targeting *miR-223-3p*. Oncol Transl Med. 2022;8(6): 293-300.

Oncology and Translational Medicine
DOI 10.1007/s10330-022-0605-5

December 2022, Vol. 8, No. 6, P301–P310

ORIGINAL ARTICLE

Treatment-related adverse events of combined anti-angiogenic and immune checkpoint inhibitors: systematic review and meta-analysis

Lian Chen[1], Ling Wu[2], Zhang Lu[1], Qin Huang[1], Liu Huang[1] (✉)

[1] Department of Oncology, Tongji Hospital, Tongji Medical College, Huazhong University of Science and Technology, Wuhan 430022, China
[2] Union Hospital, Tongji Medical College, Huazhong University of Science and Technology, Wuhan 430022, China

Abstract

Objective Immune checkpoint inhibitor (ICI) plus angiogenesis inhibitor (AI) combination therapy is a novel treatment model for multiple cancers that normalizes vascular-immune crosstalk to potentiate cancer immunity. In this review, we summarize the characteristics of adverse effects (AEs) and all fatal cases reported in clinical studies involing ICI + AI therapy.

Methods Four databases were systematically searched for eligible studies, and 28 relevant studies were selected for inclusion.

Results Of the patients included, 58.1% developed grade ≥ 3 AEs. The most common fatal AEs were cardiovascular events, severe infections, and hemorrhage. Compared with AI alone, ICI + AI therapy resulted in more cases of grade ≥ 3 proteinuria, liver injury, and fatal AEs (2.49% *vs.* 1.28%, $P = 0.0041$), especially respiratory toxicities and severe infections; however, ICI + AI therapy reduced hematological toxicity.

Conclusion We shared comprehensive and practical safety data to review the adverse events associated with ICI + AI treatment.

Received: 28 October 2022
Revised: 15 November 2022
Accepted: 5 December 2022

Key words: combination therapy, immune checkpoint inhibitor, angiogenesis inhibitor, treatment-related adverse events, systematic review, meta-analysis

Immune checkpoint inhibitors (ICIs) are now the cornerstones of cancer therapy, with approval for use in 17 different cancer types [1, 2]. In clinical practice, the main concern when choosing an ICI is the low response rate [3]. Recent studies have indicated that the efficacy of combination therapy with ICIs and angiogenesis inhibitors (AI) is superior to monotherapy with ICIs or AIs [4–6]. AI therapy not only prunes blood vessels, which are essential for cancer growth and metastasis but also reprograms the tumor immune microenvironment [7]. For this novel therapy, whether the severity and frequency of adverse events (AEs) are synergistic or additive is unclear. To the best of our knowledge, the spectrum of treatment-related adverse events (TRAEs) associated with ICI + AI therapy has its own characteristics; however, no relevant article has summarized them. Therefore, a systematic review of such AE data is necessary to guide informed decisions in clinical trials and in clinics, for both clinicians and patients. Herein, we conducted a systematic review and meta-analysis of the incidence of all-grade AEs, grade ≥ 3 AEs, and all deaths associated with ICI + AI therapy *vs.* ICI or AI monotherapy to synthesize an accurate and comprehensive toxicity profile that can help clinicians manage patients and rapidly respond to fatal AEs.

Materials and methods

Search strategy

Relevant studies were identified using the following electronic databases: (1) PubMed, (2) Embase, (3) Web of Science, and (4) Cochrane library. The following keywords were used: "Immune Checkpoint Inhibitors," "ipilimumab," "tremelimumab," "nivolumab,"

✉ Correspondence to: Liu Huang. E-mail: huangliu@tjh.tjmu.edu.cn

"pembrolizumab," "atezolizumab," "avelumab," "durvalumab," "PD-1," "PD-L1," "CTLA-4," "ICI," "anti-angiogenic," "Anti-VEGF," "ramucirumab," "bevacizumab," "TKI," "axitinib," and "sunitinib." Only studies published in English from conception of the database to November 28, 2020, were included. Further efforts to identify additional 29 studies included hand-searching of reviews and reference lists as well as attempts to contact authors. The eligibility assessment for study selection was performed independently in a blinded, standardized manner by two reviewers. Disagreements between the two reviewers were resolved by discussion and consensus.

Selection criteria

The inclusion criteria were as follows: (1) studies based on histologically or cytologically confirmed solid tumors, (2) studies on ICI + AI therapy, (3) studies including reported tabulated data on TRAEs, and (4) articles published in English. The exclusion criteria were as follows: (1) review articles, meta-analyses, and case reports, and (2) studies based on ICI + AI therapy in combination with chemotherapy.

Data extraction

A data extraction form was developed a priori, two reviewers conducted data extraction in tandem, and the final results were reviewed by a third reviewer. If overlapping data were identified, the most recent or comprehensive study was included in the analysis. Disagreements were resolved through discussions among the three reviewers. The following information was extracted from each study: (1) study name/clinical trial ID; (2) author; (3) year of publication; (4) cancer type; (5) drugs studied; (6) treatment arms; (7) trial phase; and (8) AE data including the total number of patients affected and incidence of all-grade AEs and grade ≥ 3 AEs.

Quality assessment

Two investigators independently assessed the risk of bias in the included randomized controlled trials (RCTs) using the Cochrane Collaboration's tool, which includes the following five domains: sequence generation, allocation concealment, blinding, incomplete data, and selective reporting. Blinding can't be applied in studies with specific designs (such as open-label or cross-over) for unavoidable reasons. If such reasons were clearly stated in the included studies, they were rated as "+." An RCT was judged to have a "low risk of bias," a "high risk of bias," or an "unclear risk of bias" if all domains indicated low risk, one or more domains indicated high risk or more than three domains indicated unclear risk, respectively.

Statistical analysis

The meta-analysis was conducted using Review Manager (version 5.3, The Nordic Cochrane Center) and the package "metafor" of the R-project (version 3.6.3). Pooled risk ratios (RR) with 95% confidence intervals (CI) were used to analyze the all-grade TRAEs (RR > 1 favored the combination group; RR < 1 favored the monotherapy group). Among the selected studies, only those containing both combination therapy and monotherapy groups were included in the calculation of the pooled RR, whereas all studies were included in the calculation of the pooled incidence of selected TRAEs. If a study included more than one monotherapy arm, the combination arm was compared twice with each monotherapy arm.

Results

Search results and study quality assessment

The initial database search yielded 1527 studies. After screening (Fig. 1), 27 studies involving 5,138 patients were included in the final analysis. Of the 27 studies, 9 were control experiments (8 RCTs; 1 retrospective study) and 18 were single-arm experiments. The rationale for the addition and exclusion of each study is summarized in Fig. 1. The ICIs administered included atezolizumab (n = 7), pembrolizumab (n = 10), nivolumab (n = 4), avelumab (n = 1), and others (n = 5). The trials involved the treatment of renal cell carcinoma (RCC; n = 8), hepatocellular carcinoma (HCC; n = 3), ovarian cancer (n = 3), cervical cancer (n = 2), other cancers (n = 8), and mixed cancer types (n = 3; Table 1).

Overall, the risk of bias across studies was relatively low; one abstract and one retrospective study were rated as having a high risk of bias. The funnel plot analysis didn't indicate any evident risk of publication bias for all-grade AEs and grade ≥ 3 AEs.

Pooled incidence of TRAEs in the ICI + AI and AI groups

Collectively, 27 studies (including 9 RCTs and 18 single-arm studies involving ICI + AI, AI, and ICI regimens) reported more than 100 different types of AEs. Overall, 4,970 (96.7%) of 5,138 patients patients ICI + AI [3052 (97.0%) of 3,146 patients], AI [1,724 (98.5%) of 1,751 patients], and ICI [194 (80.5%) of 241 patients)] from the 27 studies developed at least one AE of any grade, and 2,964 (58.1%) of 5,102 patients ICI + AI [1783 (56.8%) of 3140 patients], AI [1127 (64.4%) of 1751 patients], and ICI [54 (25.6%) of 211 patients] from 27 studies developed at least one AE of grade ≥ 3.

For the meta-analysis, we focused on AEs that were reported by at least 10% of the studies or were likely to be

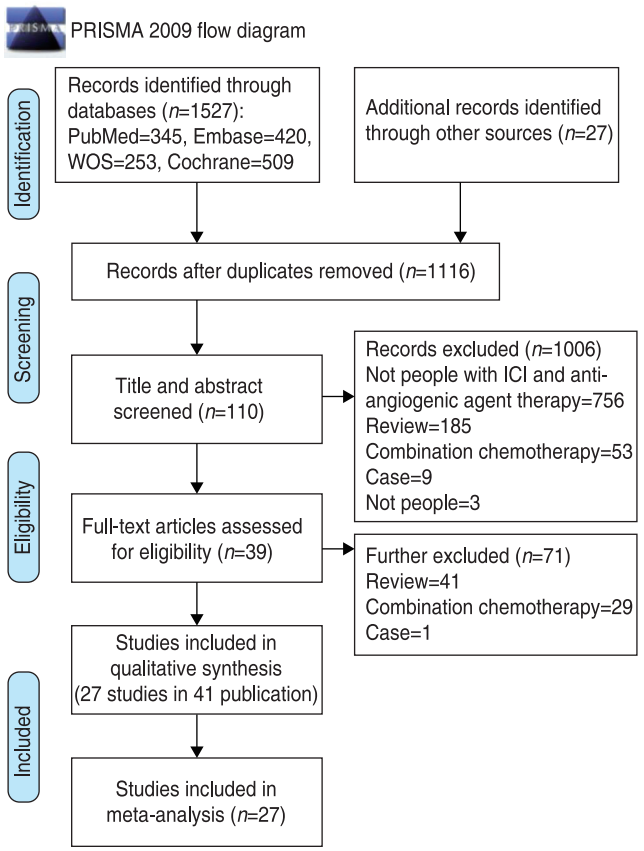

Fig. 1 Database search and study selection

TRAEs. Using these criteria, we focused on 58 AEs, which included the most clinically relevant AEs commonly seen in practice. The overall mean incidence of all-grade AEs in the ICI + AI and AI groups were 96.0% (95% CI: 94.2%–97.8%) and 98.8% (95% CI: 97.8%–99.7%), respectively, and the mean incidence of grade ≥ 3 AEs was higher in the AI group (53.9%; 95% CI: 47.4%–60.4%) than in the ICI + AI group (63.3%; 95% CI: 55.8%–70.7%). However, no significant difference in the risk of all-grade AEs and grade ≥ 3 AEs were observed between the two groups.

Common categories of AEs (grade ≥ 3) associated with ICI + AI and AI therapies

Clinicians are usually more concerned about common serious AEs; thus, we listed the top five grade ≥ 3 AEs sorted by different systems in Table 2. In the ICI + AI group, >10% of the AEs were hypertension (18.4%; 95% CI: 14.3%–22.5%), and 5%–10% AEs were rash (9.6%; 95% CI: 6.4%–12.9%), pruritus (6.9%; 95% CI: 2.8%–11%), decreased platelet count (5.6%; 95% CI: 3.40%–7.8%). Other life-threatening AEs were severe diarrhea (4.4%; 95% CI: 2.9%–5.8%), gastrointestinal hemorrhage (1.8%; 95% CI: 1.0%–4.2%), adrenal insufficiency (2.0%; 95% CI: 0.5%–3.5%), pulmonary embolism (2.1%; 95% CI: 0.7%–3.5%), and cerebrovascular accident (2.0%; 95% CI: 0.2%–3.9%). Severely abnormal biochemical indicators were increased lipase levels (5.5%; 95% CI: 2.6%–8.3%), alanine aminotransferase (ALT) elevation (5.4%; 95% CI: 3.5%–7.3%), and creatine kinase elevation (5.3%; 95% CI: 0.70%–9.9%), indicating pancreatic, liver, and cardiac damage, respectively.

In the AI group, >10% of the AEs were hypertension (16.7%; 95% CI: 14.3%–19.2%), 5%–9% AEs were decreased platelet counts (7.6%; 95% CI: 2.4%–12.9%), palmar-plantar erythrodysesthesia syndrome (PPE) (6.0%; 95% CI: 3.5%–8.6%), and anemia (5.7%; 95% CI: 3.5%–7.8%). Severely abnormal biochemical indicators were aspartate aminotransferase (AST) elevation (2.5%; 95% CI: 1.3%–3.6%) and ALT elevation (2.3%; 95% CI: 1.4%–3.3%), indicating liver injury.

Characteristics and incidence of fatal AEs (grade 5) in the ICI + AI and AI groups

(1) Eleven studies, including 2,991 patients, reported fatal AEs in the ICI + AI group, with a total of 57 deaths. The overall incidence of fatal AEs was 2.50% (57/2291). As shown in Table 3, fatal hemorrhage at any site [n = 13 (0.57%)], cardiovascular toxicities [n = 12 (0.52%)], and severe infection [n = 10 (0.44%)] accounted for more than half of the fatal AEs. Other important fatal AEs included respiratory, gastrointestinal, and hepatic toxicities, such as pneumonitis [n = 6 (0.26%)], ulcer perforation [n = 4 (0.17%)], and hepatic injury [n = 4 (0.17%)]. Myasthenia gravis and adrenal insufficiency led to 6 (0.26%) and 1 death, respectively.

(2) In the AI group, 5 studies reported at least 1 fatal AE, with a total of 20 reported deaths. The overall incidence of fatal AEs was 1.28% (20 of 1,566). The most common cause of fatal AEs in the AI group was cardiovascular toxicity [n = 8 (0.51%)], including cardiac arrest [n = 3 (0.19%)) and sudden death [n = 3 (0.19%)]; and hepatic toxicities and hemorrhage were both observed in 4 [0.26%] cases; together accounting for 80% of fatal AEs. Sudden death and cardiac arrest are common causes of medical disputes in China and thus need attention. Informing about the risk in advance rather than acting after its occurrence usually helps reduce medical disputes. As shown in Table 3 , the ICI + AI group had a significantly higher risk of fatal AEs than the AI group [57 (2.50%) *vs.* 20 (1.28%), P = 0.0041], especially with regard to respiratory toxicities [8 (0.35%) *vs.* 1 (0.06%), P = 0.04] and severe infection [10 (0.44%) *vs.* 0 (0.00%), P < 0.01].

The total number of fatal AEs in the ICI + AI group (n = 59) was slightly higher than the total number of deaths (n = 57); the percentage values were calculated from 57. One study [10] reported four treatment-related deaths that occurred in 451 patients (one patient had cerebral infarction, one patient had adrenal insufficiency and hypotension, one patient had multiple organ dysfunction

Table 1 Study characteristics

Study	NCT number	Phase	Cancer	Treatment arm	Monotherapy arm	Patients (*n*)	Number of all-grade AEs	Number of grade 3 AEs
[8]	IMmotion150	II	RCC	[a]atezolizumab+bevacizumab	[b]sunitinib	101/100	101/99	67/71
[8]	IMmotion150	II	RCC	[a]atezolizumab+bevacizumab	[a]tezolizumab	101/103	101/101	67/43
[9]	NCT02684006	Ib	RCC	[c]avelumab+axitinib	[b]sunitinib	434/439	432/436	309/314
[10]	NCT02420821	III	RCC	[a]atezolizumab+bevacizumab	[b]sunitinib	451/446	411/429	187/245
[11]	NCT02853331	III	RCC	[d]pembrolizumab+axitinib	[b]sunitinib	429/425	422/423	325/300
[12]	-	-	LUAD	ICI + AI	AI	25/49	23/39	3/3
[13]	NCT03434379	III	HCC	[a]atezolizumab+bevacizumab	[e]sorafenib	329/156	323/154	201/95
[14]	NCT02337491	II	glioblastoma	[f]pembrolizumab+bevacizumab	pembrolizumab	50/30	50/30	-
[15]	ORIENT-32	III	HCC	[g]sintilimab+bevacizumab	[e]sorafenib	380/185	376/181	217/93
[16]	NCT02715531	IB	HCC	[a]atezolizumab+bevacizumab	atezolizumab	60/58	57/52	41/24
[16]	NCT02715531	IB	HCC	atezolizumab+bevacizumab	None	104	91	55
[17]	-	-	glioblastoma	ipilimumab+bevacizumab	None	20	20	7
[18]	CheckMate 016	I	RCC	nivolumab+sunitinib	None	33	33	27
[18]	CheckMate 016	I	RCC	nivolumab+pazopanib	None	20	20	14
[19]	NCT02133742	Ib	RCC	pembrolizumab+axitinib	None	52	52	34
[20]	NCT02443324	Ia/b	mixed	pembrolizumab+ramucirumab	None	92	75	22
[21]	NCT02501096	II	endometrial cancer	pembrolizumab+lenvatinib	None	53	51	36
[22]	NCT02636725	II	sarcomas	pembrolizumab+axitinib	None	33	33	13
[23]	NCT02873962	II	ovarian cancer	nivolumab+bevacizumab	None	38	34	9
[24]	NCT02921269	II	cervical cancer	atezolizumab+bevacizumab	None	11	11	4
[25]	NCT02821000	1b	melanoma	toripalimab+axitinib	None	33	32	13
[26]	-	1b/II	mixed	pembrolizumab+lenvatinib	None	137	133	94
[27]	NCT03136627	Ib	RCC	nivolumab+tivozanib	None	25	25	20
[28]	EPOC1706	II	gastric cancer	pembrolizumab+lenvatinib	None	29	29	14
[29]	NCT02496208	I	urothelial carcinoma	nivolumab+cabozantinib	None	24	24	18
[30]	BTCRC-GU14-003	Ib/II	RCC	pembrolizumab+bevacizumab	None	60	60	27
[31]	-	II	cervical cancer	camrelizumab+apatinib	None	45	43	32
[32]	NCT01633970	Ib	ovarian cancer	atezolizumab+bevacizumab	None	20	19	7
[33]	NCT02853318	II	ovarian cancer	pembrolizumab+bevacizumab	None	40	33	13
[34]	NCT02942329	Ib	mixed	SHR-1210+apatinib	None	33	-	-

[a] atezolizumab 1200mg + bevacizumab 15mg/kg; [b] sunitinib 50mg; [c] avelumab 10mg/kg + axitinib 5mg; [d] pembrolizumab 200mg + axitinib 5mg; [e] sorafenib 400mg; [f] pembrolizumab + bevacizumab; [g] sintilimab 200mg + bevacizumab 15mg/kg; LUAD: lung adenocarcinoma cells

syndrome and post-radiation ulcer with cecum perforation, and one patient had sepsis and pneumonia). The total number of fatal AEs in the AI group was 20; the percentage values were calculated from 20.

Characteristics and risk of all-grade and grade ≥ 3 TRAEs in the ICI + AI versus AI groups in RCT studies

The meta-analysis included nine studies based on all-grade AEs, grade ≥ 3 AEs, fatal AEs, and dose modifications/interruptions. Of these, five studies compared the ICI + AI group with the AI group, three studies compared the ICI + AI group with the ICI group, and one study compared the ICI + AI group with both the AI and ICI groups.

The ICI + AI group had a higher risk in grade ≥ 3 TRAEs [RR, 1.70; (95%CI: 1.33–2.18)] (Fig. 3b) than the ICI group. However, compared to the AI group, the ICI + AI group showed no significant differences in the risk of all-grade [RR, 0.90; (95%CI: 0.97–1.01)] (Fig. 2a), grade ≥ 3 [RR, 1.00; (95%CI: 0.89–1.13)] (Fig. 3a) and fatal AEs [RR, 0.96; (95%CI: 0.59–1.58)] (Fig. 4). Compared to the ICI group, the ICI + AI group also showed no significant differences in the risk of all-grade [RR, 1.12; (95%CI: 0.94-1.32)] (Fig.2b). The ICI + AI group had similar incidences of drug discontinuation and dose modification to the AI group (RR, 1.47; 95% CI: 0.89–2.43), (RR, 0.92; 95% CI: 0.65–1.31) (Fig. 5a and 5b).

In other words, compared with AI, adding ICI to AI didn't increase the total incidence of AEs. However, analysis of the top 20 reported AEs (hypertension, fatigue, diarrhea, PPE, decreased platelet count, decreased appetite, dyspepsia, pruritis, proteinuria, hypothyroidism,

Table 2 Incidences of the most common grade ≥ 3 adverse events in the ICI + AI *vs* AI groups

Outcome	ICI + AI	AI
	Incidence (95% CI)	Incidence (95% CI)
General		
Fatigue	0.039 (0.025-0.052)	0.045 (0.031-0.058)
Weight loss	0.028 (0.019-0.037)	0.004 (0.002-0.007)
Fever	0.014 (0.004-0.025)	-
Asthenia	0.013 (0.001-0.025)	0.029 (0.019-0.040)
Decreased appetite	0.012 (0.006-0.018)	0.013 (0.004-0.022)
Gastrointestinal		
Diarrhea	0.044 (0.029-0.058)	0.039 (0.028-0.049)
Gastrointestinal hemorrhage	0.018 (0.001-0.042)	-
Colitis	0.013 (0.004-0.022)	-
Vomiting	0.010 (0.001-0.019)	0.011 (0.005-0.016)
Stomatitis	0.008 (0.004-0.013)	0.016 (0.007-0.025)
Nausea	0.007 (0.002-0.012)	0.007 (0.001-0.013)
Cutaneous		
Rash	0.096 (0.064-0.129)	0.005 (0.001-0.009)
Pruritis	0.069 (0.028-0.110)	-
PPE	0.044 (0.032-0.055)	0.060 (0.035-0.086)
Mucosal inflammation	0.006 (0.001-0.013)	-
Endocrine dysfunction		
Proteinuria	0.037 (0.025-0.048)	0.007 (0.002-0.012)
Adrenal insufficiency	0.020 (0.005-0.035)	-
Hyperthyroidism	0.006 (0.002-0.014)	-
Hypothyroidism	0.003 (0.001-0.005)	0.004 (0.001-0.009)
Pain		
Myalgia	0.024 (0.001-0.057)	-
Headache	0.022 (0.003-0.041)	-
Abdominal pain	0.014 (0.008-0.020)	0.013 (0.001-0.017)
Arthralgia	0.012 (0.007-0.018)	0.004 (0.001-0.007)
Oral pain	0.009 (0.006-0.041)	-
Respiratory		
Pulmonary embolism	0.021 (0.007-0.035)	-
Dyspnea	0.011 (0.001-0.026)	-
Cough	0.010 (0.002-0.018)	-
Pneumonia	0.010 (0.004-0.017)	-
Dysphonia	0.003 (0.001-0.007)	-
Cardiovascular		
Hypertension	0.184 (0.143-0.225)	0.167 (0.143-0.192)
Cerebrovascular accident	0.020 (0.002-0.039)	-
Hematologic		
Decreased platelet count	0.056 (0.340-0.078)	0.076 (0.024-0.129)
Leukopenia	0.030 (0.005-0.055)	-
Anemia	0.016 (0.006-0.026)	0.057 (0.035-0.078)
Neutropenia	0.010 (0.002-0.021)	0.010 (0.002-0.021)
Biochemical abnormalities		
Increased lipase	0.055 (0.026-0.083)	-
ALT elevation	0.054 (0.035-0.073)	0.023 (0.014-0.033)
Creatine kinase elevation	0.053 (0.007-0.099)	-
AST elevation	0.047 (0.029-0.064)	0.025 (0.013-0.036)
GGT elevation	0.040 (0.001-0.086)	-

Table 3 Cases and fatality rates of treatment-related deaths in clinical trials of ICI + AI and AI groups

Cause of death	Number (%)		
	ICI + AI 57 (2.49)	AI 20 (1.28)	*P* value (0.0041)
Respiratory	8 (0.35)	1 (0.06)	0.04
Pneumonia	6 (0.26)	1 (0.06)	0.08
Respiratory distress	1 (0.04)	0 (0.00)	0.20
Respiratory failure	1 (0.04)	0 (0.00)	0.20
Cardiovascular	12 (0.52)	8 (0.51)	0.48
Sudden death	4 (0.17)	3 (0.19)	0.45
Cardiac arrest	2 (0.09)	3 (0.19)	0.19
Myocarditis	2 (0.09)	0 (0.00)	0.12
Myocardial infarction	1 (0.04)	1 (0.06)	0.39
Hypotension	1 (0.04)	0 (0.00)	0.20
Thromboembolic event	1 (0.04)	0 (0.00)	0.20
Heart failure	0 (0.00)	1 (0.06)	0.11
Hemorrhage	13 (0.57)	4 (0.26)	0.08
Gastrointestinal hemorrhage	6 (0.26)	1 (0.06)	0.08
Intracranial hemorrhage	4 (0.17)	2 (0.13)	0.36
Pulmonary hemorrhage	1 (0.04)	0 (0.00)	0.20
Esophageal varices hemorrhage	1 (0.04)	0 (0.00)	0.20
Hematemesis	1 (0.04)	0 (0.00)	0.20
Peritoneal hemorrhage	0 (0.00)	1 (0.06)	0.11
Gastrointestinal	6 (0.26)	1 (0.06)	0.08
Ulcer perforation	4 (0.17)	1 (0.06)	0.17
Necrotizing pancreatitis	1 (0.04)	0 (0.00)	0.20
Bowel obstruction	1 (0.04)	0 (0.00)	0.20
Hepatic	8 (0.35)	4 (0.26)	0.30
Liver injury	4 (0.17)	2 (0.13)	0.36
Hepatic cirrhosis	2 (0.09)	2 (0.13)	0.35
Hepatic failure	2 (0.09)	0 (0.00)	0.12
Cerebrovascular	1 (0.04)	0 (0.00)	0.20
Cerebral infarction	1 (0.04)	0 (0.00)	0.20
Sever infectious	10 (0.44)	0 (0.00)	< 0.01
Sepsis	5 (0.22)	0 (0.00)	0.03
Bacterial peritonitis	2 (0.09)	0 (0.00)	0.12
Empyema	1 (0.04)	0 (0.00)	0.20
Necrotizing fasciitis	1 (0.04)	0 (0.00)	0.20
Bacteremia	1 (0.04)	0 (0.00)	0.20
Other	3 (0.13)	2 (0.13)	0.49
Myasthenia gravis	1 (0.04)	0 (0.00)	0.20
Adrenal insufficiency	1 (0.04)	0 (0.00)	0.20
MODS	1 (0.04)	0 (0.00)	0.20
General physical health deterioration	0 (0.00)	1 (0.06)	0.11
Malignant neoplasm progression	0 (0.00)	1 (0.06)	0.11

stomatitis, arthralgia, mucosal inflammation, rash, elevated liver enzymes, dysphonia, anemia, constipation, headache, neutropenia), revealed differences between them. When ICI was added to AI, some AEs increased in line with our speculation; however, other AEs decreased beyond our expectations. (1) For all-grade AEs, ICI + AI group displayed significantly higher rates of dysphonia

a

Study or subgroup	Experimental Events	Total	Control Events	Total	Weight	Risk ratio M·H, Random, 95% CI
David1	101	101	99	100	15.3%	1.01 [0.98, 1.04]
Finn	323	329	154	156	16.9%	0.99 [0.97, 1.02]
Motzer	432	434	436	439	21.3%	1.00 [0.99, 1.01]
Rinia	411	451	429	446	13.0%	0.95 [0.92, 0.98]
Rinib	413	429	415	425	16.7%	0.99 [0.96, 1.01]
Zhengguang	376	380	181	185	16.7%	1.01 [0.99, 1.04]
Total (95% CI)		2124		1751	100.0%	0.99 [0.97, 1.01]
Total events	2056		1714			

Heterogeneity: Tau²=0.00; Chi²=22.55, df=5 (*P*=0.0004); I²=78%
Test for overall effect: Z=0.67 (*P*=0.50)

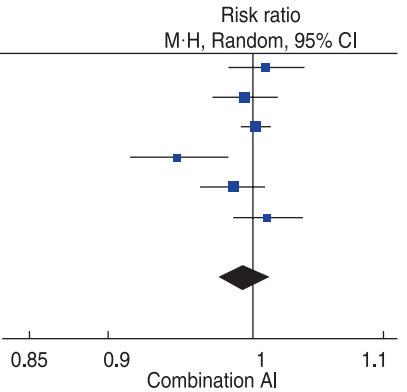

b

Study or subgroup	Experimental Events	Total	Control Events	Total	Weight	Risk ratio M·H, Random, 95% CI
David2	101	101	101	103	31.9%	1.02 [0.99, 1.05]
Di huang	23	25	39	49	23.4%	1.16 [0.96, 1.39]
Lee	41	60	24	59	13.3%	1.68 [1.18, 2.39]
Nayak	50	50	30	30	31.3%	1.00 [0.95, 1.05]
Total (95% CI)		236		241	100.0%	1.12 [0.94, 1.32]
Total events	215		194			

Heterogeneity: Tau²=0.02; Chi²=53.22, df=3 (*P*=0.00001); I²=94%
Test for overall effect: Z=1.27 (*P*=0.20)

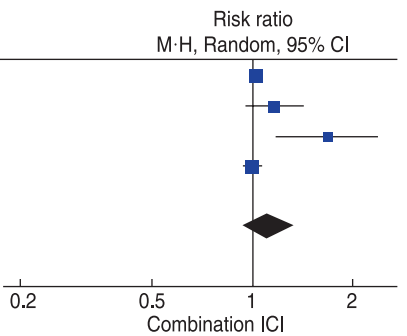

Fig. 2 Risk of all-grade AEs in combination therapy vs. monotherapy (a) show all-grade AEs in combination therapy vs. AI therapy. (b) show all-grade AEs in combination therapy vs. ICI therapy.

a

Study or subgroup	Experimental Events	Total	Control Events	Total	Weight	Risk ratio M·H, Random, 95% CI
David1	60	101	42	100	9.9%	1.41 [1.07, 1.87]
Finn	211	329	95	156	16.5%	1.05 [0.91, 1.22]
Motzer	309	434	314	439	20.1%	1.00 [0.92, 1.08]
Rinia	187	451	245	446	17.2%	0.75 [0.66, 0.87]
Rinib	325	429	300	425	20.2%	1.07 [0.99, 1.16]
Zhengguang	217	380	93	158	16.1%	0.97 [0.83, 1.13]
Total (95% CI)		2124		1724	100.0%	1.00 [0.89, 1.13]
Total events	1309		1089			

Heterogeneity: Tau²=0.02; Chi²=25.85, df=5 (*P*<0.0001); I²=81%
Test for overall effect: Z=0.05 (*P*=0.96)

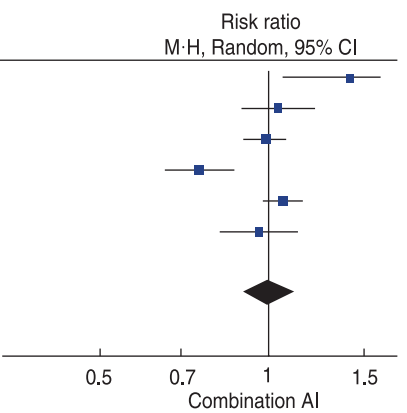

b

Study or subgroup	Experimental Events	Total	Control Events	Total	Weight	Risk ratio M·H, Random, 95% CI
David2	67	101	43	103	85.7%	1.59 [1.22, 2.08]
Di huang	3	25	3	49	2.6%	1.96 [0.43, 9.02]
Lee	22	60	8	59	11.6%	2.70 [1.31, 5.58]
Total (95% CI)		186		211	100.0%	1.70 [1.33, 2.18]
Total events	92		54			

Heterogeneity: Tau²=0.00; Chi²=1.97, df=2 (*P*=0.37); I²=0%
Test for overall effect: Z=4.20 (*P*<0.0001)

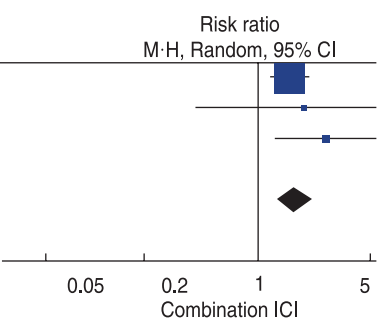

Fig. 3 Risk of grade ≥ 3 AEs in combination vs monotherapy (a) show grade ≥ 3 AEs in combination therapy vs. AI therapy. (b) show grade ≥ 3 AEs in combination therapy vs. ICI therapy

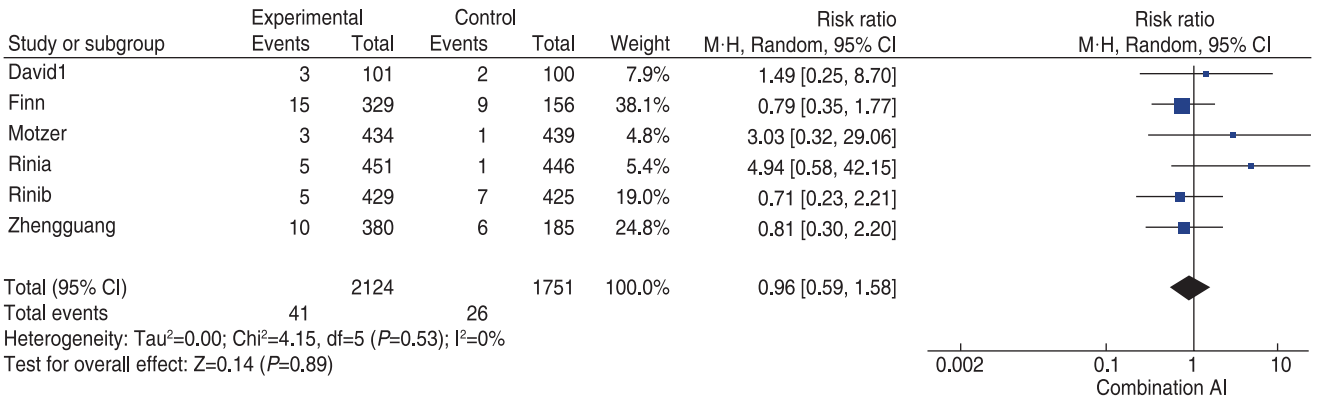

Fig. 4 Risk of treatment-related deaths in combination therapy vs. monotherapy

(21.90% *vs* 3.40%; 95% CI: 2.86–12.46, $P < 0.001$), proteinuria (20.40% *vs* 7.90%; 95% CI: 1.67–4.80, $P = 0.0001$), pruritis (17.00% *vs* 6.00%; 95% CI: 2.18–3.40, $P < 0.001$), arthralgia (18.40% *vs* 8.00%; 95% CI: 1.72–3.17, $P < 0.001$), ALT elevation (19.70% *vs* 12.50%; 95% CI: 1.35–2.01, $P < 0.001$), AST elevation (20.10% *vs* 14.40%; 95% CI: 1.12–1.69, $P = 0.002$), fatigue (33.6% *vs* 27.3%; 95% CI: 1.02–1.64, $P = 0.04$), and headache (16.8% *vs* 13.7%; 95% CI: 1.01–1.52, $P = 0.04$). In contrast, the ICI + AI group reported lower rates of PPE (16.6% *vs* 35.9%; 95% CI: 0.08–0.50, $P < 0.0006$), neutropenia (1.2% *vs* 16.6%; 95% CI: 0.05–0.13, $P < 0.001$), decreased platelet counts (4.9% *vs* 15.5%; 95% CI: 0.09–0.97, $P = 0.04$), anemia (5.7% *vs* 20.4%; 95% CI: 0.22–0.36, $P < 0.001$), mucosal inflammation (12.1% *vs* 22.0%; 95% CI: 0.32–0.92, $P = 0.02$), stomatitis (15.9% *vs* 22.4%; 95% CI: 0.44–0.99, $P = 0.04$) and dyspepsia (5.1% *vs* 16.6%; 95% CI: 0.16–0.53, $P < 0.001$). (2) For grade ≥ 3 AEs, the ICI + AI group induced significantly higher rates of proteinuria (3.0% *vs* 0.9%; 95% CI: 1.42–7.18, $P = 0.005$) and liver enzymes (ALT elevation (8.0% *vs* 2.5%; 95% CI: 2.17–5.12, $P < 0.001$) and AST elevation (5.9% *vs* 2.6%; 95% CI: 1.29–3.20, $P = 0.002$)) but had lower rates of fatigue (2.4% *vs* 4.4%; 95% CI: 032–0.93, $P = 0.03$), neutropenia (0.3% *vs* 6.1%; 95% CI: 0.02–0.16, $P < 0.001$), anemia (0.8% *vs* 5.8%; 95% CI: 0.08–0.30, $P < 0.001$), and decreased platelet count (0.3% *vs* 24.5%; 95% CI: 0.02–0.21, $P < 0.001$) (Table 4).

Discussion

The overall response rate to ICI remains suboptimal [3]. AI drugs have been shown to synergize with ICIs in multiple cancers. However, TRAEs resulting from the combination of these two modalities aren't fully understood. Although the toxicity profile of this new treatment is favorable, a unique set of AEs including fatal hemorrhage, liver injury, severe infection, and pneumonitis has been observed. To help clinicians better understand the safety data of ICI + AI therapy and learn more about the toxicity of this new regimen, we conducted this systematic review and meta-analysis. To the best of our knowledge, our meta-analysis is the largest and most comprehensive study on the TRAEs associated with ICI + AI therapy.

Compared with traditional chemotherapy, AI or ICI + AI treatment has shown advantages in safety and efficacy in many cancer types [9, 11, 16, 18, 35–37]. However, more than 90% of patients suffered all-grade AEs, and grade ≥ 3 AEs were reported in more than 50% of cancer patients. From the standpoint of patients and clinicians, we cannot ignore TRAEs and should pay attention to toxicity monitoring and control.

In the analysis of the top 20 reported all-grade AEs, we observed that adding ICI to AI increased the incidence rates of proteinuria, liver injury, dysphonia, pruritis, arthralgia, fatigue, and headache. This reminds clinicians of the following when using ICI + AI therapy: (1) For symptoms that may lead to serious organ injury and adverse clinical outcomes, such as proteinuria (20.40%), liver injury [AST elevation (20.10%)], and ALT elevation (19.70%), monitoring of these AEs and medication optimization are suggested. (2) Symptoms that may affect a patient's quality of life, such as dysphonia (increased from 3% to 22%), pruritus (increased from 6% to 17%), arthralgia (increased from 8% to 18%), fatigue (increased from 27% to 33%), and headache (increased from 13% to 16%), should be shared with patients before they accept ICI + AI treatment, and symptomatic treatment and management need to be strengthened during treatment [3]. Interestingly, compared to the AI group, the ICI + AI group had lower rates of PPE, hematologic toxicity (neutropenia, decreased platelet counts, anemia), mucosal inflammation, and stomatitis. The mechanisms involved are currently unclear, probably because in the ICI + AI group, AIs (such as bevacizumab and axitinib) [9, 16] had lower blood, skin, and mucosal toxicities than those used

Table 4 Significantly different adverse effects (all-grade and grade ≥ 3) associated with ICI + AI vs AI

Items	ICI + AI group (event/total)	AI group (event/total)	RR (95% CI)	*P* value	Heterogeneity	
					I^2 (%)	*P* value
All-grade adverse effects						
Dysphonia	288/1314	44/1310	5.97 (2.86–12.46)	< 0.001	82	0.004
Proteinuria	267/1310	89/1127	2.83 (1.67–4.80)	0.0001	78	0.004
Pruritis	297/1744	94/1566	2.72 (2.18–3.40)	< 0.001	0	0.42
Arthralgia	261/1415	113/1410	2.34 (1.72–3.17)	< 0.001	51	0.11
ALT elevation	235/1192	128/1020	1.65 (1.35–2.01)	< 0.001	0	0.72
AST elevation	239/1192	147/1020	1.38 (1.12–1.69)	0.002	14	0.31
Fatigue	79/235	66/242	1.29 (1.02–1.64)	0.04	0	0.59
Headache	238/1415	193/1410	1.24 (1.01–1.52)	0.04	23	0.07
PPE	290/1744	562/1566	0.20 (0.08–0.50)	0.0006	97	< 0.001
Mucosal inflammation	171/1415	310/1410	0.54 (0.32–0.92)	0.02	88	< 0.001
Neutropenia	16/1314	218/1310	0.08 (0.05–0.13)	< 0.001	0	0.48
Decreased platelet count	59/1192	158/1020	0.29 (0.09–0.97)	0.04	92	< 0.001
Anemia	75/1314	267/1310	0.28 (0.22–0.36)	< 0.001	0	0.42
Stomatitis	225/1415	316/14410	0.66 (0.44–0.99)	0.04	83	0.0005
Dyspepsia	67/1314	217/1310	0.29 (0.16–0.53)	< 0.001	78	0.01
Grade 3 adverse effects						
Proteinuria	36/1209	9/1027	3.19 (1.42–7.18)	0.005	9	0.33
ALT elevation	95/1192	26/1020	3.33 (2.17–5.12)	< 0.001	0	0.42
AST elevation	70/1192	27/1020	2.03 (1.29–3.20)	0.002	7	0.34
Fatigue	41/1744	69/1566	0.55 (0.32–0.93)	0.03	41	0.16
Neutropenia	4/1314	80/1310	0.06 (0.02–0.16)	< 0.001	0	0.43
Anemia	11/1314	76/1310	0.16 (0.08–0.30)	< 0.001	0	0.46
Decreased platelet count	4/1314	76/1310	0.07 (0.02–0.21)	< 0.001	13	0.32

in the AI group (such as sunitinib and sorafenib) [15, 38], as shown in Table 1.

This meta-analysis showed that the ICI + AI group had a significantly higher risk of fatal AEs than the AI group, especially for respiratory toxicities and severe infections. Moreover, cardiovascular events, hemorrhage, and liver injury were the most common fatal AEs in both groups. Based on our results, we suggest that (1) for both ICI + AI and AI groups, clinicians need to closely monitor the symptoms or signs associated with hemorrhage, blood pressure (BP), ECG recordings, and liver function of patients; (2) for the ICI + AI group, clinicians need additional monitoring of symptoms or signs associated with respiratory system toxicity (e.g., dyspnea, dyspnea, and cough) [39] and indices of severe infection (such as C-reactive protein, procalcitonin, blood lactate, and index of fungal infection) [40]. Such knowledge is essential for identifying potentially fatal AEs, and early recognition and prompt treatment of fatal AEs are warranted; and (3) some fatal AEs, such as adrenal insufficiency, necrotizing pancreatitis, myasthenia gravis, cardiac arrest, thromboembolic events, and myocarditis, are relatively rare and tend to be overlooked by clinicians. If clinicians can keep these rare fatal AEs in mind, the rate of missed diagnoses can be reduced.

Moreover, what is particularly interesting is that the incidence of severe infections in the ICI + AI group was significantly higher than that in the AI group. We speculated that PD1/PDL1 inhibitors activate immune killer cells, which is beneficial for anti-tumor therapy; however, activation of the immune system may amplify microorganisms associated with immune damage. For example, vaccination of patients with COVID-19 with cancer will cause CRS, a vaccine-related adverse event, and anti-PD1 blockade is a potential contributor [41].

This study had some limitations. First, in RCTs, the AIs used in the ICI + AI group were different from those used in the AI group, which may have influenced the comparison results. Furthermore, the type of cancer was limited in the present study, and it is uncertain whether the results are consistent with those of other cancer types. Finally, although the number of cases was large, it was not sufficient to represent the real world and special patients. It is necessary to continue follow-up research reports to further improve ICI + AI adverse reaction cognition.

Conclusion

Clinicians should pay close attention to monitoring AEs associated with ICI + AI treatment. Understanding the characteristics of severe or fatal AEs is necessary because prompt diagnosis and optimal treatment of severe AEs are important to improve patient survival.

Acknowledgements

Not applicable

Funding

This research did not receive any specific grants from funding agencies in the public, commercial, or not-for-profit sectors.

Conflicts of interest

The authors indicated no potential conflicts of interest.

Author contributions

All authors contributed to data acquisition and interpretation and reviewed and approved the final version of this manuscript.

Data availability statement

Not applicable.

Ethical approval

Not applicable.

References

1. Yarchoan M, Hopkins A, Jaffee EM. Tumor Mutational Burden and Response Rate to PD-1 Inhibition. N Engl J Med. 2017;377(25):2500-2501.
2. Wolchok JD. PD-1 Blockers. Cell. 2015;162(5):937. Yi M, Jiao D, Xu H, Liu Q, Zhao W, Han X, Wu K. Biomarkers for predicting efficacy of PD-1/PD-L1 inhibitors. Mol Cancer. 2018;17(1):129.
3. Yi M, Jiao D, Qin S, et al. Synergistic effect of immune checkpoint blockade and anti-angiogenesis in cancer treatment. Mol Cancer. 2019;18(1):60.
4. Yasuda S, Sho M, Yamato I, et al. Simultaneous blockade of programmed death 1 and vascular endothelial growth factor receptor 2 (VEGFR2) induces synergistic anti-tumour effect in vivo. Clin Exp Immunol. 2013;172(3):500-506.
5. Wu FTH, Xu P, Chow A, et al. Pre- and post-operative anti-PD-L1 plus anti-angiogenic therapies in mouse breast or renal cancer models of micro- or macro-metastatic disease. Br J Cancer. 2019;120(2):196-206.
6. Tada Y, Togashi Y, Kotani D, et al. Targeting VEGFR2 with Ramucirumab strongly impacts effector/ activated regulatory T cells and CD8(+) T cells in the tumor microenvironment. J Immunother Cancer. 2018;6(1):106.
7. McDermott DF, Huseni MA, Atkins MB, et al. Clinical activity and molecular correlates of response to atezolizumab alone or in combination with bevacizumab versus sunitinib in renal cell carcinoma. Nat Med. 2018;24(6):749-757.
8. Motzer RJ, Penkov K, Haanen J, et al. Avelumab plus Axitinib versus Sunitinib for Advanced Renal-Cell Carcinoma. N Engl J Med. 2019;380(12):1103-1115.
9. Rini BI, Powles T, Atkins MB, et al. Atezolizumab plus bevacizumab versus sunitinib in patients with previously untreated metastatic renal cell carcinoma (IMmotion151): a multicentre, open-label, phase 3, randomised controlled trial. Lancet. 2019;393(10189):2404-2415.
10. Rini BI, Plimack ER, Stus V, et al. Pembrolizumab plus Axitinib versus Sunitinib for Advanced Renal-Cell Carcinoma. N Engl J Med. 2019;380(12):1116-1127.
11. Huang D, Cui PF, Huang ZW, et al. Anti-PD-1/L1 plus anti-angiogenesis therapy as second-line or later treatment in advanced lung adenocarcinoma. J Cancer Res Clin. 2021;147(3):881-891.
12. Finn RS, Qin S, Ikeda M, et al. Atezolizumab plus Bevacizumab in Unresectable Hepatocellular Carcinoma. N Engl J Med. 2020;382(20):1894-1905.
13. Nayak L, Molinaro AM, Peters K, et al. Randomized Phase II and Biomarker Study of Pembrolizumab plus Bevacizumab versus Pembrolizumab Alone for Patients with Recurrent Glioblastoma. Clin Cancer Res. 2021;27(4):1048-1057.
14. Ren Z, Xu J, Bai Y, et al. Sintilimab plus a bevacizumab biosimilar (IBI305) versus sorafenib in unresectable hepatocellular carcinoma (ORIENT-32): a randomised, open-label, phase 2-3 study. Lancet Oncol. 2021;22(7):977-990.
15. Lee MS, Ryoo BY, Hsu CH, et al. Atezolizumab with or without bevacizumab in unresectable hepatocellular carcinoma (GO30140): an open-label, multicentre, phase 1b study. Lancet Oncol. 2020;21(6):808-820.
16. Carter T, Shaw H, Cohn-Brown D, et al. Ipilimumab and Bevacizumab in Glioblastoma. Clin Oncol (R Coll Radiol). 2016;28(10):622-626.
17. Amin A, Plimack ER, Ernstoff MS, et al. Safety and efficacy of nivolumab in combination with sunitinib or pazopanib in advanced or metastatic renal cell carcinoma: the CheckMate 016 study. J Immunother Cancer. 2018;6(1):109.
18. Atkins MB, Plimack ER, Puzanov I, et al. Axitinib in combination with pembrolizumab in patients with advanced renal cell cancer: a non-randomised, open-label, dose-finding, and dose-expansion phase 1b trial. Lancet Oncol. 2018;19(3):405-415.
19. Herbst RS, Arkenau HT, Santana-Davila R, et al. Ramucirumab plus pembrolizumab in patients with previously treated advanced non-small-cell lung cancer, gastro-oesophageal cancer, or urothelial carcinomas (JVDF): a multicohort, non-randomised, open-label, phase 1a/b trial. Lancet Oncol. 2019;20(8):1109-1123.
20. Makker V, Rasco D, Vogelzang NJ, et al. Lenvatinib plus pembrolizumab in patients with advanced endometrial cancer: an interim analysis of a multicentre, open-label, single-arm, phase 2 trial. Lancet Oncol. 2019;20(5):711-718.
21. Wilky BA, Trucco MM, Subhawong TK, et al. Axitinib plus pembrolizumab in patients with advanced sarcomas including alveolar soft-part sarcoma: a single-centre, single-arm, phase 2 trial. Lancet Oncol. 2019;20(6):837-848.
22. Liu JF, Herold C, Gray KP, et al. Assessment of Combined Nivolumab and Bevacizumab in Relapsed Ovarian Cancer: A Phase 2 Clinical Trial. JAMA Oncol. 2019;5(12):1731-1738.
23. Friedman CF, Snyder Charen A, et al. Phase II study of atezolizumab in combination with bevacizumab in patients with advanced cervical cancer. J Immunother Cancer. 2020;8(2).
24. Sheng X, Yan X, Chi Z, et al. Axitinib in Combination With Toripalimab, a Humanized Immunoglobulin G4 Monoclonal Antibody

Against Programmed Cell Death-1, in Patients With Metastatic Mucosal Melanoma: An Open-Label Phase IB Trial. J Clin Oncol. 2019;37(32):2987-2999.
25. Taylor MH, Lee CH, Makker V, et al. Phase IB/II Trial of Lenvatinib Plus Pembrolizumab in Patients With Advanced Renal Cell Carcinoma, Endometrial Cancer, and Other Selected Advanced Solid Tumors. J Clin Oncol. 2020;38(11):1154-1163.
26. Albiges L, Barthélémy P, Gross-Goupil M, et al. TiNivo: safety and efficacy of tivozanib-nivolumab combination therapy in patients with metastatic renal cell carcinoma. Ann Oncol. 2021;32(1):97-102.
27. Kawazoe A, Fukuoka S, Nakamura Y, et al. Lenvatinib plus pembrolizumab in patients with advanced gastric cancer in the first-line or second-line setting (EPOC1706): an open-label, single-arm, phase 2 trial. Lancet Oncol. 2020;21(8):1057-1065.
28. Apolo AB, Nadal R, Girardi DM, et al. Phase I Study of Cabozantinib and Nivolumab Alone or With Ipilimumab for Advanced or Metastatic Urothelial Carcinoma and Other Genitourinary Tumors. J Clin Oncol. 2020;38(31):3672-3684.
29. Dudek AZ, Liu LC, Gupta S, et al. Phase Ib/II Clinical Trial of Pembrolizumab With Bevacizumab for Metastatic Renal Cell Carcinoma: BTCRC-GU14-003. J Clin Oncol. 2020;38(11):1138-1145.
30. Lan C, Shen J, Wang Y, et al. Camrelizumab Plus Apatinib in Patients With Advanced Cervical Cancer (CLAP): A Multicenter, Open-Label, Single-Arm, Phase II Trial. J Clin Oncol. 2020;38(34):4095-4106.
31. Moroney JW, Powderly J, Lieu CH, et al. Safety and Clinical Activity of Atezolizumab Plus Bevacizumab in Patients with Ovarian Cancer: A Phase Ib Study. Clin Cancer Res. 2020;26(21):5631-5637.
32. Zsiros E, Lynam S, Attwood KM, et al. Efficacy and Safety of Pembrolizumab in Combination With Bevacizumab and Oral Metronomic Cyclophosphamide in the Treatment of Recurrent Ovarian Cancer: A Phase 2 Nonrandomized Clinical Trial. JAMA Oncol. 2021;7(1):78-85.
33. Xu J, Zhang Y, Jia R, et al. Anti-PD-1 Antibody SHR-1210 Combined with Apatinib for Advanced Hepatocellular Carcinoma, Gastric, or Esophagogastric Junction Cancer: An Open-label, Dose Escalation and Expansion Study. Clin Cancer Res. 2019;25(2):515-523.
34. Finn RS, Cheng AL. Atezolizumab and Bevacizumab in Hepatocellular Carcinoma. Reply. N Engl J Med. 2020;383(7):695.
35. Makker V, Taylor MH, Aghajanian C, et al. Lenvatinib Plus Pembrolizumab in Patients With Advanced Endometrial Cancer. J Clin Oncol. 2020;38(26):2981-2992.
36. Rini BI, Motzer RJ, Powles T, et al. Atezolizumab plus Bevacizumab Versus Sunitinib for Patients with Untreated Metastatic Renal Cell Carcinoma and Sarcomatoid Features: A Prespecified Subgroup Analysis of the IMmotion151 Clinical Trial. Eur Urol. 2021;79(5):659-662.
37. Motzer RJ, Robbins PB, Powles T, et al. Avelumab plus axitinib versus sunitinib in advanced renal cell carcinoma: biomarker analysis of the phase 3 JAVELIN Renal 101 trial. Nat Med. 2020;26(11):1733-1741.
38. Baldomero AK, Melzer AC, Greer N, et al. Effectiveness and Harms of High-Flow Nasal Oxygen for Acute Respiratory Failure: An Evidence Report for a Clinical Guideline From the American College of Physicians. Ann Intern Med. 2021;174(7):952-966.
39. Li M, Shao H, Wang C. Risk factors and their predictive value for intensive care unit acquired weakness in patients with sepsis. Zhonghua Wei Zhong Bing Ji Jiu Yi Xue. 2021;33(6):648-653.
40. Au L, Fendler A, Shepherd STC, et al. Cytokine release syndrome in a patient with colorectal cancer after vaccination with BNT162b2. Nat Med. 2021;27(8):1362-1366.

DOI 10.1007/s10330-022-0605-5
Cite this article as: Chen L, Wu L, Lu Z, *et al*. Treatment-related adverse events of combined anti-angiogenic and immune checkpoint inhibitors: systematic review and meta-analysis. Oncol Transl Med. 2022;8(6):301-310.

Oncology and Translational Medicine
DOI 10.1007/s10330-022-0554-4
December 2022, Vol. 8, No. 6, P311–P313

CASE REPORT

Case report of a mixed pulmonary large cell neuroendocrine carcinoma

Xiaoying Quan, Xiaoyan Chen, Lei Lei, Xiaoli Jia, Chunzhi Wu, Bin Ye (✉)

Department of Medical Oncology, The Sixth People's Hospital of Chengdu, Chengdu 610051, China

Abstract

A 57 year-old male patient was found to have a lesion in the middle lobe of his right lung using chest computed tomography (CT). Tumor cells were detected, and surgical excision was performed. The patient was diagnosed with mixed large cell neuroendocrine carcinoma, and underwent six cycles of a chemotherapy regimen comprising etoposide combined with cisplatin. Genetic testing revealed an EGFR mutation, which prompted oxitinib-targeted therapy. To date, no signs of recurrence or metastasis have been reported.

Received: 17 January 2022
Revised: 17 June 2022
Accepted: 21 August 2022

Key words: pulmonary large cell neuroendocrine carcinoma; pulmonary adenocarcinoma; diagnosis; treatment

Case presentation

A 57 year-old male patient presenting in our hospital (the Sixth People's Hospital of Chengdu, China) in December 2020 was found to have a lesion (approximately 3.1 cm × 2.8 cm) in the middle lobe of his right lung using chest computed tomography (CT) (Fig. 1), with no cough, sputum, hemoptysis, or chest pain.

For further treatment, in January 2021, he was admitted to Sichuan Provincial Cancer Hospital, China, where enhanced CT of chest and abdomen revealed a soft tissue mass measuring 3.2 cm × 2.9 cm × 2.6 cm located in the middle lobe of the right lung, and suspected to be carcinoma. Metastases were not observed in lymph nodes or at distant sites. Enhanced magnetic resonance imaging of the head and bone scintigraphy revealed no signs of metastasis, while fibrobronchoscopic biopsy revealed the presence of tumor cells.

On January 19, 2021, radical resection of a right middle lobe carcinoma, including systematic lymph node dissection was performed to diagnose non-metastatic lung cancer and exclude surgical contraindications. Postoperative pathology revealed a macroscopic tumor size of 2.5 cm × 2.2 cm × 2 cm (Fig. 2). The tumor was hard and grey-white or grey-brown in color. Histological examination revealed a malignant tumor with some areas of adenoid structure, and a solid arrangement. Immunohistochemical analysis of the primary tumor showed CK7 (+), TTF-1 (–), NapsinA (–), Syn (few+), CgA (few+), P40 (–), ALK-V (–), ROS1 (–), BRAF V600E (–), and Ki67 (dense areas, 70%+). Combining histologic morphology and immunohistochemistry supported a diagnosis of mixed small cell carcinoma. Approximately 90% of this tissue was adenocarcinoma (mainly acinar type) and 10% was small cell neuroendocrine carcinoma. Histopathologic grading was scored as visceral pleura (+), bronchial margin (–), vascular margin (–), intravascular tumor plug (–), and airway spread (–). Lymph node

Fig. 1 Chest computed tomography shows that lesion is located in right lung middle lobe

✉ Correspondence to: Bin Ye. Email: 354539616@qq.com

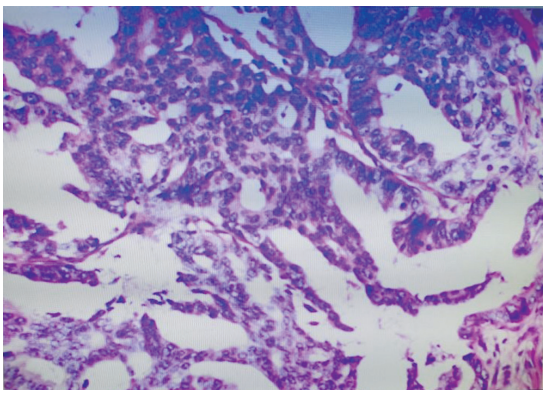

Fig. 2 Postoperative pathology shows that tumor cells (HE ×40)

metastasis was present in the second and fourth group lymph nodes (1/2), seventh group lymph nodes (2/5), a tenth group lymph node (1/1), and a bronchial root lymph node (1/1). The pathological stages were pT2N2M0 and IIIA. Genetic testing revealed an EGFR exon 21 mutation (L858R). Paraffinized tissue sent to the West China Hospital (Chengdu, China) for pathological consultation diagnosed as mixed large cell neuroendocrine carcinoma, with the adenocarcinoma component accounting for 90% of the mass. Large cell neuroendocrine carcinoma accounted for approximately 10% of the mass. Metastatic carcinoma was found in all lymph node sections. Immunophenotypic results suggested adenocarcinoma component metastasis.

After excluding chemotherapy contraindications, six cycles of etoposide combined with cisplatin chemotherapy (etoposide 160 mg ivgtt d1–3 + cisplatin 40 mg ivgtt d1–3) were administered from March 2021 to August 2021. Grade III myelosuppression occurred during chemotherapy and was enhanced by leukocyte promotion therapy. CT reexamination after completing chemotherapy showed no signs of tumor recurrence or metastasis.

In September 2021, the patient began taking oxitinib (Astrazeneca, trade name Terissa) 80 mg po qd. Skin rashes appeared on his face after one month of oxitinib administration. This condition improved upon symptomatic treatment without serious adverse reactions.

To date, the patient has had no signs of tumor recurrence or metastasis.

Discussion

Pulmonary large-cell neuroendocrine carcinoma (PLCNEC) is a rare type of non-small cell lung carcinoma characterized by high malignancy and poor prognosis, accounting for approximately 3% [1, 2] of lung carcinomas. Most patients are already in an advanced stage at time of initial diagnosis. Due to lack of large cohort clinical studies, the current treatment remains controversial [3, 4].

Surgical resection is the main treatment for PLCNEC and achieves improved prognosis in early-stage patients [5, 6]. Postoperative adjuvant chemotherapy can reduce the recurrence rate in patients with stage II disease or above [7]. Some studies have found that the efficacy of platinum-containing chemotherapy regimens is better than that of platinum-free chemotherapy. Thus, the etoposide-platinum regimen currently seems to be the better choice [8, 9]. Most scholars currently recommend etoposide combined with a platinum regimen as the first-line chemotherapy for patients with PLCNEC. The therapeutic efficacy of radiotherapy for patients with PLCNEC is unclear. However, it may prolong the overall survival of patients who were unsuitable for surgery, had postoperative residual lesions, or were in an advanced stage [10, 11]. PLCNEC patients with EGFR mutation have shown good responses to EGFR-tyrosine kinase inhibitors [12, 13]. Since gene mutations are extremely rare in patients with PLCNEC, their clinical value requires further study. Some studies have found that the expression of programmed cell death-ligand 1 can be detected in patients with PLCNEC, suggesting that immunotherapy may be effective [14, 15].

Mixed pulmonary large cell neuroendocrine carcinoma with high malignancy had a worse prognosis than PLCNEC in our study, and was characterized by large cell neuroendocrine carcinoma in some regions and adenocarcinoma in other regions. Its treatment is still in an exploratory stage. The patient in our case study was a middle-aged male diagnosed with pulmonary large cell neuroendocrine carcinoma with adenocarcinoma stage III. He was actively treated with surgical resection and etoposide combined with a platinum chemotherapy regimen. Genetic testing revealed an EGFR mutation which prompted oxitinib-targeted therapy. The patient is still under close follow-up, with no signs of tumor recurrence or metastasis; therefore, the efficacy and safety of this regimen remains to be clarified in follow up studies.

Conclusion

In conclusion, a standard treatment regimen has not yet been determined for mixed pulmonary large cell neuroendocrine carcinoma because of its rarity and complex pathological manifestations. We expect that more therapeutic methods will be examined, leading to improved prognosis for future patients.

Acknowledgments

Not applicable.

Funding

Not applicable.

Conflicts of interest

The authors indicated no potential conflicts of interest.

Author contributions

All authors contributed to data acquisition, data interpretation, and reviewed and approved the final version of this manuscript.

Data availability statement

Not applicable.

Ethical approval

Not applicable.

References

1. Fasano M, Della Corte CM, Papaccio F, et al. Pulmonary large-cell neuroendocrine carcinoma: from epidemiology to therapy. J Thorac Oncol. 2015;10(8):1133-1141.
2. Kinslow CJ, May MS, Saqi A, et al. Large-cell neuroendocrine carcinoma of the lung: a population-based study. Clin Lung Cancer. 2020;21(2):e99-e113.
3. Zombori T, Juhász-Nagy G, Tiszlavicz L, et al. Large-cell neuroendocrine carcinoma of the lung – challenges of diagnosis and treatment. Orv Hetil (Hungarian). 2020;161(8):313-319.
4. Ferrara MG, Stefani A, Simbolo M, et al. Large cell neuro-endocrine carcinoma of the lung: current treatment options and potential future opportunities. Front Oncol. 2021;11:650293.
5. Roesel C, Terjung S, Weinreich G, et al. A single-institution analysis of the surgical management of pulmonary large cell neuroendocrine carcinomas. Ann Thorac Surg. 2016;101(5):1909-1914.
6. Chen Y, Zhang J, Huang C, et al. Survival outcomes of surgery in patients with pulmonary large-cell neuroendocrine carcinoma: a retrospective single-institution analysis and literature review. Orphanet J Rare Dis. 2021;16(1):82.
7. Kim KW, Kim HK, Kim J, et al. Outcomes of curative-intent surgery and adjuvant treatment for pulmonary large cell neuroendocrine carcinoma. World J Surg. 2017;41(7):1820-1827.
8. Derks JL, van Suylen RJ, Thunnissen E, et al. Chemotherapy for pulmonary large cell neuroendocrine carcinomas: does the regimen matter? Eur Respir J. 2017;49(6):1601838.
9. Shen Y, Hu F, Li C, et al. Clinical features and outcomes analysis of surgical resected pulmonary large-cell neuroendocrine carcinoma with adjuvant chemotherapy. Front Oncol. 2020;10:556194.
10. Jiang Y, Lei C, Zhang X, et al. Double-edged role of radiotherapy in patients with pulmonary large-cell neuroendocrine carcinoma. J Cancer. 2019;10(25):6422-6430.
11. Cao L, Wu HF, Zhao L, et al. The role of radiotherapy in pulmonary large cell neuroendocrine carcinoma: propensity score matching analysis. J Radiat Res. 2020;61(4):594-601.
12. Wang Y, Shen YH, Ma S, et al. A marked response to icotinib in a patient with large cell neuroendocrine carcinoma harboring an EGFR mutation: A case report. Oncol Lett. 2015;10(3):1575-1578.
13. Muto S, Ozaki Y, Okabe N, et al. Successful treatment of combined large cell neuroendocrine carcinoma harboring an EGFR mutation with EGFR-TKIs plus Bevacizumab: A case report. Case Rep Oncol. 2020;13(3):1387-1392.
14. Eichhorn F, Harms A, Warth A, et al. PD-L1 expression in large cell neuroendocrine carcinoma of the lung. Lung Cancer. 2018;118:76-82.
15. Arpin D, Charpentier MC, Bernardi M, et al. PD-L1-expression patterns in large-cell neuroendocrine carcinoma of the lung: potential implications for use of immunotherapy in these patients: the GFPC 03-2017 "EPNEC" study. Ther Adv Med Oncol. 2020;12:1758835920937972.

DOI 10.1007/s10330-022-0554-4
Cite this article as: Quan XY, Chen XY, Lei L, et al. Case report of a mixed pulmonary large cell neuroendocrine carcinoma. Oncol Transl Med. 2022;8(6): 311-313.

Oncology and Translational Medicine
DOI 10.1007/s10330-022-0607-7
December 2022, Vol. 8, No. 6, P314–P317

CASE REPORT

Adnexal tumor found during a brain-dead donor organ retrieval: a case report*

Bo Zhang[1, 2, 3, 4], Huibo Shi[5], Jing Xu[5], Xiaoqin Li[5], Mengjun Zeng[5], Ying Tao[5], Xing Wu[5], Jipin Jiang[5] (✉)

[1] Institute of Organ Transplantation, Tongji Hospital, Tongji Medical College, Huazhong University of Science and Technology, Wuhan 430030, China
[2] Key Laboratory of Organ Transplantation, Ministry of Education, Wuhan 430030, China
[3] NHC Key Laboratory of Organ Transplantation, Wuhan 430030, China
[4] Key Laboratory of Organ Transplantation, Chinese Academy of Medical Sciences, Wuhan 430030, China
[5] Organ Procurement Organization (OPO), Tongji Hospital, Tongji Medical College, Huazhong University of Science and Technology, Wuhan 430030, China

Abstract

Pre-donation evaluation of organ donors is important. Organ quality directly affects both short- and long-term survival rates of transplanted organs and recipients after transplantation. Contraindications to donation are directly related to recipient survival and medical ethics. The following information is included in this organ donation case report: detailed medical history (primary disease and surgical history), blood type, infectious diseases, coagulation function, biochemical function, tumor biomarker, indicators related to tuberculosis infection, microbial culture indicators, lung computed tomography (CT) scan, and abdominal ultrasound (heart, liver, gallbladder, pancreas, spleen, kidneys, ureters, bladder, adnexa). We found a 10 cm × 10 cm space-occupying lesion in the abdominal cavity in this donor organ retrieval surgery. Frozen or paraffin sections showed that the space-occupying lesion was malignant. The organ donor was not suitable due to the malignant tumor, and the transplantation surgery was canceled. We analyzed this case of organ donation to provide a reference for the follow-up donation evaluation process. This case study reveals the limitations of preoperative non-invasive assessment, the necessity of preoperative multi-dimensional assessment of organ function, and the exclusion of donation contraindications.

Received: 31 October 2022
Revised: 24 November 2022
Accepted: 10 December 2022

Key words: organ donation; donation evaluation; tumor

Organ donation after a citizen's death has become the main source of organ transplantation in China [1]. The quantity and quality of donated organs have become a new topic in organ donation. To match the growing organ demand, an increasing number of marginal organ donors are being covered by our evaluation and maintenance system. Therefore, balancing the use of donated organs and ensuring organ quality and recipient safety has become a major challenge for Organ Procurement Organizations (OPO) and transplant surgeons [2]. Currently, a complete system has been developed for the functional evaluation of donated organs; however, due to the limitations of emergency acquisition and preoperative evaluation, contraindications for donation may not be noticed [3]. In 2016, the "Expert Consensus on the Function Evaluation and Maintenance of Donated Organs Donated for Chinese Citizens after the Death," published by the Chinese Journal of Transplantation, clearly stated that organs containing malignant tumors (except intracranial tumors) cannot be donated [4]. Therefore, all donations from individuals with malignant tumors are contraindicated to ensure the safety of the recipient. In combination with previous cases in which adnexal tumors were found in organ donation surgeries, this study will allow the process of evaluation and contraindication exclusion for donation cases to be further optimized and will provide evaluation

✉ Correspondence to: Jipin Jiang. Email: 87148236@qq.com
* Supported by grants from the National Natural Sciences Foundation of China (No. 81800580), Wuhan Federation of Social Sciences (No. WHSKL2020140), and the Sichuan Medical Law Research Center (No. YF20-Y05).

experience for subsequent cases.

Case introduction

Medical history

The patient's family members described the patient as follows: 41 years of age, female sex, a 4-year history of hypertension, and a cesarean section. The patient was unconscious when found on the ground by family members one day prior, with no convulsions in her limbs. She presented with dyspnea and incontinence and was immediately sent to the emergency department of the local hospital. Head CT scan showed brain herniation, a large left cerebral hemorrhage in the lateral cerebral hemisphere, and a rupture into the ventricle. Emergency tracheal intubation and ventilator-assisted ventilation were subsequently performed, and the patient was transferred to the intensive care unit for treatment and symptomatic support, including dehydration and hemostasis. The neurosurgeon suggested surgical treatment, but the family refused after being informed about the patient's current condition and the risks of the operation. Therefore, she was transferred to our hospital (Tongji Hospital, Tongji Medical College, Huazhong University of Science and Technology, Wuhan, China) for further treatment with a diagnosis of "ventricular herniation and massive cerebral hemorrhage." The patient was in a deep coma without spontaneous breathing, and brainstem reflexes were not observed. Cerebral blood flow and somatosensory-evoked potentials were consistent with brain death. According to the standard protocol, the family members have signed to discontinue all rescue therapies and proceed with organ donation.

Donation evaluation

Vital signs: The patient was in a deep coma with tracheal intubation and synchronized intermittent mandatory ventilation: FiO_2, 80%; BP, 91/64 mmHg (under the treatment of vasopressors); heart rate, 91 bpm; SpO_2, 95%. Body check: bilateral pupils were unequal (left D = 4.5 mm, right D = 5.0 mm), light reflex not observed; bilateral lung breath sounds slightly thicker; scattered moist rales could be heard; and abdominal soft, mobile, dull, negative, and bowel sounds could still be heard. There was no edema in the lower extremities, and no pathological signs were elicited on either side. The assessment of clinical brain death was completed, and the donation of medical ethics materials was completed.

Laboratory tests for blood were as follows: white blood cell count, 13.95×10^9 /L↑; neutrophil percentage, 88.7%↑; neutrophil count, 12.37×10^9 /L↑; lymphocyte percentage, 7.7%↓; lymphocyte count, 1.07×10^9 /L↓; eosinophil percentage, 0.1%↓; eosinophil count, 0.01×10^9 /L↓; mean hemoglobin concentration, 309 g/L↓; RBC distribution width, SD, 50.2 fL↑. For biochemical tests: albumin, 25.4 g/L↓; urea, 15.20 mmol/L↑; sodium, 164.3 mmol/L↑; creatinine, 223 μmol/L↑; eGFR (based on the CKD-EPI equation), 22.9 mL/min/1.73m^2↓; chlorine, 127.9 mmol/L↑; high-sensitivity cardiac troponin I, 824.3 pg/mL↑↑↑. For coagulation tests: D-D dimer quantification, 0.65 μg/mL↑; prothrombin time, 19.0 seconds↑; prothrombin activity, 51.0%↓; international normalized ratio, 1.57↑; fibrinogen, 7.04 g/L↑; activated partial thromboplastin time, 51.0 seconds↑; procalcitonin, 5.92 ng/mL↑; amino-terminal pro-brain natriuretic peptide (NT-proBNP), 515 pg/mL↑; creatine kinase (CK), 1175 U/L↑. For tumor markers: Alpha-Feto protein (AFP), 6.8 ng/mL; carcinoembryonic antigen (CEA), 1.91 ng/mL; Carbohydrate antigen 199 (CA199), 19.32 U/L. Abdominal B-ultrasound showed no obvious abnormalities of the liver, gallbladder, pancreas, spleen, or any fluid in the right pleural cavity, and an abnormal echo in the abdominal cavity was suspected to be due to a dilated bowel with fecal accumulation.

Results

Abdominal space-occupying was found during the organ retrieval operation, as shown in the intraoperative image (Fig. 1), and the frozen and paraffin section reports during the operation showed that the space-occupying tumor was of adnexal mesenchymal origin, suspected to be an endometrial stromal sarcoma accompanied by implantation of the liver capsule (Fig. 2). The donor was not suitable for organ donation due to the malignant tumor, and the liver and kidney transplantation surgery was canceled.

Discussion

In cases where the organ donor has a malignant tumor, the life safety of the recipient is directly impacted, the occurrence of early cancer and carcinoma *in situ* is hidden, and the methods of preoperative exclusion are limited. For donors with primary central system tumors, related risks can be excluded according to the pathological results before donation. However, it is more difficult to identify abdominal tumors, such as those in the gastrointestinal tract, breast, and adnexa.

A case report was published by Frederike Bemelman at the Amsterdam Academic Medical Center in the *American Journal of Transplantation*. Four patients who successfully received lung, left kidney, liver, and right kidney transplants developed breast cancer with similar histological types within 16 months to 6 years after surgery. All the organs donated to these four patients came from the same donor, but no evidence of breast cancer was found at the time of donation [5]. A DNA test proved that the breast cancer cells came from the organ

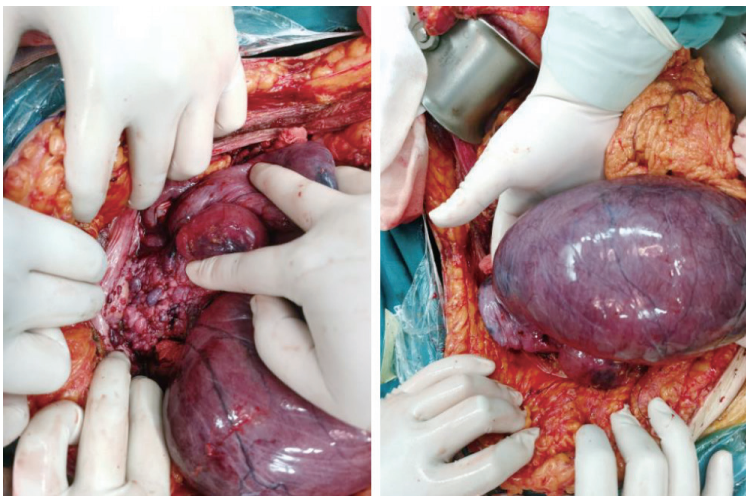

Fig. 1 During the operations, abdominal space-occupying was found

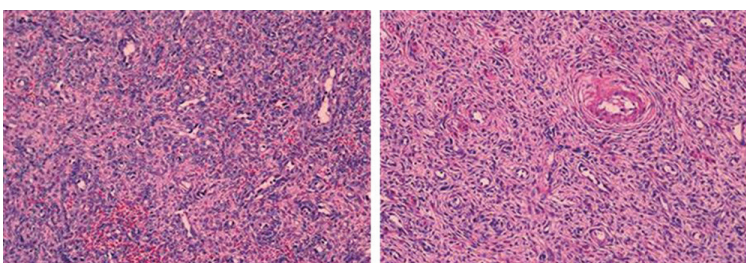

Fig. 2 Rapid biopsy results during the operation showed that the space-occupying tumor was adnexal mesenchymal, suspected to be endometrial stromal sarcoma, and accompanied by implantation of the liver capsule. Pathological diagnosis (HE ×200): (1) Tumor of mesenchymal origin, low potential malignancy, endometrial stromal sarcoma. IHC: CD10 (+), CD34 (–), SMA (+), DES (+), Caldesmon (–), ER (+), PR (+), RB1 (+), ALK1 (–), CD31 (–), CD117 (–), DOG1 (–), S-100 (–), SOX10 (–), H3K27Me3 (+), INT1 (+), HMB45 (–), Melan-A (–), Cathepsin K (–), STAT6 (–), FH (+), Ki-67 (–), and EBER CISH (–). (2) Tumor tissue similar to ovarian and uterine walls was seen on the liver capsule surface, which was considered to be implantable dissemination of the tumor

donor, but the donor had no prior history of tumors and no abnormalities had been found during the preoperative examination. In this report, although the preoperative non-invasive evaluation did not detect the tumor, the presence of *in situ* or early-stage carcinoma could not be excluded, and tumor-infecting events occurred in the circulating tumor cells after transplantation. Therefore, a preoperative examination cannot completely exclude the presence of a tumor. This case also confirmed that organ transplantation may transfer the malignant tumor from the donor to the organ recipient. Even if no obvious tumor metastasis is found, individuals with tumors are not suitable donors.

Some cancer patients are permitted to donate organs, and some scholars have compared the data of the British Transplant Registry with the national data of England, Wales, and Northern Ireland (1985–2001). In a previous study, 495 organs from 177 donors with intracranial malignant tumors were transplanted into 448 recipients, but no metastasis from donor-derived tumors was found [6]. This study concluded that the organs of patients with primary intracranial malignancies are safe for organ transplantation. Although cancer metastasis may occur after organ donation from patients with such primary diseases, the risk is very low. In all malignancies, the risk of intracranial tumor metastases outside the central nervous system is very low, and studies have shown that when individuals with high-risk factors and glioblastoma multiforme are excluded, those with primary intracranial tumors are suitable donors [7].

A clinical decision support system can facilitate living kidney donor assessments [8]. Our center has established a set of standardized evaluation procedures for early donation evaluation. This evaluation includes the following: detailed medical history (primary disease and surgical history), blood type, infectious diseases, coagulation function, biochemical function, tumor biomarkers, indicators related to tuberculosis infection, microbial culture indicators, lung CT, abdominal ultrasound (heart, hepatobiliary, and pancreas, spleen, kidneys, ureters, bladder, and appendages), as well as contrast-enhanced ultrasonography and preoperative

needle biopsy of the liver and kidneys.

Routinely, the relevant inspections and tests should be completed before donation surgery, and the maintenance and evaluation team, including the transplant physician, will complete the standardized evaluation. In this case, the relevant preoperative examinations were comprehensive, abdominal B-ultrasound abnormalities were reported, and an abnormal echo in the abdominal cavity was suspected to be due to a dilated bowel with fecal accumulation. The adnexal tumor was found during the kidney and liver retrieval, although the preoperative evaluation had been well-established. This discrepancy was mainly due to the low resolution of the bedside B-ultrasound and the lack of clinician experience. In addition, the evaluation team failed to clarify the lesions indicated by abnormal echoes in the abdominal cavity, such as through further non-invasive examinations with CT or MRI, to clarify the relationship between the lesions and surrounding tissues. However, our center has developed a whole-process evaluation procedure, abnormal information reporting, and a discussion system. Although the tumor lesions could not be accurately detected before donation surgery, the abnormal information tracking procedure was implemented in the donation process because of the abnormal inspection indicators before donation. However, because of the accurate judgment of the surgeon during the operation, the consultation of the relevant clinical department during the operation, and the pathological diagnosis of the tumor lesion, the OPO finally terminated the donation.

Organ donation assessment is not an independent unit but runs throughout the entire organ donation process and requires the support of various systems and departments. For example, detailed case records, assessment techniques, and strategies will all affect the accuracy of the assessment. Therefore, when setting up an evaluation process, different processes should be set up according to the situation in each case, and a flexible evaluation method should be established to improve evaluation accuracy.

Based on this case, the donation evaluation process has been further improved, and clinical surgeons have been established to participate in the entire evaluation process. The medical staff of the pre-donation maintenance group should start the operation after evaluation, the relevant special information should be reevaluated during the operation, and the pathological diagnosis should be processed to reevaluate organ quality. Considering the current status of organ donation evaluation, we hope that the evaluation process described in this study will be beneficial to our organ donation evaluation work and ensure the safety of the recipients' operations.

Acknowledgments

Not applicable.

Funding

This study was supported by grants from the National Natural Sciences Foundation of China (No. 81800580), Wuhan Federation of Social Sciences (No. WHSKL2020140), and the Sichuan Medical Law Research Center (No. YF20-Y05).

Conflicts of interest

The authors indicated no potential conflicts of interest.

Author contributions

All authors contributed to data acquisition and data interpretation, and reviewed and approved the final version of this manuscript.

Data availability statement

Not applicable.

Ethical approval

Not applicable.

References

1. Luo AJ, Xie WZ, Wei W, et al. Public opinion on organ donation after death and its influence on attitudes toward organ donation. Ann Transplant. 2016;21:516-524.
2. Abt PL, Marsh CL, Dunn TB, et al. Challenges to research and innovation to optimize deceased donor organ quality and quantity. Am J Transplant. 2013;13(6):1400-1404.
3. Knight SR, Cao KN, South M, et al. Development of a clinical decision support system for living kidney donor assessment based on national guidelines. Transplantation. 2018;102(10):e447-e453.
4. Chinese Society of Organ Transplantation of Chinese Medical Association, Organ Transplantation Branch of Chinese Medical Doctor Association. Expert consensus on organ function evaluation and maintenance of donation after citizen's death in China (2016). Chin J Transplant (Electronic Edition)(Chinese). 2016;10(4):145-153.
5. Matser YAH, Terpstra ML, Nadalin S, et al. Transmission of breast cancer by a single multiorgan donor to 4 transplant recipients. Am J Transplant. 2018;18(7):1810-1814.
6. Watson CJ, Roberts R, Wright KA, et al. How safe is it to transplant organs from deceased donors with primary intracranial malignancy? An analysis of UK Registry data. Am J Transplant. 2010;10(6):1437-1444.
7. Cacciatori A, Godino M, Bengochea M, et al. Organ donation and primary central nervous system tumors. Transplant Proc. 2020;52(4):1024-1029.
8. Bugeja A, Clark EG. A clinical decision support system can help facilitate living kidney donor assessments. Transplantation. 2018;102(10):1601-1602.

DOI 10.1007/s10330-022-0607-7
Cite this article as: Zhang B, Shi HB, Xu J, et al. Adnexal tumor found during a brain-dead donor organ retrieval: a case report. Oncol Transl Med. 2022;8(6): 314-317.

Call For Papers
Oncology and Translational Medicine

(CN 42-1865/R, ISSN 2095-9621)

Dear Authors,

Oncology and Translational Medicine (OTM), a peer-reviewed open-access journal, is very interested in your study. If you have unpublished papers in hand and have the idea of making our journal a vehicle for your research interests, please feel free to submit your manuscripts to us via the Paper Submission System.

Aims & Scope

- Lung Cancer
- Liver Cancer
- Pancreatic Cancer
- Gastrointestinal Tumors
- Breast Cancer
- Thyroid Cancer
- Bone Tumors
- Genitourinary Tumors
- Brain Tumor
- Blood Diseases
- Gynecologic Oncology
- ENT Tumors
- Skin Cancer
- Cancer Translational Medicine
- Cancer Imageology
- Cancer Chemotherapy
- Radiotherapy
- Tumors Psychology
- Other Tumor-related Contents

Contact Us
Editorial office of Oncology and Translational Medicine
Tongji Hospital
Tongji Medical College
Huazhong University of Science and Technology
Jie Fang Da Dao 1095
430030 Wuhan, China
Tel.: 86-27-69378388
Email: dmedizin@tjh.tjmu.edu.cn;
dmedizin@sina.com

Oncology and Translational Medicine (OTM) is sponsored by Tongji Hospital, Tongji Medical College, Huazhong University of Science and Technology, China (English, bimonthly).

OTM mainly publishes original and review articles on oncology and translational medicine. We are working with the commitment to bring the highest quality research to the widest possible audience and share the research work in a timely fashion.

Manuscripts considered for publication include regular scientific papers, original research, brief reports and case reports. Review articles, commentaries and letters are welcome.

About Us

- Peer-reviewed
- Rapid publication
- Online first
- Open access
- Both print and online versions

For more information about us, please visit:
http://otm.tjh.com.cn

中国科技核心期刊

（中国科技论文统计源期刊）

收录证书

CERTIFICATE OF SOURCE JOURNAL

FOR CHINESE SCIENTIFIC AND TECHNICAL PAPERS AND CITATIONS

ONCOLOGY AND TRANSLATIONAL MEDICINE

经过多项学术指标综合评定及同行专家评议推荐，贵刊被收录为“中国科技核心期刊”（中国科技论文统计源期刊）。

特颁发此证书。

中国科学技术信息研究所

Institute of Scientific and Technical Information of China

北京复兴路 15 号 100038　　www.istic.ac.cn

2022年12月

证书编号：2021-G616-0123

有效期至：2023年12月